ELECTROPHORETIC DEPOSITION OF ORGANIC-INORGANIC NANOCOMPOSITES

Electrophoretic Deposition of Organic - Inorganic Nanocomposites

By

YANCHAO SUN, B.Eng.

A Thesis

Submitted to the School of Graduate Studies

In Partial Fulfillment of the Requirements

For the Degree

Master of Science

McMaster University

MASTER OF SCIENCE (2012)………………...……..McMaster University

(Materials Science & Engineering)……………………….Hamilton, Ontario

TITLE: Electrophoretic Deposition of Organic-Inorganic Nanocomposites

AUTHOR: Yanchao Sun, B.Eng. (Shanghai University)

SUPERVISOR: Professor Igor Zhitomirsky

NUMBER OF PAGES: XII, 112

Abstract

Electrochemical deposition methods have been developed for the fabrication of organic － inorganic nanocomposite coatings. The methods are based on electrophoretic deposition of ceramic nanoparticles and polymers.

EPD method has been developed for the deposition of nanostructured TiO_2 films using new dispersing agents. The stabilization and charging of the nanoparticles in suspensions was achieved using these organic molecules, which belong to catecholate and salicylate families. Anodic deposition was achieved using caffeic acid, 2,3－dihydroxybenzoic acid, 2,6－dihydroxybenzoic acid and 5－sulfosalicylic acid. Cathodic deposition was performed using 2,4 dihydroxycinnamic acid, p－coumaric acid and trans cinnamic acid. The deposition yield has been studied as a function of the additive concentration and deposition time. The deposition mechanism has been investigated. The fundamental adsorption mechanism is based on the complexation of metal ions at the surfaces of oxide nanoparticles. The method enabled the co-deposition of TiO_2 and other oxides and the formation of composite films.

Electrophoretic deposition method has been used for the deposition of TiO_2 nanoparticles modified with organic dyes. Alizarin red, alizarin yellow, pyrocatechol violet and Aurintricarboxylic acid dyes were used for the dispersion and charging of TiO_2. The microstructures of the nanocomposite coatings were studied. The deposition yield was investigated under a variety of conditions. Obtained results could pave the way for the fabrication of dye-sensitized TiO_2 films.

EPD method has also been developed for the fabrication of (Poly[3-(3-N,N-diethylaminopropoxy)thiophene]) PDAOT－TiO_2, (polyethylenimine) PEI－TiO_2 and PEI－hydrotalcite composite films. The microstructures of the nanocomposite coatings were studied by Scanning Electron Microscopy, Thermogravimetric Analysis, which showed the co－deposition of inorganic nanoparticles and organic polymer. Electrochemical test of the composite film has been conducted. The results showed that PEI film provided corrosion protection of the stainless steel substrates.

Acknowledgement

I would like to express my gratitude to all those who gave me the possibility to complete this thesis.

First of all, I would like to express my sincere appreciation to my supervisor, Professor Igor Zhitomirsky, whose help, stimulating suggestions and encouragement helped me in all the time of research and writing of this thesis.

Also I would give many thanks to all the team members, Kangmin Wu, Xiaofei Li, Yaohui Wang, Lijia Yang, Imran Deen, Mustafa Ata, Shilei Chen, Yisong Su for their kindness and friendship.

Last but not the least; I take this opportunity to express my profound gratitude to my beloved parents for the moral support and patience during my study in Canada.

Table of Contents

List of Figures

List of Tables

1 Introduction

The field of nanocomposite materials has attracted attention of scientists and engineers in recent years. Organic - inorganic composite nanomaterials have attracted more and more interest for the purpose of creating high performance or high functional materials that are expected to provide many advanced properties. Organic - inorganic materials can be used to modify organic polymer materials or to modify inorganic materials. The composites exhibit very different properties from their original components. Thus, the materials built from them can be multifunctional. Composites are one of the most important classes of engineered materials, as they offer several outstanding properties as compared to conventional materials. These materials have found increasingly wider applications in the general areas of chemistry, physics, nanotechnology, material science and engineering.

The most convincing examples of such composites are naturally occurring materials such as bone, which is a hierarchical nanocomposite built from ceramic nanoparticles and organic materials. The organic—inorganic nanocomposite materials are widely used in photovoltaics. The finite supply of traditional fossil fuels (oil, natural gas, coal, etc.) underscores the urgency of searching for alternative energy sources. Nowadays the most important role is attributed to solar energetics. Photovoltaics are important solar technology which produces electricity from solar radiation using solar cells encapsulated in panels [1]. Photovoltaic devices are based on the concept of charge separation at an interface of two materials of different conduction mechanism.

Dye-Sensitized Solar Cells (DSSC) is among the most promising solar energy conversion devices of new generation. The dye-sensitized solar cell (DSSC) appears to have significant potential as a low-cost alternative to conventional p-n junction solar cells. A DSSC consists of a nanocrystalline, mesoporous network of a wide band gap semiconductor (usually TiO_2), which is covered with a monolayer of dye molecules (usually a Ru dye) [2]. DSSC are based on the sensitization to visible light of mesoporous, nanocrystalline metal oxide films achieved by means of the adsorption of molecular dyes.

However, the approach to the fabrication of organic and inorganic composition deposits has technological problems. Frequently people use drop casting, spin-coating and vapor phase deposition. Each method has certain disadvantages and technological problems. In our research, electrodeposition method was used. Compared with other methods, electrodeposition can overcome most of the drawbacks. The major challenge is to electrodeposit composite materials, which, in most cases, are electrically neutral. Another challenge is to avoid particle agglomeration during the deposition of polymer and metal oxide particle composites. The possibility to obtain the suspension, containing well dispersed and charged particles of different materials is important for the electrodeposition process [3].

The subject of this research thus involves the development electrodeposition methods for the fabrication of composite coating and development of advanced dispersing and charging agents with strong interfacial adhesion and pH—dependent charge.

2 Literature Review

2.1 Electrophoretic Deposition (EPD)

Electrodeposition is a promising technology. Generally, electrodeposition is defined as the deposition of a substance on an electode by the action of electricity, especially by electrolysis [4, 5]. Electrodeposition was invented by the Indian scientist G. M. Bose during the 1740s in a liquid-siphon experiment. In 1807, the Russian Reuss first observed the electric-field-induced motion of solid particles (clay) in water [6]. However, electrodeposition indeed took off with the development of effective electrolytes for silver and gold deposition in the 1840s. These have been the basis of an extraordinarily successful decorative plating industry. But the electrolytes were extremely poisonous, as they incorporated cyanide, and the search for safer, better substitutes continues [7, 8].

Electrodeposition of organic and inorganic materials can be achieved by cathodic or anodic methods. Two processes are commonly used to prepare organic and inorganic coatings: the electrophoretic process (EPD) which is based on the use of suspensions of ceramic particles or polyelectrolytes and the electrolytic process (ELD) which starts from solutions of metal salts. The range of thickness of coating deposited by these techniques is shown in Figure 2-1 [5]. EPD enables the formation of thick films, whereas ELD is an important tool for the preparation of nanostructured thin films.

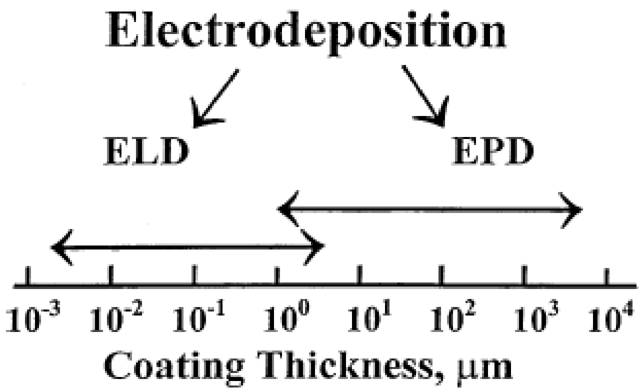

Figure 2-1 Thickness of coatings deposited using EPD and ELD [5]

EPD is an electrochemical method attracting increasing interest as a material processing technique. EPD is widely used for coating application, but there was also new and advanced applications using different templates, which can be used for the fabrication of photonic crystals, nanowires, composite materials, fiber reinforced materials. EPD is a combination of two processes: electrophoresis and deposition. Electrophoresis is the motion of charged particles in a suspension under the influence of an electric field. In a second step the particles accumulate at the electrode surface and create a relatively compact and homogeneous film. The EPD process is schematically shown in Figure 2-2 [6]. It is important to note, that electrode reactions are not involved in the EPD [3]. A post-EPD processing step is always necessary, which includes a proper heat-treatment (firing or sintering) in order to further densify the deposits to eliminate porosity. The interest in EPD is not only based on its high versatility to be used with different materials and combinations of materials but also EPD provides a lot of advantages for surface modification over other techniques:

- Uniform coating

- Applicable to substrates of complex shape
- Relatively high deposition rate
- High purity of deposited materials
- Wide range of materials (metals, polymers, ceramics, etc.)
- Precise control of the composition and microstructure of deposit
- Low cost of equipment and materials

All these properties contribute to a significant interest in the application of EPD techniques for the fabrication of films and coatings for organic and inorganic nanomaterials.

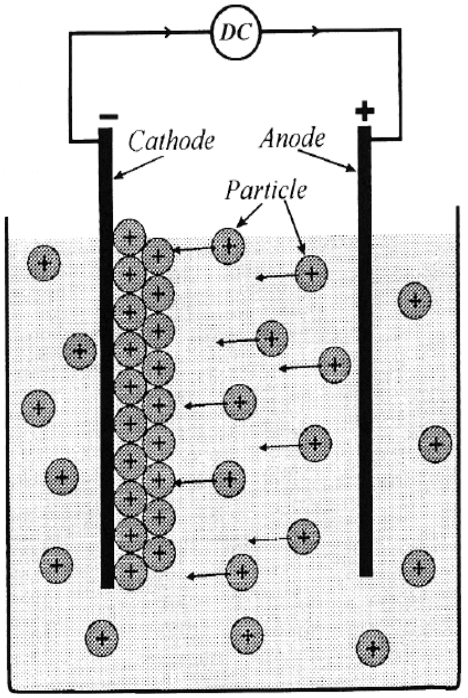

Figure 2-2 Schematic drawing of electrophoretic deposition (EPD) cell showing the process [6]

In several experiments, EPD of ceramic particles was performed in the presence of electrolytes and polyelectrolytes. Presently, various electrochemical methods are under development, which are based on the EPD of polyelectrolytes, polymer–metal ion complexes and inorganic particles. The properties, composition, nanostructure, and morphology of the composite films can be tailored according to specific requirements for various applications. This can be obtained by variation of bath composition, deposition parameters such as deposition time and voltage, and mass transport conditions for organic and inorganic materials [4].

2.2 The DLVO theory

Dejaguin and Landau and Verwey and Overbeek developed a theory to explain the relationship between stability of a colloid suspension and energies of interactions between colloidal particles and other surfaces in a liquid [9, 10], which is now known as a classic DLVO theory. The fundamental mechanisms of EPD have been largely depicted in the literature primarily in the framework of the DLVO theory. In terms of this theory, the stability of a colloidal system is dependent upon the total pair interaction between colloidal particles, which is the combination of two parts, coulombic double-layer repulsion and Van der Waals' attraction.

There are some critical assumptions in the DLVO theory [11]:

1) Infinite flat solid surface,
2) Uniform surface charge density,
3) No redistribution of surface charge,
4) No change of concentration profiles of both counter ions and surface charge determining ions,
5) Solvent exerts influences via the dielectric constant only.

The DLVO considers two particles dispersed in a suspension. This theory successfully describes the interactions between two approaching particles and thus is widely accepted.

The total energy V_T of interaction of two isolated, identically charged particles is defined as [5]:

$$V_T = V_A + V_R \tag{2-1}$$

The Van der Waals' attraction (V_A) between two spherical particles can be expressed by [11]:

$$V_A = -\frac{A}{6}\left(\frac{2}{s^2-4} + \frac{2}{s^2} + \ln\frac{s^2-4}{s^2}\right) \tag{2-2}$$

where A is the Hamaker constant and s = 2 + D/r, with D the shortest distance between the two spheres and r the particle radius. If D << r, Equation (2-2) can be simplified to:

$$V_A = -A\frac{r}{12D} \tag{2-3}$$

The coulombic double-layer repulsion (V_R) can be expressed by [5]:

$$V_R = 2\pi\varepsilon\varepsilon_0 r\psi^2 \ln[1+e^{-\kappa D}] \tag{2-4}$$

where ε is the dielectric constant of the solvent, ε_0 is the vacuum dielectric permittivity, ψ is the surface potential, 1/κ is the Debye length, which is [5]:

$$\kappa = \sqrt{\left(\frac{{e_0}^2\sum n_i z_i^2}{\varepsilon\varepsilon_0 kT}\right)} \tag{2-5}$$

where e_0 is the electron charge, k is the Boltzmann constant, T is the absolute temperature, n_i is the concentration of ions with valence z_i. Repulsion between colloidal particles is directly related to the diffuse double layer charge on the particles.

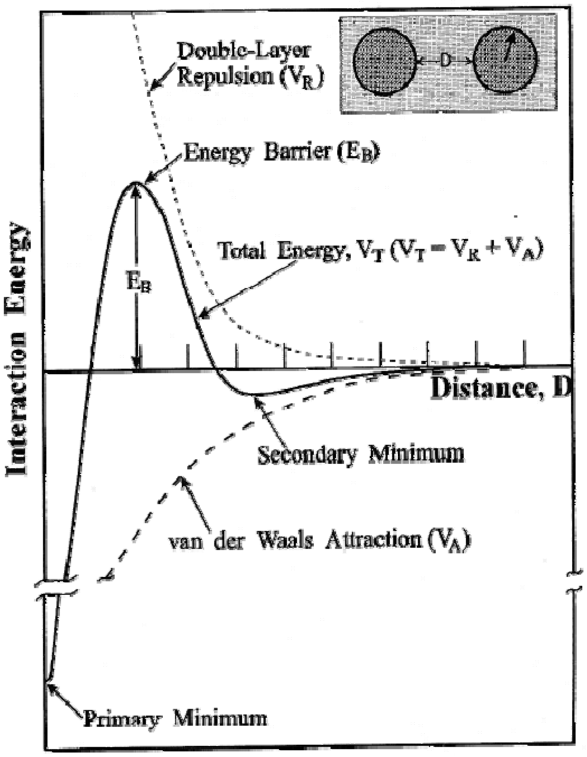

Figure 2-3 Schematic of the interaction energy as a function of separation between two particles in suspension [6]

A schematic plot of V_R, V_A with D is shown in Figure 2-3 [6]. It shows the Van der Waals attraction energy, coulombic double-layer repulsion energy, and the resultant total energy as a function of distance from the surface of a spherical particle. The DLVO theory explains the potential energy curve for the interaction. A peak of height E_B is located slightly away from the surface, as the coulombic double-layer repulsion energy dominates the Van der Waals attraction energy. The peak is known as the energy barrier and this is the energy barrier to particle coagulation [11]. If the particles are closer than the energy barrier (E_B) the adhesion of particles is irreversible. Since the coulombic double-layer repulsion energy is determined by the concentration and valence state of electrolyte ions as shown in Equations (2-4) and (2-5) and the Van der Waals attraction energy is almost independent on the concentration and valence state of electrolyte ions, the total energy is strongly influenced by the concentration and valence state of counter-ions.

The thickness of the double layer is characterized by the Debye length, 1/κ. It is sensitive to the electrolyte concentration. According to the DLVO theory, there is a critical electrolyte concentration (flocculation value) for coagulation, which reduce with the valence state of the electrolyte ions of a charge opposite to that of the colloidal particles (rule of Schulze and Hardey) [10]. It was illustrated that the energy barrier reduces as the electrolyte concentration increases. As the potential energy peak vanishes, coagulation happens as shown in Figure 2-4 [5].

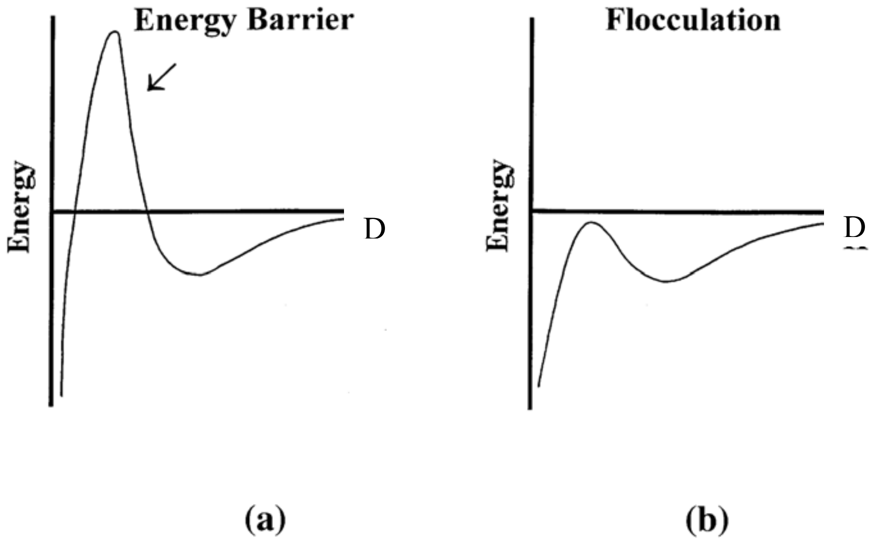

Figure 2-4 Total interaction energy between spherical particles as a function of interparticle separation at (a) low and (b) high electrolyte concentrations [5]

Flocculation by ions compressing the thickness of double layer also obeys the Hofmeister series [10]. So at the same valence, compared to small cations, a negatively charged sol is flocculated by large cations at a smaller concentration [5]. Besides, the flocculation can also be influenced by many factors such as the sol concentration, temperature, particle size of the colloid, and chemical nature of the sol.

2.3 Other interparticle forces

According to the DLVO theory, no other force is present besides van der Vaals and electrostatic interactions. Various aspects of the accuracy of the DLVO theory have been discussed in the literature. It should be noticed that besides these two forces, other physical interactions also exist.

For isolated pairs of particles, the DLVO theory is valid. But, in a system containing many particles, the attractive ion correlation force could be prominently high to induce aggregation and flocculation of colloidal particles. The Sogami-Ise theory illustrates that coulombic attraction exists between highly charged colloidal particles [12, 13].

Recent studies showed that geometrical confinement can cause a significant effect on the interaction between particles such as long-range attractions, which are not considered in the DLVO theory [14]. Other forces like electrohydrodynamic flows-induced interaction, polarization interaction and capillary interactions can also exist between the particles [15-17].

2.4 Other deposition theories

Although the DLVO theory is the fundamental mechanisms of EPD, additional theoretical studies are in progress in order to understand the deposition process and interactions between solvent and particles in an electric field.

2.4.1 Particle charge neutralization mechanism

One mechanism suggests that charged particles are involved in reactions near the electrode that decrease the surface charge of the particles and neutralize them. It is believed that a difference in pH of the electrodes and bulk suspension plays an important role in this process.

In aqueous solutions, the primary electrochemical process is the decomposition of water, which is shown by the following two electrode reactions:

$$\text{Anode: } 2H_2O \rightarrow O_2 + 4H^+ + 4e^- \qquad (2\text{-}6)$$

$$\text{Cathode: } 4H_2O \rightarrow 4OH^- + 2H_2 \qquad (2\text{-}7)$$

In anodic EPD process, the hydrogen ions (protons) which are electrogenerated by the reaction (2-6) react with the negatively charged colloidal particles near the anodic electrode and neutralize. Then the neutralized particles produce deposits at the anodic electrode. On the contrary, in the cathodic EPD process, the positively charged particles are neutralized by the base caused by the reaction (2-7) and form cathodic deposits at the electrode.

This mechanism describes the deposition of powders charged by the addition of salts to the suspension and the deposition of single particles and monolayers. Whereas, it could not explain deposition of thick layers achieved for longer times, or for processes in which the particle-electrode contact is not allowed [18].

2.4.2 Flocculation by particle accumulation

Through the observation and comparison between the formation of deposits by electrophoresis and gravitation, Hamaker and Verwey found the similarities between these two processes [19, 20]. Actually, in both processes, the pressure applied to the arriving particles dominates the interparticle repulsion. Hence, the principal function of the applied electric field in EPD is to force the particles moving towards the electrode to accumulate [18]. This mechanism can also apply to the deposits onto membranes that are not working as electrodes.

2.4.3 Electrochemical particle coagulation mechanism

Through the calculation of the rising of the ionic strength at the electrode when electric potential was exerted, Koelmans proposed a theory that a decrease of the repulsion between the particles close to the electrode (lower ζ-potential) results from an increase of the electrolyte concentration and as a consequence, the particles coagulate [21]. He found the fact that the value of ionic strength at the electrode surface was sufficient for flocculating a suspension. Given that a finite time is required to increase the electrolyte concentration close to the electrode, we can assume that a period of time is needed for getting deposition, and this time is inversely proportional to the square of the applied voltage [18].

2.4.4 Electrical double layer (EDL) distortion and thinning mechanism

Sarkar and Nicholson presented a theory that is based on the distort of the particle double layer [6, 22]. This theory is supposed to interpret the invalidation of the electrochemical particle coagulation mechanism when there is no raise in electrolyte concentration close to the electrode. Sarkar and Nicholson found that the double layer is distorted when a positive particle and its shell are moving towards the cathodic electrode, as shown in Figure 2-5 [18]. Consequently, the anions around the tail experience a smaller coulombic attraction to the positive particles and are able to more easily react with other positively charged particles close to the cathodic electrode and as a result the thickness of the double layer decreases. So when two particles with a thin double layer are close enough, the interaction through Van der Waal attractive forces and coagulation could happen.

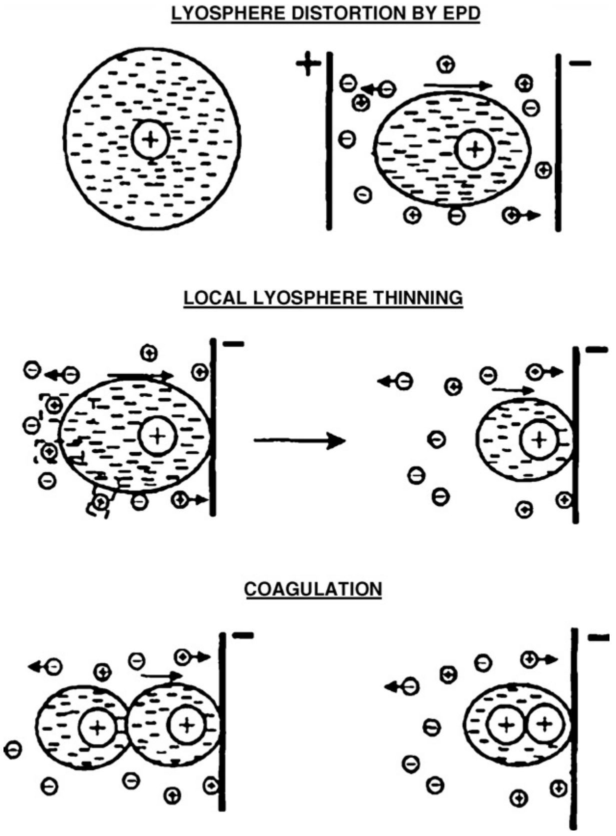

LYOSPHERE DISTORTION BY EPD

LOCAL LYOSPHERE THINNING

COAGULATION

Figure 2-5 Schematic representation of the deposition mechanism due to electrical double layer distortion and thinning [18]

This mechanism is valid for a high concentration of particles near the electrode and for incoming particles with thin double layer coagulating with particles already in the deposit [18].

2.5 Suspension stability and particle charging

2.5.1 Double layer and zeta potential

A suspension for EPD is a complex system, in which each component has a certain effect on deposition efficiency. It is critical to gain well dispersed and stable suspensions.

The charged particles in a suspension are forced to move toward an electrode under the influence of an applied electric field. This process is called electrophoresis. Very often charged particles in a suspension are covered by counter ions, and the concentration of counter ions around the particles is much higher near the surface of the particles and decreases as the distance from the surface increases. Such inhomogeneous distributions of ions close to the particle surface result in the formation of so called double-layer, as shown in Figure 2-6 [11]. The double layer is composed of Stern layer and diffuse double layer or Gouy layer, and these two layer is separated by Helmholtz plane. The electric potential reduces linearly in the Stern layer. However, in diffuse double layer, the counter ions diffuse freely and the potential does not decrease linearly.

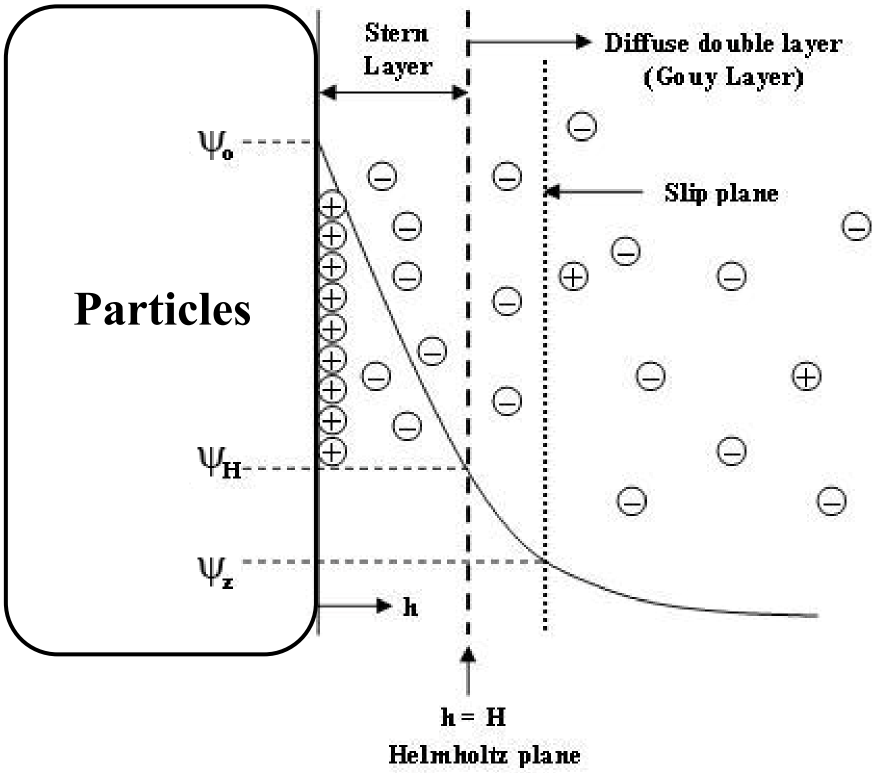

Figure 2-6 Schematic illustrating electrical double layer structure and the electric potential near the solid surface with both Stern and Gouy layers indicated [11]

The motion of these ions and the particle are in opposite directions when an electric field is applied. But, some ions are also attached to the particle, and as a consequence, a fraction of these ions which are surrounding the particle will not move in the opposite direction but move along with the particles. The potential at the surface of shear, the boundary between the electrolyte solution moving with the particle and the electrolyte solution, which does not move with the particle, is called the zeta-potential, ψ_ζ, which is schematically illustrated in Figure 2-7 [23]. Zeta-potential is the principal parameter determining the electrokinetic behaviour of the particle. In principle, a particle with a negative surface charge can show a positive zeta-potential.

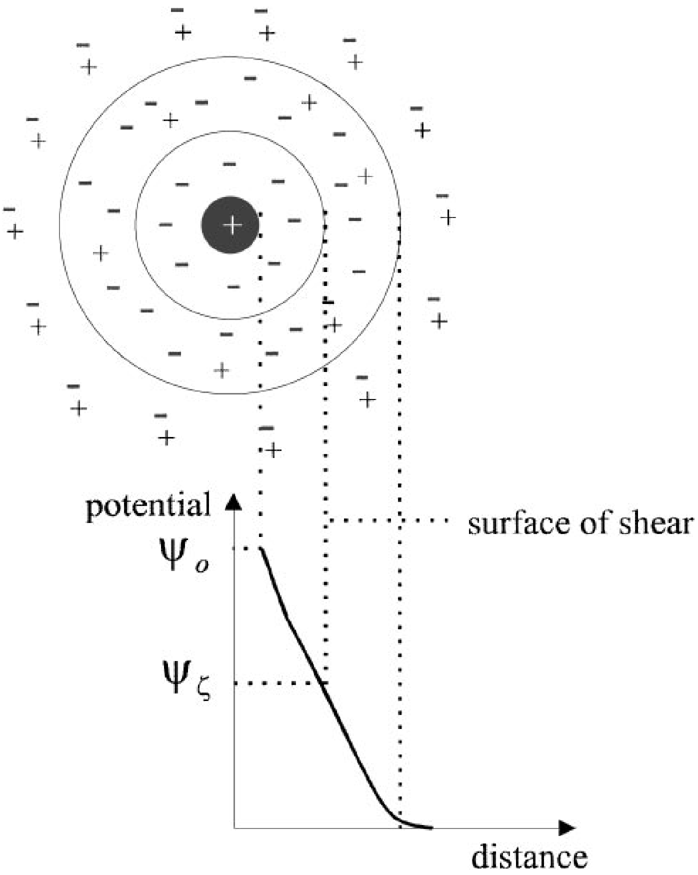

Figure 2-7 Schematic of the double layer surrounding a charged particle and evolution of the electric potential from the surface potential, ψ_0, to zero far from the particle [23]

For aqueous suspensions of ceramic powders, especially oxides, the ζ potential changes with pH value if H^+ and OH^- are potential-determining ions, showing an isoelectric point (IEP), as illustrated in Figure 2-8 [5]. ζ potential is positive at low pH and negative at high pH.

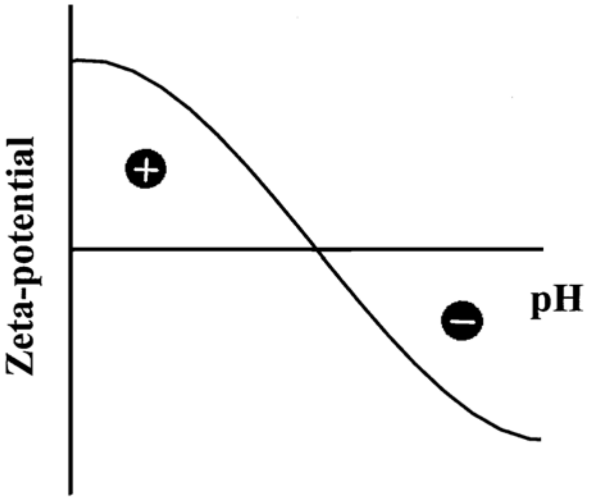

Figure 2-8 Zeta-potential of ceramic particles versus pH of suspension [5]

According to the DLVO theory, ζ potential is important for the stability of colloidal dispersions. The ζ potential indicates the degree of repulsion between adjacent, similarly charged particles in the dispersion. A high ζ potential will confer stability, however when the potential is low, attraction overcomes repulsion and the dispersion will break and flocculate. So, colloids with high ζ potential are electrically stabilized while colloids with low ζ potentials incline to coagulate or flocculate.

2.5.2 Influence of solvents on particle charging

In aqueous suspension, the charge at the particle—solvent interface could result from adsorption or desorption of ions, or dissociation of surface groups. It is known that metal oxide is often fully or partly covered with amphoteric OH groups. Oxide particles show an isoelectric point if H^+ and OH^- are potential-determining ions. Depending on the pH of the solution, they are positively charged at low pH, and negatively charge at high pH:

$$M - OH + H^{+} \Leftrightarrow M - OH_2^{+} \tag{2-8}$$

$$M - OH + OH^{-} \Leftrightarrow M - O^{-} + H_2O \tag{2-9}$$

Particle charging is accomplished by electron transfer between the particle and solvent in non-aqueous media [24]. The charge on a colloidal particle could originate from the solvent. Different solvents will cause different charging method. Alcohols, water, organic acids are viewed as proton donors and are critical for particle charging. A mixture of solvents may also be helpful to accomplish particle charging [25].

Damodaran and Moudgil [26] have suggested a mechanism of particle charging in organic solvents. They proposed that the adsorbed alcohol ionized into a protonated alcohol and an alkoxide ions, and then protonated alcohol dissociate and desorbed into the solution, leaving the proton on the particle surface.

2.5.3 Additives for particle charging

Particle charge could also be achieved by the use of various additives in order to gain well-dispersed and stable suspensions. The addition of acids [27, 28] could disperse the particles and promote the particle charging. But acids would cause corrosion of electrodes. Moreover, the acids can react with powders. It is found that a mixture of acetone, iodine and water is effective for particle charging [29, 30]. Particle charging was carried out by the adsorption of protons. The charging of ceramic particles could be accomplished by the adsorption of inorganic cations such as Mg^{2+}, Ca^{2+}, Ti^{4+}, etc [31].

Polymeric stabilization, also known as steric stabilization, is widely adopted in stabilization of colloidal dispersions. Polymeric stabilization is superior to electrostatic stabilization mechanism in the synthesis of nanoparticles, especially when narrow size distribution is required. Organic macromolecules could be used to produce steric stabilization, in which the macromolecules are adsorbed on the particle surface. It is effective for steric stabilization in both aqueous and non-aqueous suspension.

As a widely used additive, polyelectrolytes can offer steric and electrostatic stabilization to a colloidal dispersion. Moreover, polyelectrolytes are utilized for particle charging. Polyelectrolytes are macromolecules that contain charged functional groups, which can be divided into two categories: strong and weak polyelectrolytes. For strong polyelectrolytes, like poly(diallyldimethylammonium chloride) (PDDA) [32], the degree of ionization is independent of the solution pH, whereas, the degree of ionization of weak polyelectrolytes, highly relies on solution pH. Poly(ethylene imine) (PEI), chitosan (CHIT), poly(allylamine hydrochloride) (PAH) are weak polyelectrolytes, which contain amine groups [33, 34]. In addition to PDDA and PEI as additives for particle charging and steric stabilization, it is found that phosphate ester (PE) is an effective electrostatic stabilizer, which charges the particles positively in organic liquids by donating protons to the surface. Besides, PE also works as a steric dispersant by anchoring the long-chain macromolecules to the particles [35, 36]. Via the use of PE, positively charged particles like Y_2O_3 can be prepared and used for cathodic EPD [37].

2.6 Solvent

Solvents can be categorized into aqueous solvent and non-aqueous solvents or organic solvents. Another branch of solvents is protic solvents, which can exchange protons, such as methanol (CH_3OH), ethanol (C_2H_5OH). A third branch is aprotic solvents, which cannot exchange protons, such as benzene (C_6H_6). Some typical protic and aprotic solvents are shown in Table 2-1 [11].

Table 2-1 List of solvents with their dielectric constants [11]

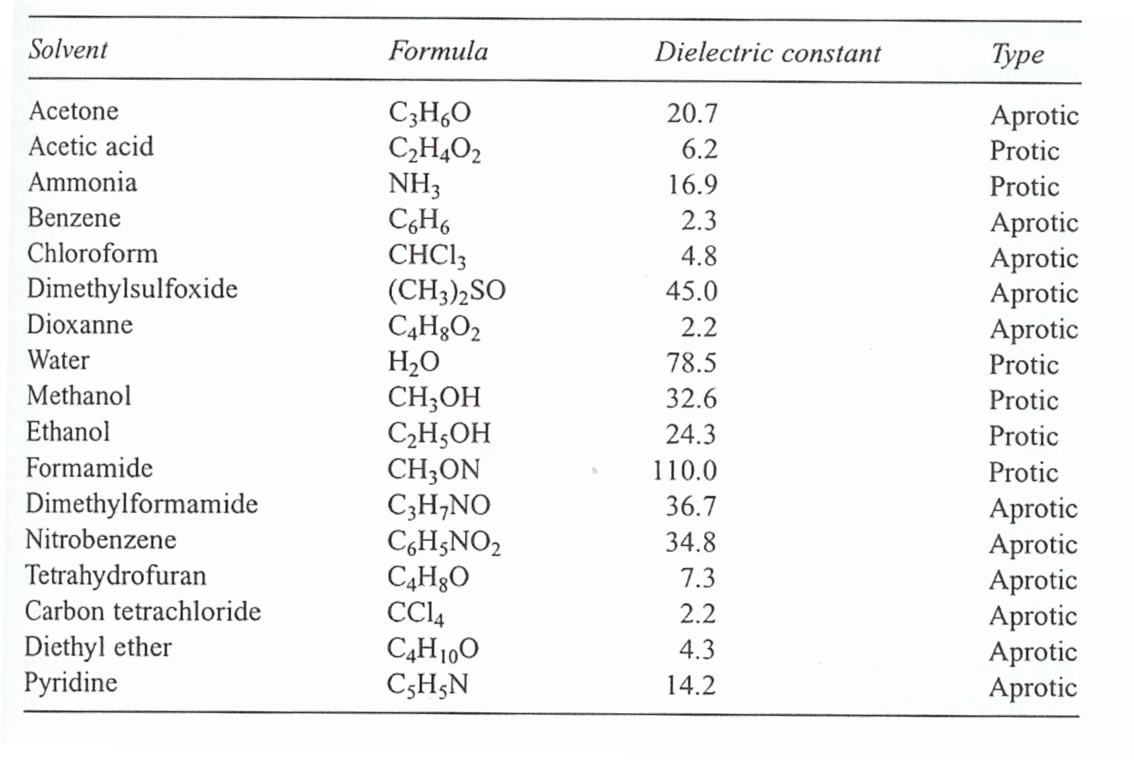

Solvent	*Formula*	*Dielectric constant*	*Type*
Acetone	C_3H_6O	20.7	Aprotic
Acetic acid	$C_2H_4O_2$	6.2	Protic
Ammonia	NH_3	16.9	Protic
Benzene	C_6H_6	2.3	Aprotic
Chloroform	$CHCl_3$	4.8	Aprotic
Dimethylsulfoxide	$(CH_3)_2SO$	45.0	Aprotic
Dioxanne	$C_4H_8O_2$	2.2	Aprotic
Water	H_2O	78.5	Protic
Methanol	CH_3OH	32.6	Protic
Ethanol	C_2H_5OH	24.3	Protic
Formamide	CH_3ON	110.0	Protic
Dimethylformamide	C_3H_7NO	36.7	Aprotic
Nitrobenzene	$C_6H_5NO_2$	34.8	Aprotic
Tetrahydrofuran	C_4H_8O	7.3	Aprotic
Carbon tetrachloride	CCl_4	2.2	Aprotic
Diethyl ether	$C_4H_{10}O$	4.3	Aprotic
Pyridine	C_5H_5N	14.2	Aprotic

The selection of a proper solvent is critical for dispersion and particle charging. Solvent works as a vehicle that carries the ceramic particles in suspensions (EPD) or ions in solutions (ELD). The solvent used in electrodeposition should dissolve both inorganic particles and organic additives. Two main types of solvents are usually used in electrodeposition: water and organic solvents.

Compared to water, organic liquids are preferable as a suspension medium for electrophoretic deposition because the generally lower dielectric constant of organic liquids limits the charge on the particles. And as a consequence, it lowers the dissociating power. In organic liquids, the problems related to electrolytic gas evolution and electrochemical attacks of the electrodes, which prevent the deposition of a uniform adherent layer and yield pinholes, could be greatly reduced. It is in this regard that much higher electric field could be applied.

Organic liquid and water mixed solution are often used in the electrolytic deposition such as methyl alcohol-water and ethyl alcohol-water, because non-aqueous solvents could prevent the deposit from hydrating. Mixed solution could reduce cracking and porosity [38]. The addition of alcohols to aqueous solutions could decrease the total dielectric constant of the solvent, and as a result, the solubility of the deposits is reduced. So that the deposition experiments [39] achieved in mixed methyl alcohol-water solutions indicate a significant enhancement of the deposition rate.

2.7 Electrophoretic deposition kinetics

The deposition rate is critical for deposit forming during EPD and control of the thickness of the deposited film. Besides, the rate is also important to achieve functionally gradient materials [40]. Since the EPD was established, the kinetics of electrophoretic deposition has been the subject of numerous investigations. In 1940, during a study of the phenomena of the EPD process, Hamaker observed that deposits weight is proportional to the concentration of the suspension, time of deposition, surface area of the deposit, and electric field. It is in this regards he proposed the following equation [23, 41]:

$$\frac{dY}{dt} = \mu ESC \tag{2-10}$$

where Y is deposition yield (kg), t is deposition time (s), μ is electrophoretic mobility ($m^2 \cdot v^{-1} \cdot s^{-1}$), S is the electrode surface area (m^2), C is solids concentration ($kg \cdot m^{-3}$). This equation, which is known as the Hamaker equation, is now viewed as the fundamental for kinetics of electrophoretic deposition. The proportionality constant is equal to the electrophoretic mobility of the particle when every particle reaching the electrode is deposited.

However, Hamaker equation ignored the change of solid concentration in the suspension during deposition. So in 1994, Zhang proposed a kinetic equation incorporating changes of particle concentration in the suspension [42]. If *dS* is an infinitesimal area of the depositing electrode on which *dw* weight of particles has been deposited in time *dt*, then [6]:

$$\int dw = \int\int fudSC(t)dt = fu\int\int dSC(t)dt \tag{2-11}$$

where u is the average velocity of the particles, *C(t)* the concentration of the particles in the suspension, and f is the efficiency factor taking into account that not all powder brought to the electrode by electrophoresis is also incorporated in the deposit ($f \leq 1$, if all the particles reaching the electrode take part in the formation of the deposit, then $f=1$).

As for electropheretic mobility, there are two different theories of electrophoresis for rigid particles and for polyelectrolytes [43, 44].

The velocity ν of a particle in an electric field E is defined as:

$$v = \mu E \tag{2-12}$$

with μ, the electrophoretic mobility. The electrophoretic mobility μ of a rigid colloidal particle can be given by the following equation [45]:

$$\mu = \frac{2\varepsilon\varepsilon_0\zeta}{3\eta} f\left(\kappa\alpha\right) \tag{2-13}$$

where η is the viscosity of the liquid. The function f(κα) increases from 1 for κα << 1 to 1.5 κα >> 1. And for particle size that are much smaller than the Debye length, the electrophoretic mobility is described by Huckel equation [5]:

$$\mu = \frac{2\varepsilon\varepsilon_0\zeta}{3\eta} \tag{2-14}$$

On the contrary, when the particles size that are large enough compared with 1/κ, like ceramic particles, the electrophortetic mobility is described by Smoluchowski formula [5]:

$$\mu = \frac{\varepsilon\varepsilon_0\zeta}{\eta} \tag{2-15}$$

Whereas, the electrophoretic mobility of a spherical polyelectrolyte, in which fixed charges are distributed at a uniform density ρ_{fix}, can be given by the following equation [46]:

$$\mu = \frac{\rho_{fix}}{\eta\lambda^2}\left[1+\frac{2}{3}\left(\frac{\lambda}{\kappa}\right)^2\frac{1+\lambda/2\kappa}{1+\lambda/\kappa}\right] \tag{2-16}$$

with $\lambda=(\gamma/\eta)^{0.5}$, and γ, the frictional coefficient of the polyelectrolyte.

Comparing equation (2-13) with equation (2-16), there is a concept of zeta potential, which was developed for rigid particles, and instead of polyelectrolytes, we use charge density.

2.8 Binders

Electrodeposition of sub-micrometer ceramic particles has the advantage of forming uniform ceramic films with dense packing and good sinterability. However, the use of fine particles induces deposit cracking. So in order to gain crack-free and compact deposits, a binder is often added to the suspensions or solutions because binder materials may enhance the effect of the van der Waals' force and as a result, the adherence and strength of the film can be increased. The optimal amount of binder added into the suspension is variable and is determined by the particle size and particle surface area.

Long-chain polymers are the most widely used binders in EPD, besides metal alkoxides and hydroxides have also been used as binders. For non-aqueous EPD, a variety of binders have been utilized, such as alkyd resin [47], dewaxed shellac [48], polyvinyl butyral [49] and so on. It is preferable to apply the binders, which also work as a dispersing agent. Many studies show that various dispersant aids with a natural binding effect. However, compared with non-aqueous suspension, the use of water-soluble binders is limited. The low adhesion strength greatly restricts their effect. There are two ways for the fabrication of polymer deposits. Positively charged ceramic particles offer electrophoretic transport of the polymeric macromolecules, which adsorb onto the surfaces of the ceramic particles, to fabricate film on substrates as shown in Figure 2-9(a). Another way is that cationic polyelectrolytes with natural binding properties, including polyethylenimine (PEI) could be utilized for particle charging and EPD (Figure 2-9(b)) [5].

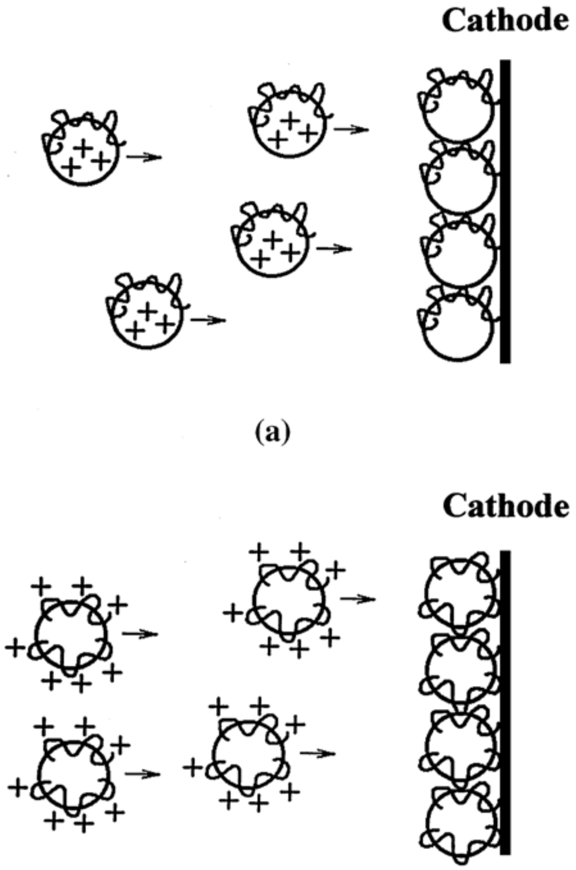

(a)

(b)

Figure 2-9 Cathodic electrophoretic deposition of ceramic particles with adsorbed (a) neutral and (b) charged polymers [5]

One important finding was the possibility of electrochemical intercalation of charged polyelectrolytes into electrolytic deposits. Through cationic polyelectrolytes with natural binding properties, problems related to cracking in electrolytic deposits could be reduced. Moreover, various organoceramic nanocomposites could be formed through electrodeposition. The intercalation of polymers is achieved by their adsorption on the surface of colloidal particles, which are produced near the cathode and form a cathodic deposit.

Binder plays a multifunctional role in the EPD processing. Polymer binders are applied to achieve adherent deposits and prevent cracks. What's more, the adsorbed polymer can offer steric stabilization of suspension of ceramic particles and reduce viscosity of the suspension [50]. In EPD process, charged ceramic particles carry adsorbed polymers to the electrode surface, allowing the polymer binders to be included in the deposits.

2.9 Codeposition of organic-inorganic composite coatings by EPD

More and more researches have focused on the organic-inorganic composite materials because of the feasibility of combining the properties of organic and inorganic materials. The so-called codeposition means the fabrication of nanocomposite films containing inorganic nanoparticles in a polyelectrolyte matrix, which is usually based on self-assembly [51, 52]. Sequential adsorption of polyelectrolytes and oppositely charged inorganic nanoparticles is critical for this method. Moreover, codeposition of organic and inorganic materials provides the critical advantage of room temperature processing of the nanocomposite materials so that the problems such as shrinkage and cracks, caused by the sintering process can be avoided. In addition to layer-by-layer fabrication of polyelectrolyte multilayers and polyelectrolyte capsules, EPD is a promising approach for fabricating composite films. A variety of researches are focusing on electrochemical strategies, including EPD of polyelectrolytes or polymer-metal ion complexes and the EPD or electrosynthesis of inorganic particles. Different electrochemical strategies were developed in order to decrease the electrostatic repulsion of the polyelectrolyte at the electrode and accomplish codeposition of ceramic particles and polyelectrolytes [4]. It is a promising strategy to use polyelectrolytes for EPD to fabricate advanced organic-inorganic nanocomposites.

In addition to polyelectrolytes, polymer-metal ion complexes provide another approach to form composites. Polymer-metal complexes consist of a polymer ligand and metal ions in which the metal ions are attached to the polymer ligand by a coordinate bond [4]. It is found that a polymer chelate is formed when metal ions are added to the solutions of polymers, such as PEI. The use of polyelectrolytes and polymer-metal ion complexes paves the way for forming advanced nanocomposites by a combined method based on EPD and electrosynthesis of inorganic particles.

2.9.1 EPD of strong polyelectrolytes and electrosynthesis of inorganic particles

The deposition of the composite film depends on the specific behavior and interactions of polyelectrolytes and inorganic nanoparticles at the electrode surface. Electrophoresis needs stable and well dispersed suspensions. However, the particles must coagulate at the electrode surface to form a film [32].

The charge compensation mechanism is proposed for the fabrication of organic-inorganic nanocomposites containing poly(diallyldimethylammonium chloride) (PDDA) [50]. This method is based on the EPD of PDDA and cathodic electrosynthesis of metal oxides and hydroxides. PDDA is positively charged in both acidic bulk solutions and basic solutions at the cathode surface. Investigations failed to achieve pure PDDA deposits because of the strong electrostatic repulsion of PDDA, but codeposition of PDDA and the ceramic particles was successfully achieved [53]. It was found that the formation of the deposit is a result of Coulombic attraction between two oppositely charged species: positively charged PDDA and negatively charged ceramic particles which are formed at the electrode surface [32]. But further researches indicated that codeposition of PDDA macromolecular and inorganic nanoparticles is governed not only by Coulombic attraction but also by hydrogen bonding and ion-dipole interactions. These interactions are important for deposits formation and microstructure of the deposit. It was reported that PDDA could be successfully codeposited with low isoelectric point inorganic particles such as oxides or hydroxides of Zr and Ce [54, 55] and high isoelectric point inorganic particles including hydroxides of Ni and Co [56, 57]. This combined method is an important technique for the manufacture of fuel cells and advanced coatings.

This method allowed the electrosynthesis of nanoparticles in-situ in a PDDA matrix, which could prevent particle agglomeration. It was proved that the properties of the complex materials can be varied by the variation of PDDA concentration in suspension. The codeposition of PDDA and ceramic particles is critical for the fabrication of thick oxide films by EPD. The PDDA also works as a binder, encouraging better adhesion of the deposits and preventing cracking. In addition, the negatively charged inorganic nanoparticles can be compensated by the positively charged PDDA. Recent studies indicated the feasibility to obtain thick ceramic coatings by small PDDA additives as a binder.

2.9.2 EPD of weak polyelectrolytes and electrosynthesis of inorganic particles

It is critical to prevent the nanoparticles to aggregate and maintain them well-dispersed. In order to achieve that, it is found that nanoparticles could be formed by electrosynthesis in situ in a polymer matrix of cationic polyelectrolytes or polymer-metal ion complexes. The high pH at the cathode, caused by the electrolysis of water, resulted in the formation of colloidal particles, which coagulated on the electrode. The charge of weak polyelectrolytes like poly(ethylene imine) (PEI) reduced with the increasing pH. As a result, the pH increased at the cathode surface, resulting in a decreasing charge and deposition of weak polyelectrolytes. In addition, composite films can be obtained when combining electrosynthesis of inorganic particles with EPD of polyelectrolytes.

Composite deposits containing nanoparticles of Fe, Co, Ni, Mn, Ce, Zr oxides or hydroxides in a PEI matrix were reported in many investigations [53, 56, 58, 59]. The EPD of PEI-Mn complex has been used for the deposition of nanocomposites with Mn_3O_4 particles [58]. This method provides advantages for the manufacture of electrode materials for supercapacitors.

The deposition mechanism is widely studied. It is proposed that PEI acquires a positive charge because of complex formation with metal ions including Ni^{2+}, Co^{2+} and Mn^{2+}. Then, electric field provides the electrophoretic motion of the polymer-metal ion complexes to the electrode. These polymer-metal ion complexes participate in cathodic reactions to form nanoparticles of metal oxides. In addition, those free metal ions, which are not captured by PEI, are also in solutions and contribute the electrosynthesis of the inorganic species.

A variety of studies were concentrated on the manufacture of composites containing poly(allylamine hydrochloride) (PAH) [60]. The method is based on the EPD of cationic PAH and electrosynthesis of ceramic particles. The recent discovery of the room temperature crystallization of complex metal oxides under the influence of PAH encourages the interests in the electrosynthesis of ceramic particles in a PAH matrix [61]. The EPD method allowed the formation of superparamagnetic films containing iron oxide particles in a PAH matrix [60]. The studies showed that the composition of the coatings can be varied by the variation of the polymer concentration in the solutions [62].

2.9.3 EPD of weak polyelectrolytes and EPD of inorganic particles

Both polyelectrolytes and inorganic nanoparticles can be electrophoretically deposited to form composite materials. The manipulation of the pH value of the suspension offers a possibility to control the charge and solubility of the polymers. As a weak polyelectrolyte, CHIT could be cathodically deposited because of its pH-responsible charge and solubility properties [63, 64]. CHIT is soluble when it is protonated. And when neutralized by the electrogeneraged base, CHIT can be deposited at the cathode to form a film:

$$\mathrm{CHIT}-\mathrm{H}^{+}+\mathrm{OH}^{-}\rightarrow \mathrm{CHIT}+\mathrm{H}_2\mathrm{O} \tag{2-17}$$

Several studies were concentrated on the electrophoretic codeposition of CHIT and nanoparticles. It was demonstrated that CHIT promotes the EPD of the latex nanoparticles, which were uniformly distributed in the CHIT film [65].

In some other studies, Gorelikov and Kumacheva found a possibility of the manufacture of composite coatings based on poly(vinyl acetate-co-crotonic acid) (PVAC) and nanoparticles of semiconductors such as CdS and CdTe [66]. However, Hasegawa et al. have concentrated on the use of PEI for the surface charging of silica nanoparticles and deposition of composites by EPD [67].

Recently the manufacture of CHIT-hydroxyapatite (HA) composite coating via EPD has been proved [68]. It was illustrated that obtained composite films provided corrosion protection of metals in the simulated body fluid solutions. This method provides the advantages of room temperature fabrication of the composite coatings. So that, the problems related to the sintering of electrophoretic HA deposits could be avoided.

2.10 Investigation of biomimetic adhesion

Adhesion is important for chemical modification of bulk material surfaces in modern chemical, biological, and materials sciences [69, 70]. A variety of methods have been widely researched for the functional modification of material surfaces such as self-assembled monolayer (SAM) formation, functionalized silanes, Langmuir-Blodgett deposition, layer-by-layer assembly and etc. The methods still have limitations for widely practical use.

Figure 2-10 Photograph of mussels attached to a rock surface

Recently, a newly developed surface modification method has published in Science by Phillip Messersmith and colleagues, which is inspired by the adhesive proteins secreted by mussels for attachment to wet surfaces (Figure 2-10) [71]. Mussels could attach to almost all types of organic and inorganic surfaces [72]. As a result of their wave-swept habits, mussels have perfected the art of adhering quickly, opportunistically and tenaciously to all manner of wet and slippery surfaces. In addition to the modification of a wide variety of materials, the resultant surface can react further, and therefore the extent for applications widens remarkably. According to the investigation of footprints of mussels on smooth substrates, researchers have found an unusual group of proteins, including Mytilus foot protein 5 (Mfp-5), of which 30% of the residues in the sequence are 3,4-dihydroxyphenyl-L-alanine (DOPA), a compound which contains catechol, and 15% are lysine, an amino acid with a side-chain ending in a primary amine group [73]. Clues to mussels' adhesion probably originate in DOPA (Figure 2-11(a)). DOPA not only participates in reactions causing bulk solidification of the adhesive, but also forms strong covalent and noncovalent interactions with substrates [74, 75]. DOPA and other catechol family compounds work as binder for adhesive inorganic surfaces, including the electropolymerization of dopamine onto conducting electrodes [76].

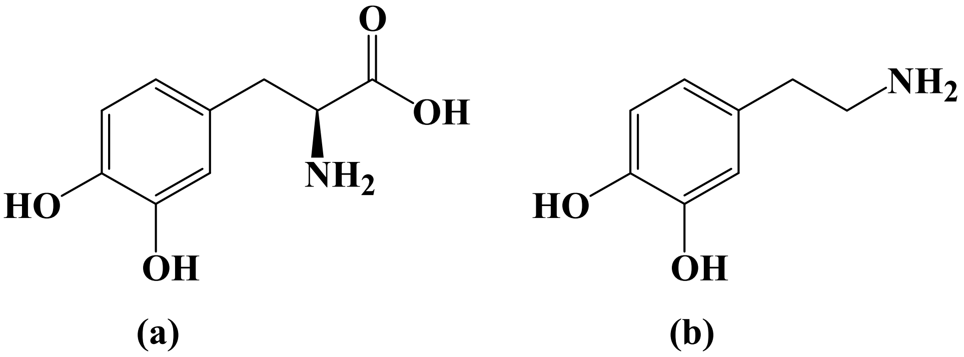

Figure 2-11 Chemical structure for DOPA (a), Dopamine (b)

Hypothesizing that the co-existence of catechol (DOPA) and amine (lysine) groups may be important for accomplishing adhesion to a variety of materials, Messersmith and colleagues combined these two compounds in their use of dopamine, which is a catecholic family (1,2-dihydroxybenzene) compound with a primary amine functional group (Figure 2-11(b)), as an alternative to natural adhesive [71]. According to Messersmith and colleagues' research, this simple structural mimic of Mfp-5 is a powerful building block for spontaneous deposition of thin polymer coatings on most bulk material surfaces and that the deposits are easily adapted for a further functional use [71]. This polydopamine coating could be formed on almost all types of material surfaces: noble metals (Au, Ag, Pt and Pd), metals with native oxide surfaces (Cu, stainless steel and NiTi shape-memory alloy), oxides (TiO_2, non-crystalline SiO_2, crystalline SiO_2 (quartz), Al_2O_3 and Nb_2O_5), semiconductors (GaAs and Si_3N_4), ceramics (glass and hydroxyapatite) and synthetic polymers (polystyrene, polyethylene, polycarbonate, polyethyleneterephthalate, polydimethylsiloxane, polyetheretherketone and polyurethanes) (Figure 2-12) [71].

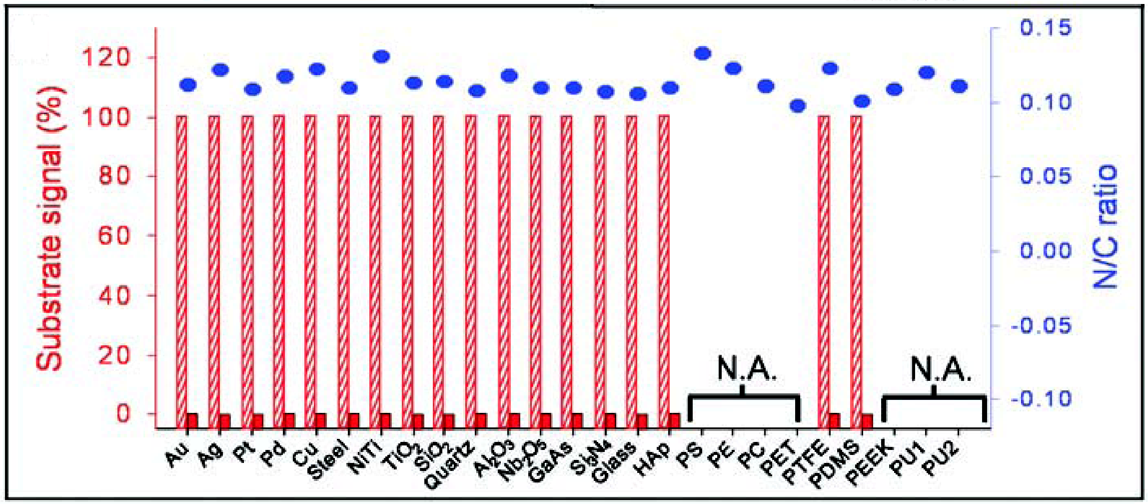

Figure 2-12 XPS characterization of 25 different polydopamine coated surfaces. The bar graph represents the intensity of characteristic substrate signal before (hatched) and after (solid) coating by polydopamine. The intensity of the unmodified substrate signal is in each case normalilzed to 100%. Substrates with characteristic XPS signals indistinguishable from the polydopamine signal are marked by "N.A.". The blue circles represent the N/C after polydopamine coating.

In addition, the polydopamine film is also an excellent stage for further reactions, which could result in tailoring of the films for different functional purposes. For instance, the metal-binding ability of catechols present in the polydopamine film was applied to deposit adherent and uniform metal coatings onto substrates [77]. Additionally, polydopamine films also support various reactions with organic agents for the application of functional organic ad-layers.

2.10.1 Properties improvement after adsorption

Adsorption at inorganic nanoparticle surfaces is a critical aspect of a variety of technological processes such as photosensitisation of semiconductors, catalysis, photodegradation of pollutants and so on [78]. Messersmith and coworkers [79] established the first example of using a catecholic monomer for surface-initiated polymerization on metal surfaces to fabricate antifouling polymer coatings.

Inspired by adhesive proteins secreted by mussels, a new bi-functional initiator was created, which adsorbs to stainless steel and titanium substrates, offering an anchor for surface immobilization of polymers. Catechols such as dopamine were used to attach to a large variety of inorganic surfaces. This biomimetic anchoring strategy is anticipated to be a highly flexible method for polymer thin film surface modification for biomedical and other applications.

Xu et al. [80] proposed a general method that used a stable anchor such as dopamine to attach functional molecules on the surface of iron oxide nanostructures. They described a simple method that is based on the use of dopamine as a strong anchor to immobilize functional molecules on the surfaces of magnetic nanoparticles such as Fe_2O_3. The use of nitrilotriacetic acid as the functional molecule for protein separation demonstrates the robustness and specificity of nanostructures created by this method. Since the increasing usage of iron oxide nanoparticles for biomedical applications, the easy connecting other biomolecules to iron oxide surfaces through a versatile anchor, such as dopamine, is expected to result in valuable applications of magnetic nanostructures in different applications including cell biology, biotechnology, and environment monitoring. Xie et al. [81] showed that iron oxide nanoparticles functionalized with dopamine linked to human serum albumin were highly efficient in labeling various types of cell lines.

TiO_2 nanoparticles have attracted extensive attention as a photocatalyst in a variety of practical applications [82] as well as part of photoeletrochemical systems [83].

Although TiO_2 is very effective from an energetic point of view, it is relatively inefficient as a photocatalyst when compared to optimized photochemical systems. Also, the use of TiO_2 for photocatalytic applications driven by solar light is limited because it has a wide band gap and thus absorbs less than 5% of the available photons of the solar spectrum. Therefore, the main attention of research for the application of semiconductor-assisted photocatalysis is to develop the separation of charges and the TiO_2 response in the visible spectral regions. Recently Ivana, Zoran et al. have reported a new route for improving the optical response of TiO_2 nanoparticles in the visible spectral region. They described surface modification of TiO_2 nanoparticles with benzene derivatives (catechol, pyrogallol and gallic acid), which was found to change optical properties of TiO_2 nanoparticles. The formation of the inner-sphere charge-transfer complexes causes a red shift of the semiconductor absorption compared to unmodified TiO_2 nanoparticles, noteworthy change in the onset of absorption and the effective band gap. They found that all investigated ligands (catechol, pyrogallol and gallic acid) are able to adjust the coordination geometry of the surface Ti atoms inducing shift of the absorption onset toward the visible region of the spectrum, compared to unmodified nanoparticles. It was reported that benzene derivatives (mainly catechol and salicylic acid) [84], which bind to Ti atoms simultaneously adjusts their coordination to octahedral geometry at the surface of nanoparticles and alter the electronic properties of TiO_2. As a consequence, absorption of light by the charge–transfer complex yields to the excitation of electrons from the chelating ligand directly into the conduction band of TiO_2 nanoparticles. This results in a red shift of the semiconductor absorption and enables competent collecting of solar photons [85].

3 Objectives

- Development of electrophoretic deposition methods for the fabrication of organic-inorganic composite films
- Development of advanced dispersing and charging agents with strong interfacial adhesion and pH-dependent charge
- Investigation of adsorption mechanism, deposition mechanism, kinetics of deposition
- Investigation of microstructure, composition and properties of the composite films

4 Experimental Procedures

4.1 Materials

4.1.1 Materials purchased from commercial suppliers

The materials listed in the following Table 4-1 were purchased from industrial suppliers and were used for the fabrication of coatings by EPD.

Table 4-1 Materials purchased from commercial suppliers

Material	Supplier	Purity and Other Specification
Titanium dioxide	Degussa	Anatase: rutile = 4:1, <25nm
Titanium dioxide	Sigma-Aldrich	Anatase, <25nm
2,6-dihydroxybenzoic acid	Sigma-Aldrich	98%
2,3-dihydroxybenzoic acid	Sigma-Aldrich	99%
Polyethylenimine (PEI)	Polyscience. Inc.	MW 250,000
Dopamine hydrochloride	Sigma-Aldrich	Reagent grade
3,4-dihyroxy-L-phenylalanine (DOPA)	Sigma-Aldrich	Reagent grade
3-Hydroxytyramine hydrochloride (Dopamine)	Sigma-Aldrich	Reagent grade
5-sulfosalicylic acid dehydrate	Sigma-Aldrich	≥99%
Pyrocatechol violet	Sigma-Aldrich	Analytical reagent

Caffeic acid	Sigma-Aldrich	≥98%
Trans-cinnamic acid	Sigma-Aldrich	97%
P-coumaric acid	Sigma-Aldrich	≥98%
2,4-dihydroxycinnamic acid	Sigma-Aldrich	97%
Alizarin red	Sigma-Aldrich	Analytical reagent
Alizarin yellow	Sigma-Aldrich	Analytical reagent, Dye content, 50%
Aurintricarboxylic acid ammonium salt (AT-NH_4)	Sigma-Aldrich	Biochemicals and reagents
Hyrotalcite	Sigma-Aldrich	Reagent grade
Multiwalled carbon nanotubes (MWCNTs)	Arkema	

4.1.2 Poly[3-(3-N,N-diethylaminopropoxy)thiophene] PDAOT

Poly[3-(3-N,N-diethylaminopropoxy)thiophene] (PDAOT) was prepared by Prof. Alex Adronov's group from Department of Chemistry, McMaster University.

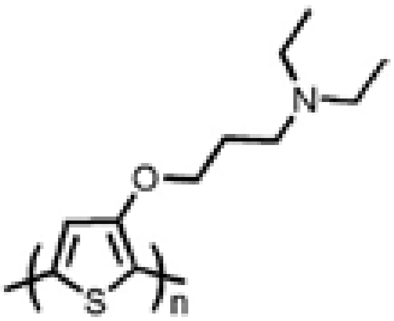

Figure 4-1 Structure of poly[3-(3-N,N-diethylaminopropoxy)thiophene] (PDAOT)

4.2 Coating fabrication by electrodeposition methods

4.2.1 Electrodeposition procedures

Anodic and cathodic composite coatings were obtained on a variety of conductive substrates under constant voltage or current conditions. These conductive substrates included stainless steel 304 foils (50×50×0.1 mm), Pt foils (50×50×0.1 mm) and platinized silicon wafers (10×50×1.5 mm).

In order to gain various coating thickness, the deposition time was varied in the range of 0-10 min. The constant voltage of 3-150 V was used for the constant voltage deposition. A minimum of three samples were prepared in each deposition experiment. All the coatings were prepared using fresh solutions. The coatings obtained were dried in air at room temperature for at least 24 hours for the further characterization.

4.2.2 Experimental setup for electrodeposition

Both anodic and cathodic electrophoretic depositions were performed for the fabrication of the polymer-ceramic, polymer-ceramic-CNTs composite coatings and nanoparticle films with various dispersants. Figure 4-2 is a schematic of the setup of the deposition cell.

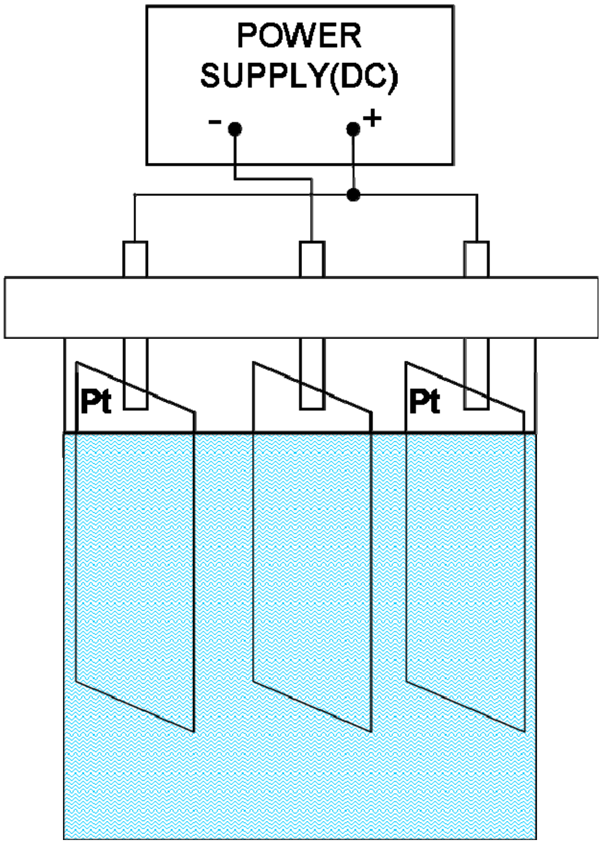

Figure 4-2 Schematic of the setup of the deposition cell

The deposition cell contained a cathodic substrate (15-30 cm^2), which is between the two parallel platinum (Pt) counter electrodes. The distance between the electrodes was 15 mm. The volume of the deposition bath ranged from 50-280 ml. An electrophoresis power supply EPS 601 (Amersham Biosciences) provided the DC electric field for electrodeposition, either in a constant current density or a constant voltage mode.

4.3 Preparation of solutions and suspensions for electrodeposion

10-30 gL^{-1} TiO_2 suspension in ethanol were prepared for EPD. Different dispersants were added to form stable and well-dispersed suspensions, in which the concentrations of dispersants were in the range of 0-1.0 gL^{-1}. For the dispersants including 2,6-dihydroxybenzoic acid (2,6-DHBA), 2,3-dihydroxybenzoic acid (2,3-DHBA), 5-sulfosalicylic acid (5-SSA), pyrocatechol violet (PV), alizarin red (AR), alizarin yellow (AY), electrophoretic deposition was performed in 10 gL^{-1} TiO_2 suspension in ethanol, for the dispersants including caffeic acid (CA), trans-cinnamic acid (TCA), p-coumaric acid (PCA), 2,4-dihydroxycinnamic acid (DCA), electrophoretic deposition was performed in 30 gL^{-1} TiO_2 suspension in ethanol. For the dispersants including aurintricarboxylic acid ammonium salt ($AT-NH_4$), electrophoretic deposition was performed in 10 gL^{-1} TiO_2 suspension in water. All the electrodepositions were performed after ultrasonication of the suspensions during 2 hours.

The neutral polymer PDAOT was protonated and dissolved in acetic acid solution to the protonation of amine side chains, resulting in complete and rapid dissolution of the polymer in water-ethanol mixture (10% / 90%), forming a purple solution of 3 g/L PDAOT.

The concentration of hydrotalcite in the suspensions was in the range of 1-10 gL^{-1}. PEI was protonated in acetic acid, dissolved in water-ethanol mixed solution (20% / 80%) and ultrasonicated for 2 hours in order to obtain a well-dispersed suspension.

Various amounts of CNT, TiO_2 nanoparticles and dispersants including pyrocatechol violet (PV), $AT-NH_4$, DOPA, dopamine were added into the solution, and ultrasonicated for 2 hours to get a well-dispersed suspension.

4.4 Characterization of the coatings

4.4.1 Investigation of electrodeposition yield

The electrophoretic deposition yield was investigated by measuring the weight of the deposited films. We used a Mettler Toledo AX105 DeltaRange analytical balance, of which the accuracy is 0.01 mg, to measure the weight of the stainless steel substrate before and after the deposition, which was dried in air at room temperature for at least 24 hours. A minimum of 3 samples were prepared in each deposition investigation. The deposition yield measurements were repeatable and the error was less than 5%.

In-situ measurement of coating mass during deposition process was performed using Quartz Crystal Microbalance (QCM 922, Princeton Applied Research). Nanobalance was used to investigate continuous deposition mass change with increasing eposition time under constant current or constant voltage conditions. In this case only dilute solution can be used. The concentration of the polymer solution ranged from 0.05-0.1 gL^{-1}. The mass gain in the QCM test was calculated using the relationship:

$$\Delta m = \frac{-\Delta F \times A\sqrt{\rho_q \mu_q}}{2F_0^{\ 2}} \tag{4-1}$$

$$\Delta m = -\Delta F \times \frac{0.196\sqrt{2.947\times10^{11}\times 2.648}}{2\times(9\times10^{6})^2} = -1.06878\times10^{-9}\Delta F \tag{4-2}$$

where ΔF is the frequency decrease of the QCM, F_0 is the parent frequency of QCM(9.00 MHz), A is the area of the gold electrode (0.196 cm^2), ρ_q is the density of the quartz (2.648 g cm^{-3}) and μ_q is the shear modulus of the quartz (2.947×10^{11} g cm^{-1} sec^{-2}). The vibration frequency of quartz deviated from its standard frequency when materials were deposited onto quartz surface.

4.4.2 Thermogravimetric and differential thermal analysis

Thermogravimetric analysis (TGA) is a helpful analytical technique, which is widely used to verify a material's thermal stability and fraction of volatile components by monitoring the weight change that takes place when a specimen is continuously heated. The weight is recorded as a function of increasing temperature in air or in an inert atmosphere. Besides the mass changes, the instruments can also record the temperature difference between the specimen and reference pans (differential thermal analysis, DTA), which is employed to monitor the energy released or absorbed through chemical reactions or phase transformations during the heating process.

In this work, TGA and DTA were employed using the deposits that had been removed from the Pt substrate after deposition and dried in air at room temperature for at least 24 hours. The thermoanalyzer (Netzsh STA-409) was operated at a heating rate of 5 °C min^{-1} up to 1200 °C.

4.4.3 Scanning electron microscopy

The scanning electron microscope (SEM) is used to observe the morphology of sample surface and cross section by scanning it with a high-energy beam of electrons in a scan pattern. Through the interaction of electrons and atoms, the images are made up producing signals that contain information about the sample's topography, composition, microstructure and other properties.

The microstructures of the deposited coatings were studied by JEOL JSM-7000F scanning electron microscope. We prepared both film surfaces and cross section samples for SEM observation by EPD of polymer, ceramic and composite films on platinized silicon wafers. The samples were placed on a conductive sample holder using a conductive adhesive copper tape and covered by a 5 nm layer of Pt in order to increase the conductivity to get a better quality of images.

4.4.4 Fourier transform infrared spectroscopy

Fourier Transform Infrared Spectroscopy (FTIR) is an analytical technique widely employed to study organic (and in some cases inorganic) materials. It measures the absorption of various infrared light wavelengths by the material of interest. FTIR spectrometer can simultaneously collect spectral data in a wide spectral range and provide a primary advantage over a dispersive spectrometer measuring intensity over a narrow range of wavelengths at a time. These infrared absorption bands identify specific molecular components and structures.

In this work, the deposits scraped from the Pt substrates were investigated by FTIR using Bio-Rad FTS-40 instrument.

4.4.5 Electrochemical analysis

Potentiostat is widely employed to test electrochemical properties of the deposited coatings. In this work, we used a potentiostat (Parstat 2273, Princeton Applied Research) connected to a computer using a PowerSuite electrochemical software. Electrochemical studies were performed using a standard three-electrode cell containing 3 wt% NaCl solution, degassed with purified nitrogen gas. The working electrode surface was a graphite rod (6mm) embedded in resin. The counter electrode was a platinum gauze, and the reference electrode was a standard calomel electrode (SCE).

Electrochemical impedance spectroscopy (EIS) has been applied in the study of corrosion systems. EIS provides measurement of impedance of an electrochemical system as a function of the frequency of an applied electric field. AC potential of a typical signal amplitude ranges from 5 to 10 mV applied to an electrochemical cell, with a frequency from 0.001Hz to 100 kHz.

Impedance is presented in the form of complex numbers. The real part represents resistance component in the system, while the imaginary part represents capacitance component. The results of impedance are typically expressed in the form of Nyquist plot (imaginary part versus real part) and Bode plots (absolute value of impedance and phase shift versus frequency).

Tafel testing is another critical way to study corrosion systems. Tafel plots reflect the potential and current density when corrosion occurring. These values are used to compare materials' corrosion properties. It is clearly shown on the Tafel plot which material prevents corrosion better and how the corrosion proceeds as potential increasing. Tafel is plotted in the form of potential versus current (logarithmical), from which corrosion rate can be calculated.

5 Experimental Results and Discussion

5.1 Electrodeposition of TiO_2 films with catechol family of additives

TiO_2 is important material for electrochemical, catalytic, electronic, photovoltaic and biomedical applications [86, 87, 88]. Electrophoretic deposition (EPD) offers many processing advantages for the fabrication of TiO_2 coatings and the increasing interest in EPD is attributed to various successful applications of this method in nanotechnology [89].

The purpose of this investigation was the EPD of TiO_2 (anatase) using caffeic acid (CA), and other similar organic acids including 2,4-dihydroxycinnamic acid (DCA), p-coumaric acid (PCA) and trans cinnamic acid (TCA). EPD was achieved from 30 gL^{-1} TiO_2 suspensions in ethanol, containing 0-1 gL^{-1} of organic acids at a deposition voltage of 50 V.

This investigation is inspired by recent advances in the research of the mechanism of mussel adhesion to metal and mineral surfaces in water, which showed that strong adhesion is attributed to the chelation of natural catecholic amino acid DOPA. The chemical structure of caffeic acid is similar to that of DOPA. Therefore, the bio-inspired chemistry of caffeic acid adhesion to inorganic nanoparticles was in the focus of this investigation. The experimental results obtained for different molecules were compared in order to understand the influence of various functional groups of the molecules on their adsorption on TiO_2 particles in ethanol.

Previous investigations of adsorption of other molecules from catechol family were mainly performed in aqueous suspensions, where adsorption was influenced by hydration of the particle surface [90, 91]. The use of ethanol as a solvent for EPD offers advantages, compared to water, because the problems related to gas evolution at the electrodes can be avoided.

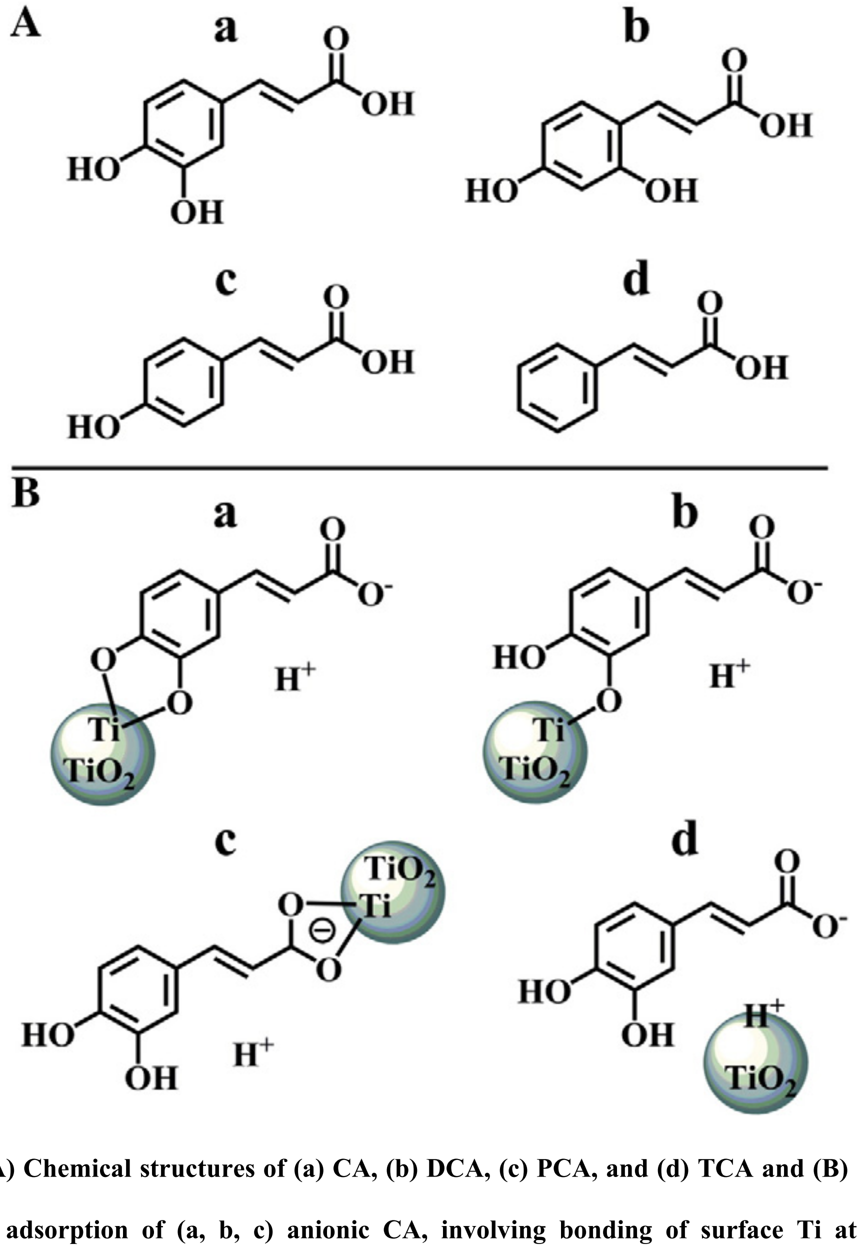

Figure 5-1 (A) Chemical structures of (a) CA, (b) DCA, (c) PCA, and (d) TCA and (B) TiO_2 particle charging by adsorption of (a, b, c) anionic CA, involving bonding of surface Ti atoms, and by adsorption of (d) H^+

Figure 5-1(A) and Figure 2-11(a) show the chemical structure of the organic additives, which were used in this investigation, including CA, DCA, PCA and TCA. These additives had similar structures, containing an aromatic ring, a hydrocarbon chain and carboxylic group. DOPA and CA belong to the catechol family of materials. Both of them had two OH groups bonded to adjacent carbon atoms of the aromatic ring, whereas DOPA also contained amino groups. Although DCA also contained two OH groups, they were bonded to non-adjacent carbon atoms of the aromatic ring. PCA contained only one OH group, whereas TCA was without OH groups. All the organic additives contained a COOH group.

Ionization of the different functional groups governs the total charge of zwitterionic DOPA [92]. The functional groups of DOPA are protonated at low pH. Therefore, the protonated amino group (NH_3^+) leads to the positive charge of DOPA at low pH [92]. When the pH increases, the deprotonation of carboxylic, phenolic and amino groups happen. As a result, DOPA is negatively charged at high pH. When the pH was below 10, amino group was protonated, reducing the total negative charge of the molecule at relatively high pH. The EPD of zwitterionic molecules and their application as charging agents presents difficulties due to charge reversal. Hence, CA molecule, containing only anionic groups, provides advantages for application in EPD. The anionic groups can be deprotonated in the bulk of suspensions and neutralized at low pH at the electrode surface. The charge neutralization is beneficial for anodic deposition of particles, containing adsorbed CA.

The adsorption is important for the efficient dispersion and charging of nanoparticles. Additionally, non-adsorbed dispersant is detrimental for dispersion and deposition. The DOPA adhesion to metals and oxides in aqueous solutions is attributed to catecholate type of bonding, involving metal atoms of the adsorbent and adjacent OH groups of DOPA. A similar mechanism can be suggested for CA adsorption. The adsorption of CA on inorganic particles is governed by the phenolic and carboxylic bonding sites. Figure 5-1B (a-d) shows possible mechanisms of particle charging in CA containing suspensions.

In order to analyze the CA adsorption mechanism, TCA, PCA, and DCA materials were investigated. The mechanisms, similar to those shown in Figure 5-1B (b-d), can be suggested for other molecules. The charge of the particles was governed by the competitive adsorption of dissociated anionic molecules and H^+. The preferred adsorption of anionic CA resulted in the negative charge of the particles, which formed anodic deposits. Preferred adsorption of H^+ in the suspensions containing other additives resulted in the formation of positively charged TiO_2 particles, which formed cathodic deposits. It is found that the catechol group is a strong complexing agent and able to coordinate metal atoms in acidic or basic pH suspensions with complete deprotonation of the OH groups [93, 94]. But the mechanism of adsorption is not known well at present. It was suggested that it involves the replacement of OH groups on the oxide surface by the deprotonated ligand [93, 94].

The CA adsorption can result from strong catecholate type bonding as depicted in Figure 5-1 B(a), which involved the complexation of surface Ti atoms with deprotonated adjacent OH groups. The interaction of carboxylic or individual OH groups of the molecules with Ti atoms on the particle surface can also result in adsorption. This adsorption was weak, compared to catecholate type adsorption of CA shown in Figure 5-1 B(a), which resulted in negatively charged particles. However, the coloration of the deposits indicated that anionic DCA, PCA and TCA were adsorbed on TiO_2 particles and incorporated into the cathodic deposits. The dispersion of materials in aqueous suspensions involves the dissociation of the dispersant and adsorption of formed anions or cations on the particle surface. In non-aqueous solvents these steps can be reversed. The dispersing agent can be adsorbed on the particle surface and then dissociate, releasing ions to the solution. The particles can contain adsorbed non-dissociated molecules. Therefore, charged particles can transport adsorbed non-dissociated molecules towards the electrode [95].

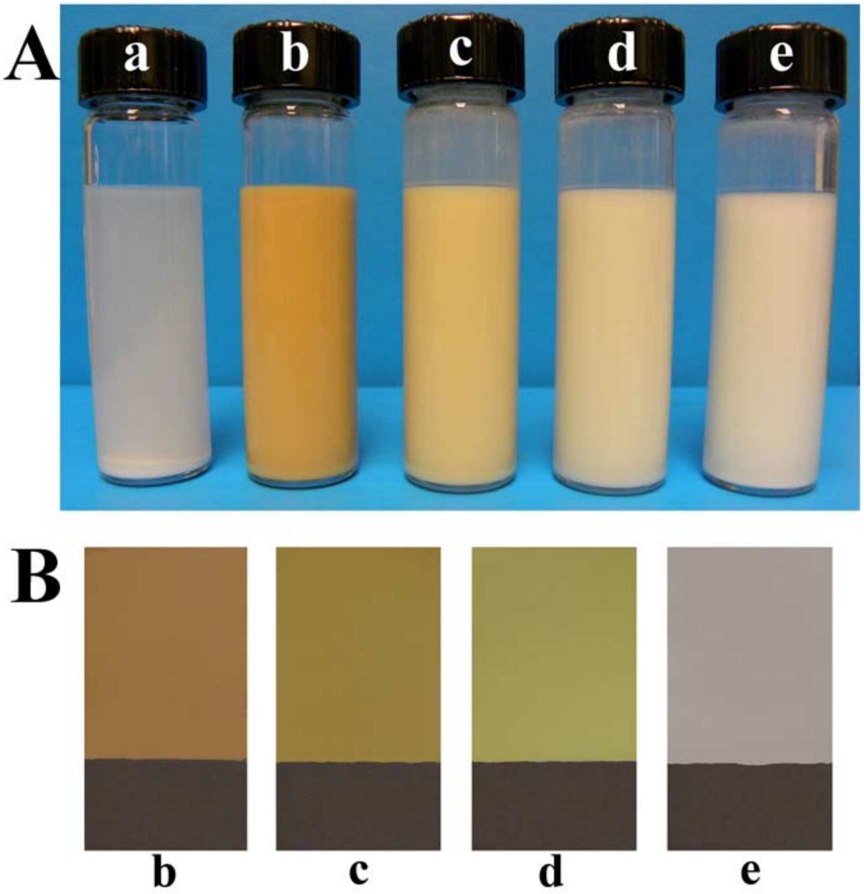

Figure 5-2 (A) TiO_2 suspensions (a) without additives, and containing 1 gL^{-1} (b) CA, (c) DCA, (d) PCA, and (e) TCA 1 h after ultrasonication; (B) deposits obtained from TiO_2 suspensions, containing 1 gL^{-1} (b) CA, (c) DCA, (d) PCA, and (e) TCA; (b) anodic, (c, d, e) cathodic deposits

The suspensions of TiO_2 in ethanol were unstable and showed significant sedimentation 1 h after the ultrasonic agitation as showed in Figure 5-2(A). The addition of the organic acids caused improved suspension stability, and the suspensions were stable at least 2-3 days. We observed that the best suspension stability was for CA containing suspensions, which were stable for more than 1 month. As you can see from Figure 5-2(A), the suspensions were coloured after the addition of the organic molecules. Anodic deposits were obtained using CA containing suspensions, whereas cathodic deposits were obtained using DCA, PCA and TCA as additives. As show in Figure 5-2(B), the colours of the deposits were similar to the colours of corresponding suspensions.

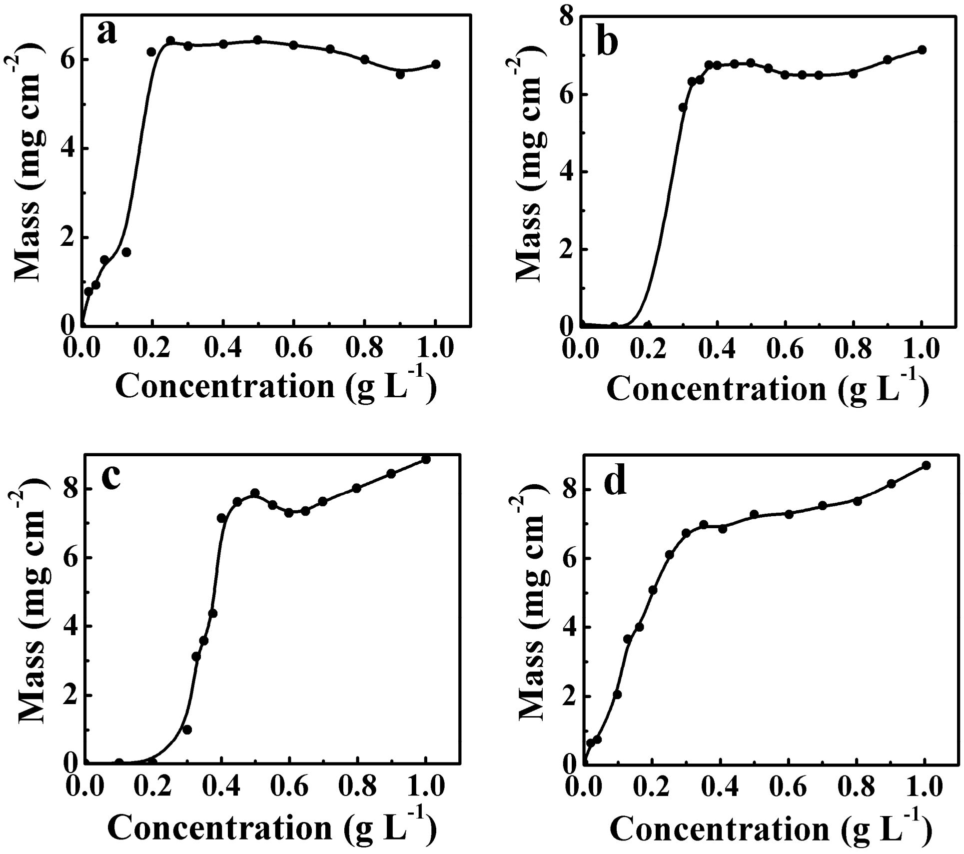

Figure 5-3 Deposit mass versus concentration of (a) CA, (b) DCA, (c) PCA, and (d) TCA at deposition time of 2 min.; (a) anodic, and (b, c, d) cathodic deposits

Figure 5-3 shows the deposit mass versus additive concentration. No deposition was observed without additives. The increase in CA and TCA concentration in the range of 0-0.2 gL^{-1} resulted in rapid increase in the anodic and cathodic deposition rates, respectively. However, very small deposition yield was observed for DCA and PCA in the same concentration range. The deposition yield increased significantly in the range of 0.2-0.4 gL^{-1} (Figure 5-3 b,c). At higher concentrations, moderate changes in the deposition yield were observed. The deposition mass versus deposition time measurements (Figure 5-4) showed that the deposit mass increased with increasing deposition time. Relatively high deposition yields were obtained for all additives. The experimental data presented in Figure 5-3 and Figure 5-4 indicated that anodic and cathodic deposition yields can be varied and controlled.

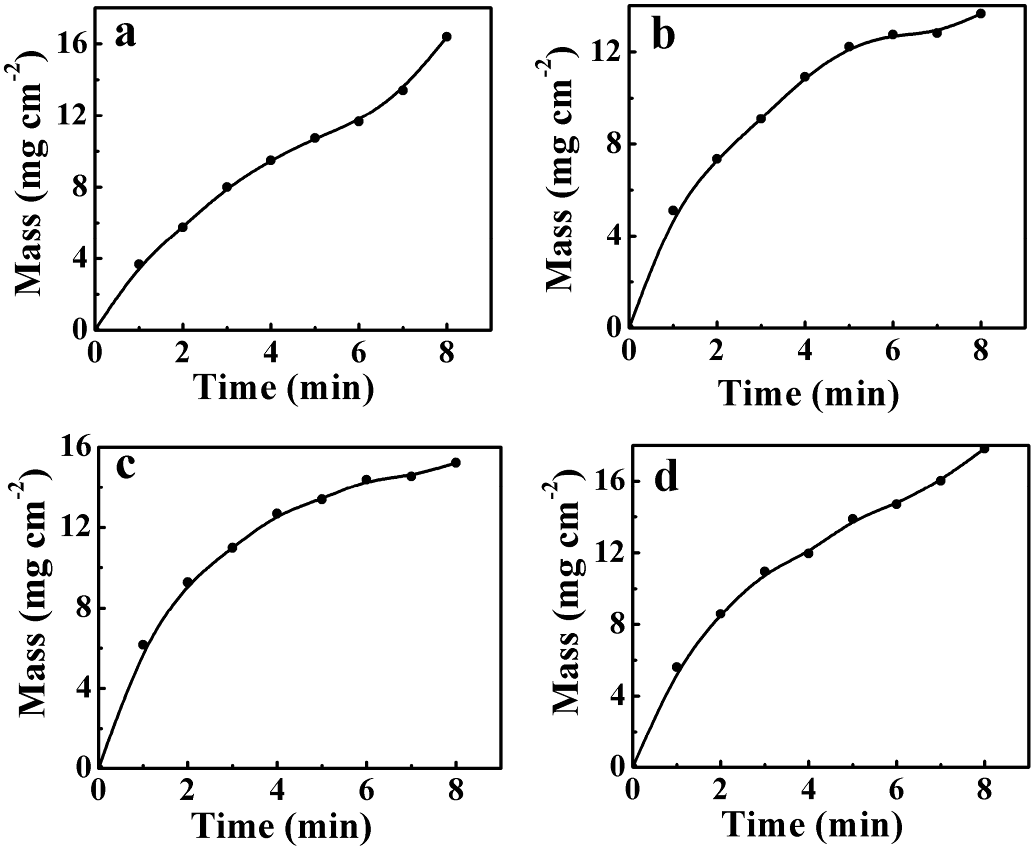

Figure 5-4 Deposit mass versus deposition time for suspensions containing 1 gL^{-1} (A) CA, (B) DCA, (C) PCA, and (D) TCA; (A) anodic, and (B, C, D) cathodic deposits

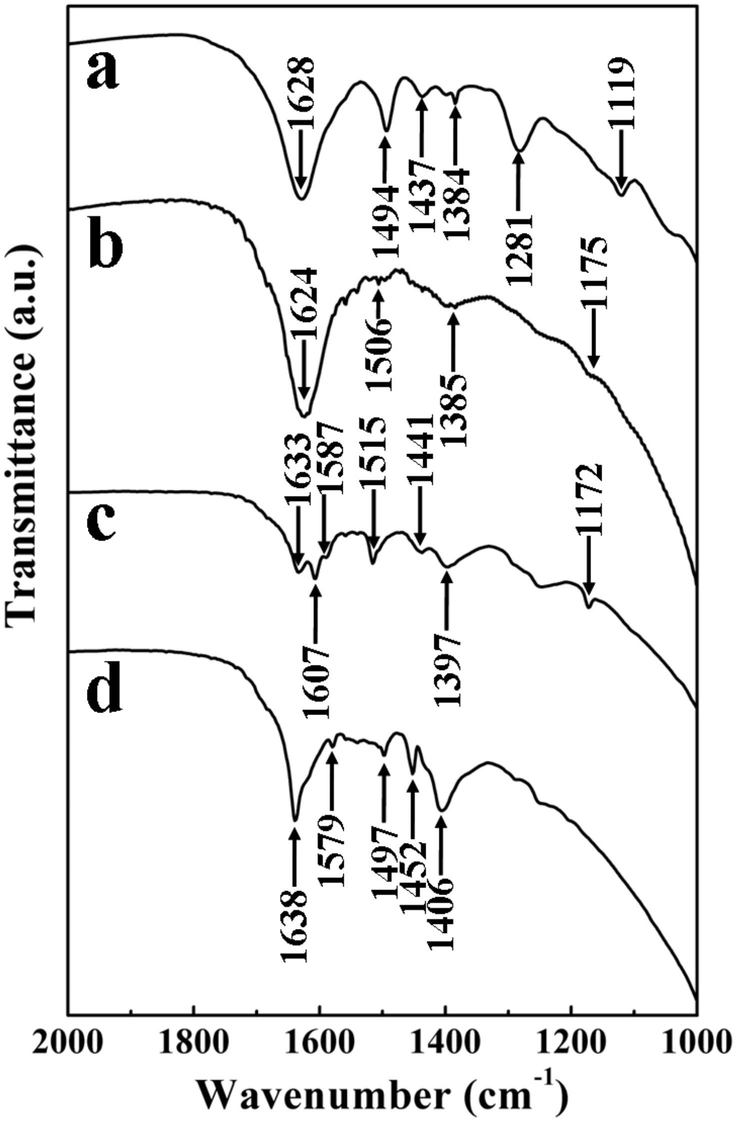

Figure 5-5 FTIR spectra of TiO_2 deposits obtained using 1 gL^{-1} (a) CA, (b) DCA, (c) PCA, and (d) TCA

Figure 5-5 shows FTIR spectra of TiO_2 deposits obtained using 1 gL^{-1} organic molecules. The peak assignments were presented in Table 5-1. The FTIR spectrum of TiO_2 deposit showed absorptions attributed to stretching vibrations of the aromatic rings of the organic molecules, bending vibrations of surface OH groups of TiO_2 and other vibrations of adsorbed additives. It is known that molecules from catechol family exhibit multiple bands in the range of 1400-1630 $\mathrm{cm^{-1}}$ related to stretching vibrations of the aromatic ring ν(C—C)/ν(C=C) [96]. Similar vibrations observed in Figure 5-5 a-d and in the FTIR spectra of as received CA, DCA, PCA and TCA indicated adsorption of the organic molecules on TiO_2. The bands at 1281 and 1119 $\mathrm{cm^{-1}}$ (Figure 5-5 a), which were attributed to the aryl—oxygen stretching vibrations of adsorbed CA, were not observed in Figure 5-5b-d [97]. However, the adsorptions attributed to the vibration of phenolic OH groups were not observed in Figure 5-5a. The FTIR data confirms the mechanism of CA adsorption, which involves the deprotonation of phenolic OH groups and complexation of Ti atoms in Figure 5-1B(a).

Table 5-1 Band assignments for TiO_2 deposits obtained using CA, DCA, PCA and TCA [a]

CA	DCA	PCA	TCA	Band Assignment
1628, 1494, 1437	1506	1607, 1587, 1515, 1441	1579, 1497, 1452	ν(ring C—C) / ν(ring C=C) vibrations [96]
	1624	1633,1397	1638, 1406	δ(OH) of TiO_2 [98]
1384	1385			ν(COO^-) vibrations [98]
	1175	1172		Ph δ(C—OH) vibrations [96]
1281, 1119				ν(C=O) / ν(C—O) vibrations [97]

[a] The wavenumbers were given in $\mathrm{cm^{-1}}$. ν = stretching mode; δ = bending mode; Ph = phenolic.

5.2 Comparing electrodeposition of TiO_2 films with catechol family and salicylate family of additives

The purpose of this investigation was the EPD of TiO_2 (anatase) using 2,3-dihydroxybenzoic acid, 2,6-dihydroxybenzoic acid and 5-sulfosalicylic acid. EPD was achieved from 10 gL^{-1} TiO_2 suspensions in ethanol, containing 0-1 gL^{-1} of organic acids at a deposition voltage of 50 V. Figure 5-6 shows the chemical structure of these three additives. As you can see, these additives had similar structures, containing an aromatic ring, a hydrocarbon chain and a carboxylic group. 2,3-dihydroxybenzoic acid had two OH groups bonded to adjacent carbon atoms of the aromatic ring. Although 2,6-dihydroxybenzoic acid also contained two OH groups, they were bonded to non-adjacent carbon atoms of the aromatic ring. 5-sulfosalicylic acid contained only one OH group All the organic additives contained a COOH group.

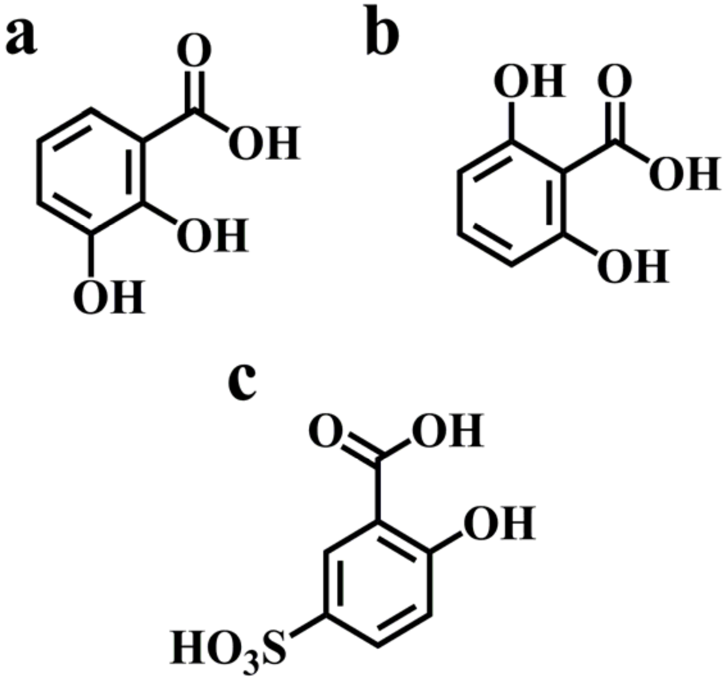

Figure 5-6 Chemical structures of (a) 2,3-dihydroxybenzoic acid, (b) 2,6-dihydroxybenzoic acid, and (c) 5-sulfosalicylic acid

Figure 5-7 shows the absorption mechanism. The 2,3-dihydroxybenzoic acid adsorption can result from strong catecholate type bonding in Figure 5-1 (a), which involved the complexation of surface Ti atoms with deprotonated adjacent OH groups. The mechanisms, shown in Figure 5-1 (b and c), can be suggested for 2,6-dihydroxybenzoic acid and 5-sulfosalicylic acid, which involved the complexation of surface Ti atoms with deprotonated adjacent OH and COOH groups. The charge of the particles was governed by the competitive adsorption of dissociated anionic molecules and H^+. The preferred adsorption of anionic organic acids resulted in the formation of negatively charged TiO_2 particles, which migrated towards the anode and formed anodic deposits.

As mentioned above, the catechol group is a strong complexing agent and able to coordinate metal atoms in acidic or basic pH suspensions with complete deprotonation of the OH groups [93, 94]. The interaction of carboxylic and adjacent OH groups of the molecules with Ti atoms on the particle surface, which is called salicylate type adsorption, can also result in adsorption. This adsorption was weak, compared to the catecholate type adsorption of 2,3-dihydroxybenzoic acid. However, the coloration of the deposits indicated that cationic 2,3-dihydroxybenzoic acid, 2,6-dihydroxybenzoic acid and 5-sulfosalicylic acid were adsorbed on TiO_2 particles and incorporated into the anodic deposits.

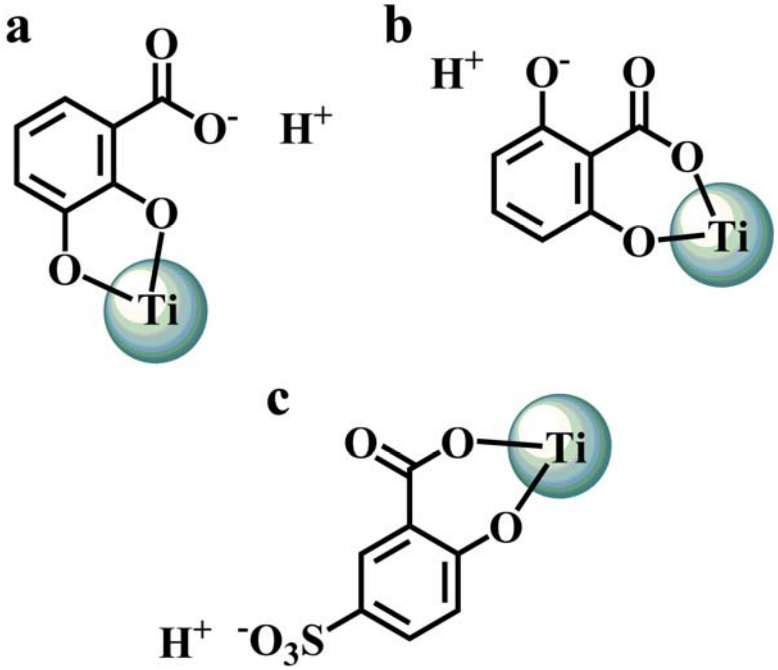

Figure 5-7 TiO_2 particle charging by adsorption of anionic (a) 2,3-dihydroxybenzoic acid, (b) 2,6-dihydroxybenzoic acid, and (c) 5-sulfosalicylic acid, involving bonding of surface Ti atoms

As pointed out above, the suspensions of TiO_2 in ethanol were unstable and showed significant sedimentation 1 h after the ultrasonic agitation (Figure 5-8A). The addition of the organic acids caused improved suspension stability, and the suspensions were stable at least 2-3 days. As it is seen from Figure 5-8(A), the suspensions were coloured after the addition of the organic molecules. Anodic deposits were obtained using 2,3-dihydroxybenzoic acid, 2,6-dihydroxybenzoic acid and 5-sulfosalicylic acid containing suspensions, respectively. As it is shown in Figure 5-8(B), the colours of the deposits were similar to the colours of corresponding suspensions.

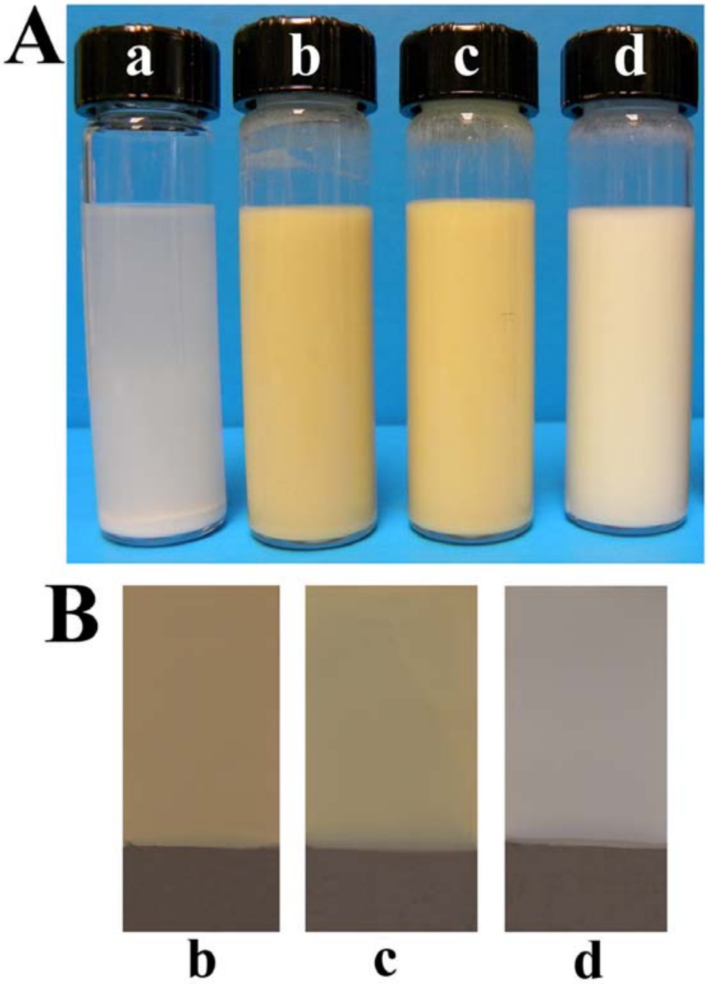

Figure 5-8 (A) TiO_2 suspensions (a) without additives, and containing 1 gL^{-1} (b) 2,3-dihydroxybenzoic acid, (c) 2,6-dihydroxybenzoic acid, and (d) 5-sulfosalicylic acid, 1 h after ultrasonication; (B) anodic deposits obtained from TiO_2 suspensions, containing 1 gL^{-1} (b) 2,3-dihydroxybenzoic acid, (c) 2,6-dihydroxybenzoic acid, and (d) 5-sulfosalicylic acid

Figure 5-9 shows deposit mass versus additive concentration dependencies. No deposition was observed without additives. The increase in 2,3-dihydroxybenzoic acid, 2,6-dihydroxybenzoic acid and 5-sulfosalicylic acid concentration in the range of 0-0.1 gL^{-1} caused a rapid increase in the anodic deposition rates, respectively. At higher concentrations, moderate changes in the deposition yield were observed for 2,3-dihydroxybenzoic acid, whereas dramatic changes were observed for 2,6-dihydroxybenzoic acid and 5-sulfosalicylic acid. After the deposition mass reaching a maximum at the concentration of about 0.1 gL^{-1}, it dropped significantly. No deposition was observed for 5-sulfosalicylic acid at concentration above 0.2 gL^{-1}. The deposition mass versus deposition time measurements (Figure 5-10) showed that deposit mass increased with increasing deposition time. The experimental data presented in Figure 5-9 and Figure 5-10 indicated that anodic deposition yields can be varied and controlled.

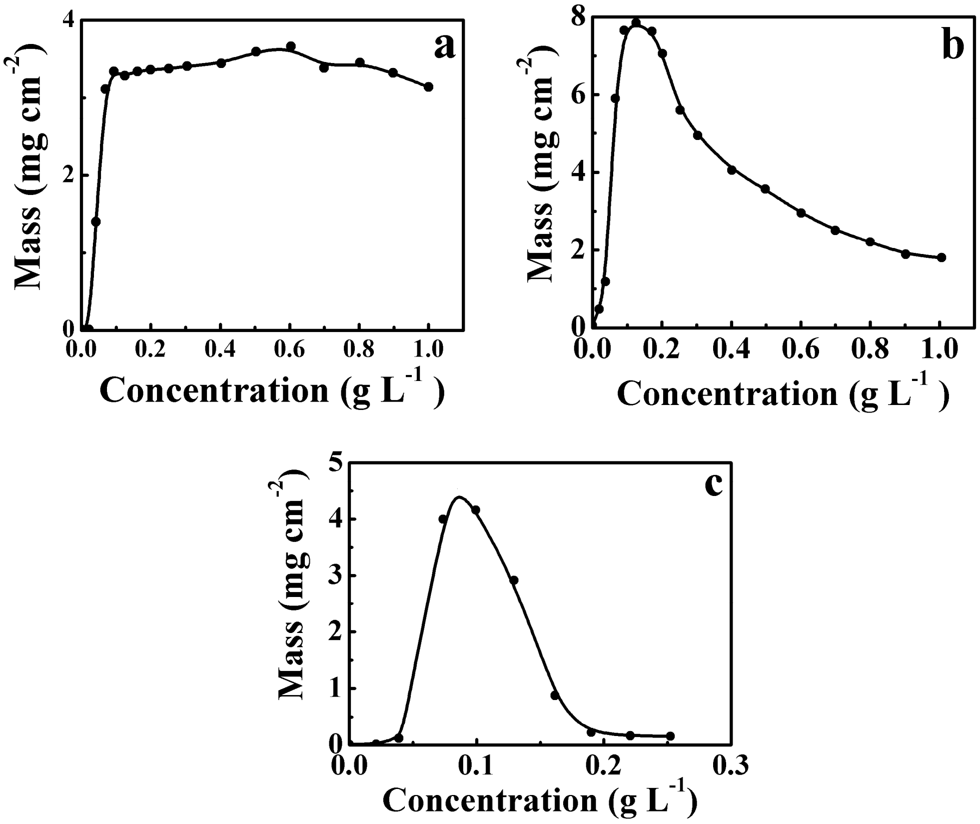

Figure 5-9 Anodic deposit mass versus concentration of (a) 2,3-dihydroxybenzoic acid, (b) 2,6-dihydroxybenzoic acid, and (c) 5-sulfosalicylic acid at deposition time of 2 min.

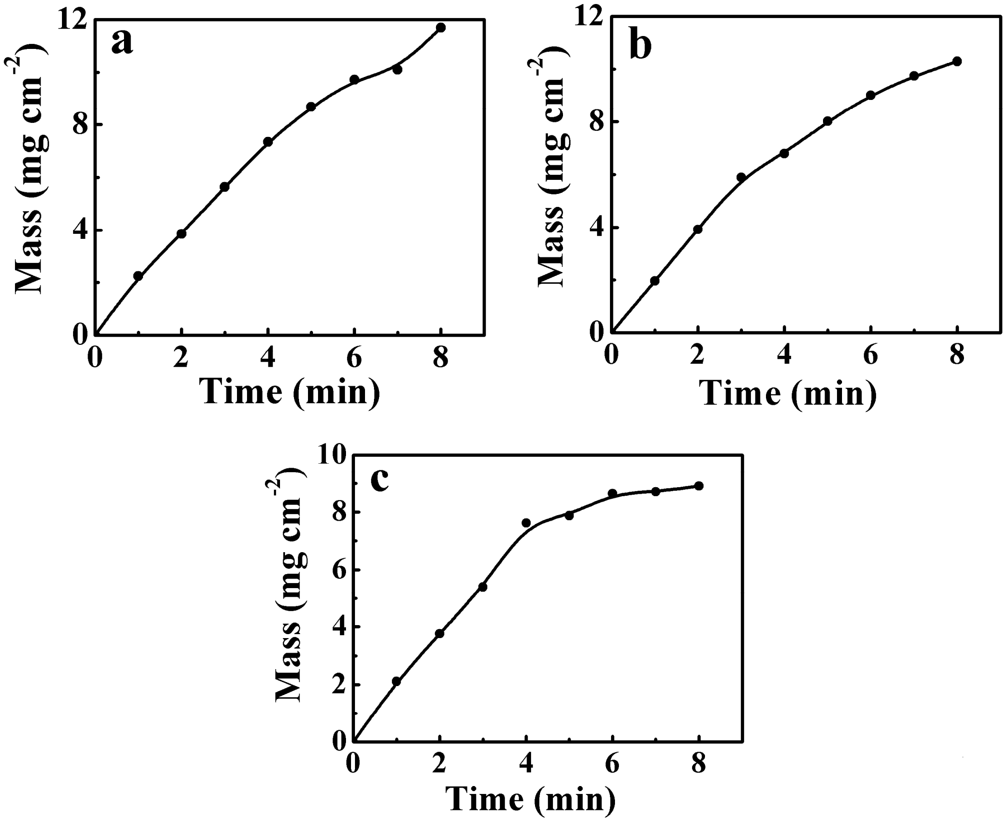

Figure 5-10 Anodic deposit mass versus deposition time for suspensions containing 1 gL^{-1} (a) 2,3-dihydroxybenzoic acid, (b) 2,6-dihydroxybenzoic acid, and (c) 5-sulfosalicylic acid

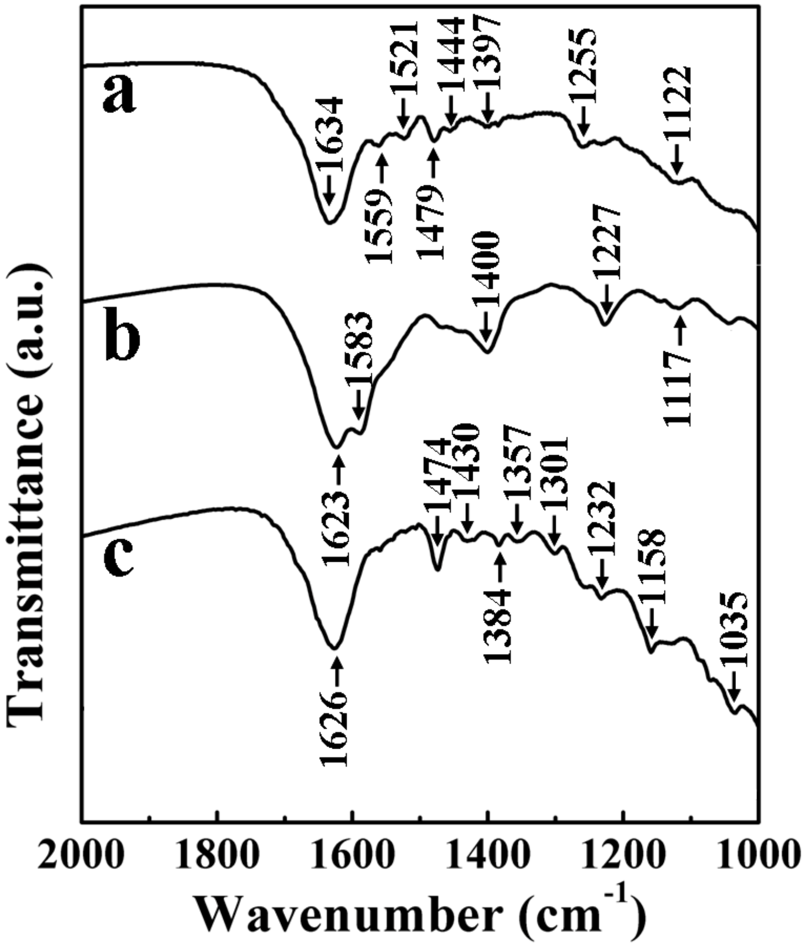

Figure 5-11 FTIR spectra of TiO_2 deposits obtained using 1 gL^{-1} (a) 2,3-DHBA, (b) 2,6-DHBA, (c) 5-SSA

The results presented above indicated that 2,3-DHBA, 2,6-DHBA and 5-SSA are efficient dispersing and charging agents for EPD of TiO_2. The adsorption of 2,3-DHBA, 2,6-DHBA and 5-SSA on TiO_2 was confirmed by the FTIR method. Figure 5-11 shows FTIR spectra of TiO_2 deposits obtained using 1 gL^{-1} organic molecules. The peak assignments were presented in Table 5-2. The FTIR spectrum of TiO_2 deposit shows absorptions attributed to stretching vibrations of the aromatic rings of the organic molecules and other vibrations of adsorbed additives. The FTIR results confirmed that additives were co-deposited with TiO_2 particles.

Table 5-2 Band assignments for TiO_2 deposits obtained using 2,3-DHBA, 2,6-DHBA and 5-SSA [a]

2,3-DHBA	2,6-DHBA	5-SSA	Band Assignment
1634, 1479, 1444	1623	1626, 1474, 1430	ν(ring C—C) / ν(ring C=C) vibrations [96, 99]
1559, 1521	1583		$\nu_{as}(COO^-)$ vibrations [99]
1397	1400	1384, 1357	$\nu_s(COO^-)$ vibrations [99, 100]
		1301	Ph ν(C—OH) vibrations [100]
1255			ν and δ(C—O—H) in carboxyl vibration [99]
		1232, 1158, 1035	SO_3^- asymmetric and symmetric vibrations [100, 101, 102]
	1227		Ph δ(C—OH) vibrations [99]
1122	1117		δ(C—H) in-plane vibrations [99]

[a] The wavenumbers were given in cm^{-1}. ν = stretching mode; δ = bending mode; Ph = phenolic.

5.3 Electrodeposition of TiO_2 nanoparticles modified with organic dyes

5.3.1 EPD of TiO_2 nanoparticles modified with alizarin red, alizarin yellow and pyrocatechol violet dyes

EPD was performed from 10 gL^{-1} TiO_2 suspensions in ethanol, containing 0–1.0 gL^{-1} AR, AY and PV, respectively. AR, AY and PV were dissolved in ethanol and used as dispersing and charging agents for EPD of TiO_2 from suspensions in ethanol.

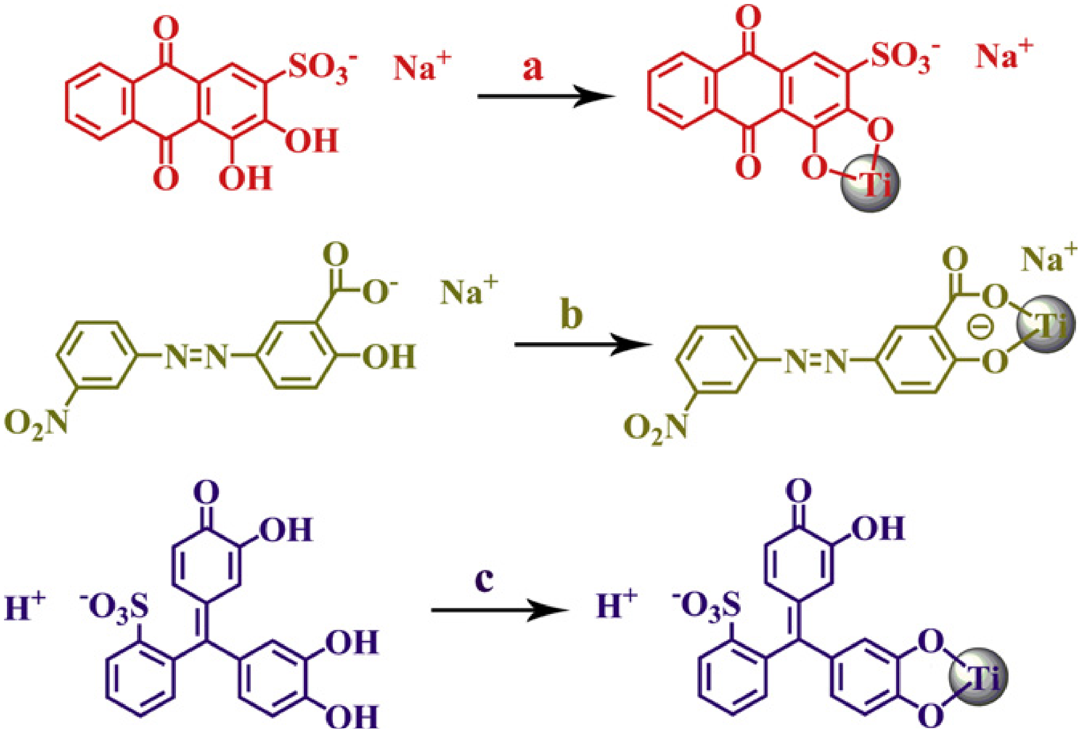

Figure 5-12 Adsorption of (a) AR, (b) AY and (c) PV on TiO_2 nanoparticles.

Figure 5-12 shows the structures of AR, AY and PV dyes used in this investigation. AR has two different complexing sites: an anionic SO_3^- group and a catechol group, containing two adjacent OH groups, bonded to the aromatic ring. It is known that SO_3^- group of AR did not play a significant role in surface anchoring process [101]. Organic molecules from the catechol family shows strong binding to TiO_2 surface [98]. The adsorption mechanism of AR involved deprotonation of two OH groups of catechol and the formation of Ti-catechol [98, 101] chelates (Figure 5-12a). The SO_3^- group of AR provided a negative charge for the anodic EPD. The adsorption of AY involved chelation of adjacent COO^- and OH groups (Figure 5-12b) [96, 98] and provided a negative charge to TiO_2 particles. The adsorption mechanism of PV was similar to that of AR and involved the complexation of a catechol group (Figure 5-12c). The adsorption resulted in negatively charged TiO_2 particles due to the SO_3^- group of PV.

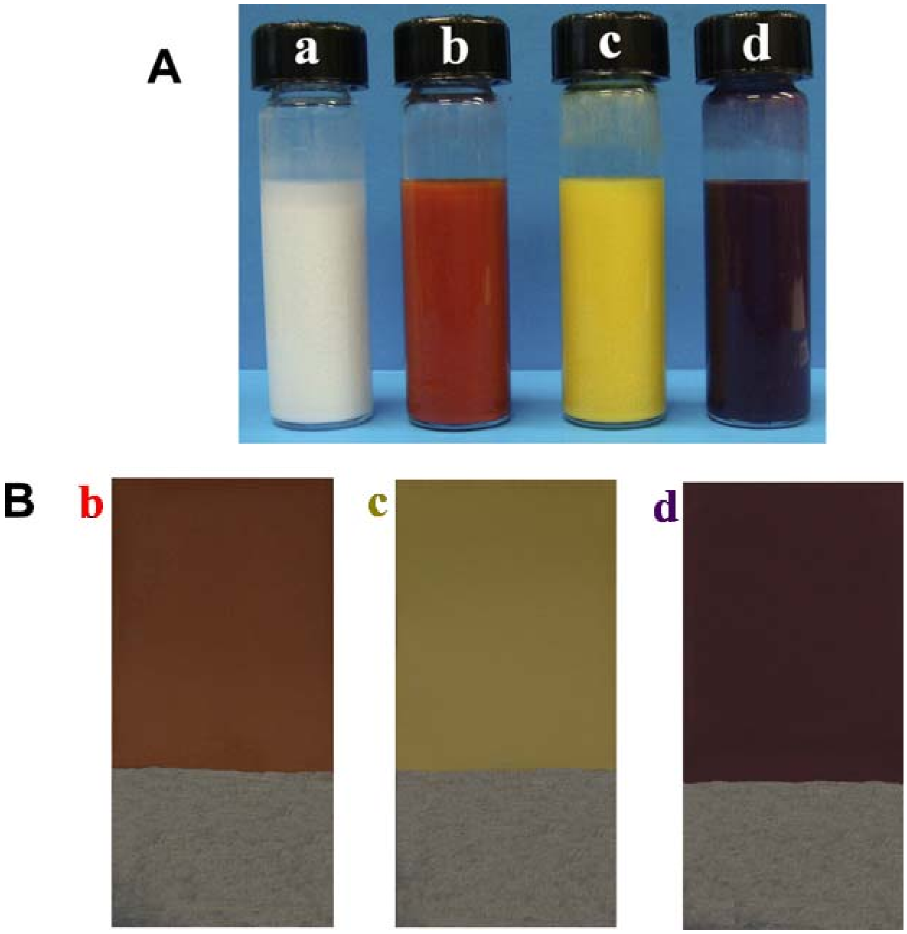

Figure 5-13(A) As prepared TiO_2 suspensions in ethanol: (a) without additives and containing, (b) AR, (c) AY and (d) PV; (B) TiO_2 films on stainless substrates prepared from suspensions in ethanol containing (b) AR, (c) AY and (d) PV

TiO_2 suspensions in ethanol without additives and with organic dyes were presented in Figure 5-13(A). The TiO_2 suspensions showed changes in color from white for pure TiO_2 to red, yellow and violet in the presence of AR, AY and PV, respectively. No EPD was achieved from pure TiO_2 suspensions because it was unstable and showed significant sedimentation 1 h after the ultrasonic agitation. In contrast, the addition of AR, AY and PV to TiO_2 resulted in improved suspension stability. Anodic deposits were obtained from TiO_2 suspensions, containing AR, AY and PV. As it is seen from Figure 5-13(B), the deposits showed red, yellow and violet colors, corresponding to the colors of the adsorbed dyes. The different colors of the deposits indicated co-deposition of TiO_2 with the dyes.

In this investigation, the deposition process was performed by measurements of deposition yield at various concentrations of additives and deposition durations. Figure 5-14 shows deposit mass versus AR, AY and PV concentration in the suspensions and deposition time dependencies. The deposit mass increased with increasing dye concentration in the suspensions, showed maxima and then decreased (Figure 5-14A). The increase in the deposit mass was attributed to the adsorption of organic dyes on TiO_2 nanoparticles, which provided particle charge and suspension stability. However, further increase in dye concentration resulted in lower deposition yield. The decrease in the deposition yield can be attributed to enhanced electrostatic repulsion of TiO_2 particles at the electrode surface, containing adsorbed dyes, which prevented particle coagulation at the electrode surface. The deposit mass increased with increasing deposition time (Figure 5-14B). Therefore, the amount of the deposited material can be varied and controlled.

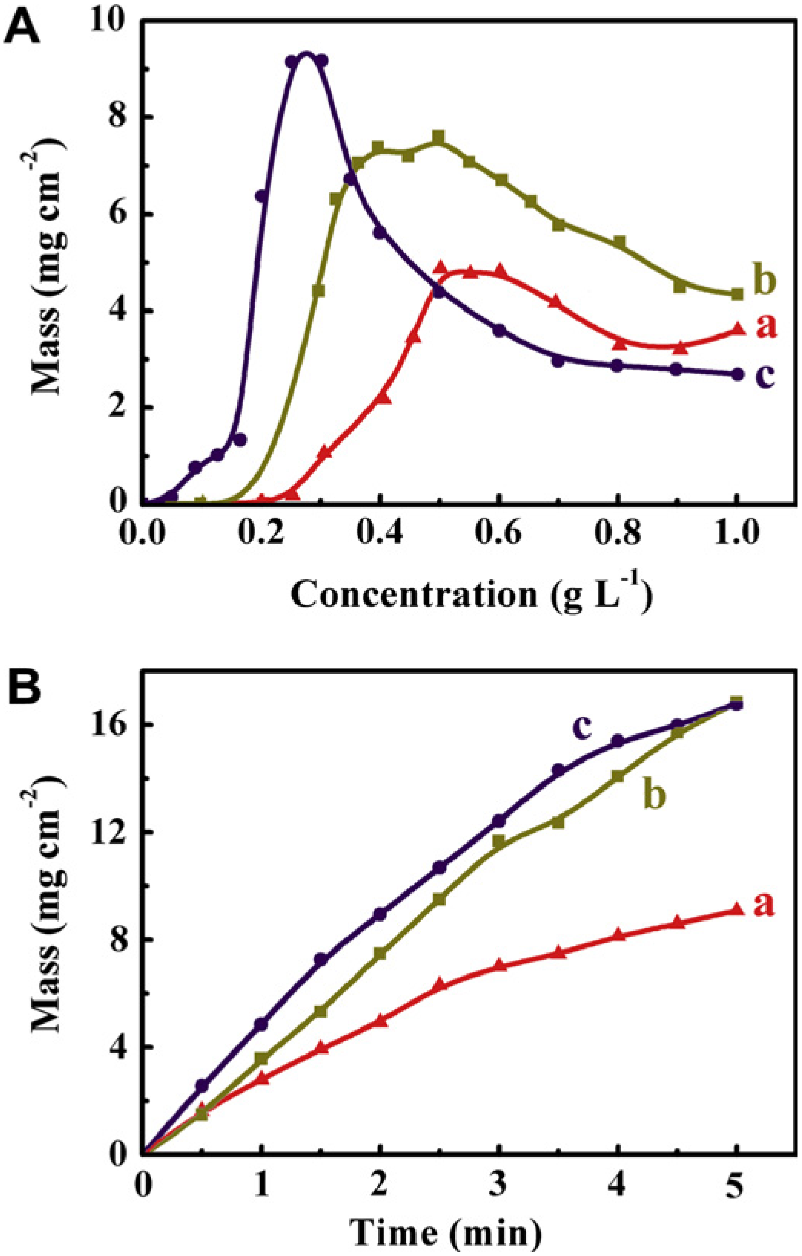

Figure 5-14 Deposition yield for deposits prepared from TiO_2 suspensions in ethanol containing (a) AR, (b) AY and (c) PV versus (A) dye concentration in suspensions at a deposition time of 2 min and (B) deposition time at dye concentration of (a and b) 0.5 gL^{-1} and (c) 0.3 gL^{-1}

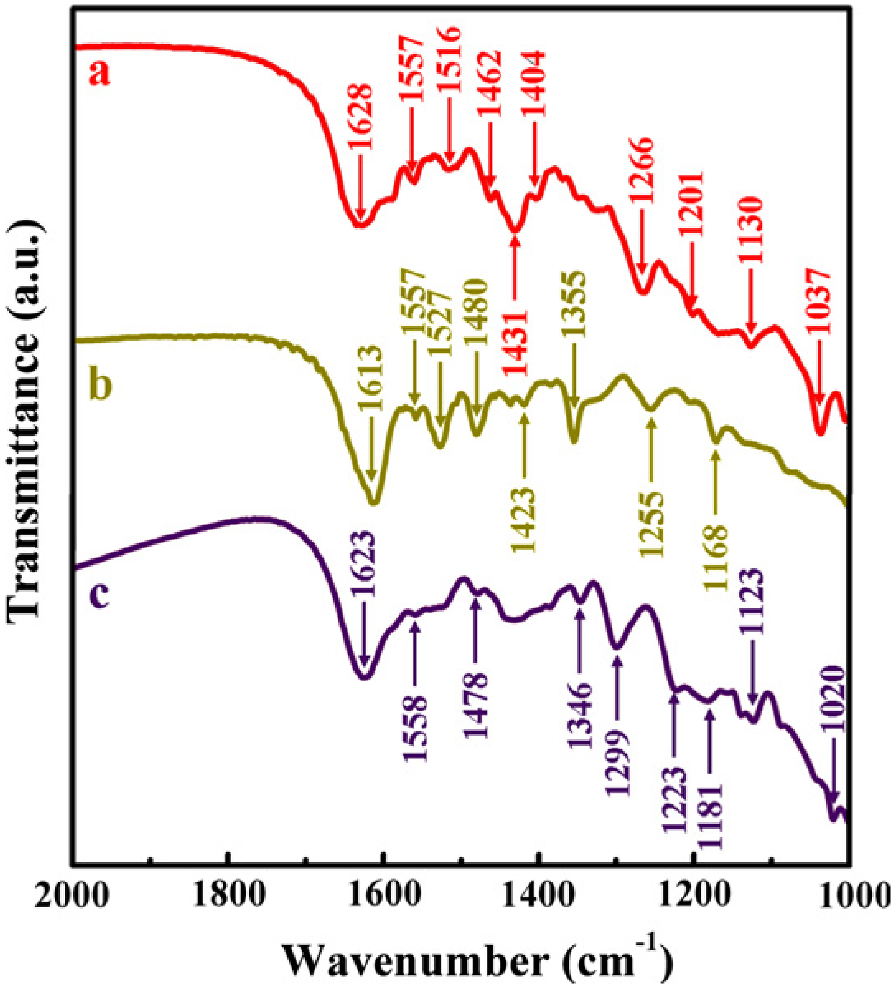

Figure 5-15 FTIR spectra of deposits prepared from TiO_2 suspensions in ethanol, containing 1.0 gL^{-1} (a) AR, (b) AY and (c) PV.

The results presented above indicated that AR, AY and PV are efficient dispersing and charging agent for EPD of TiO_2. The adsorption of AR, AY and PV on TiO_2 was confirmed by the FTIR method. Figure 5-15 shows the FTIR spectrum of deposits prepared from suspensions containing AR, AY and PV. The peak assignments were presented in Table 5-3. The FTIR results confirmed that dyes were co-deposited with TiO_2 particles.

Table 5-3 Band assignments for TiO_2 deposits obtained using AR, AY and PV [a]

AR	AY	PV	Band Assignment
1628, 1557, 1516, 1462, 1431, 1404	1613, 1557, 1527, 1480, 1423	1623, 1558, 1478	ν(ring C−C) / ν(ring C=C) vibrations [96]
1266	1355, 1255	1346, 1299	C − O vibrations [101, 103]
1201		1223	C=O vibrations [101]
1130, 1037		1181, 1123, 1020	SO_3^- asymmetric and symmetric vibrations [101, 102]
	1168		COO^- vibrations [96]

[a] The wavenumbers were given in cm^{-1}. ν = stretching mode

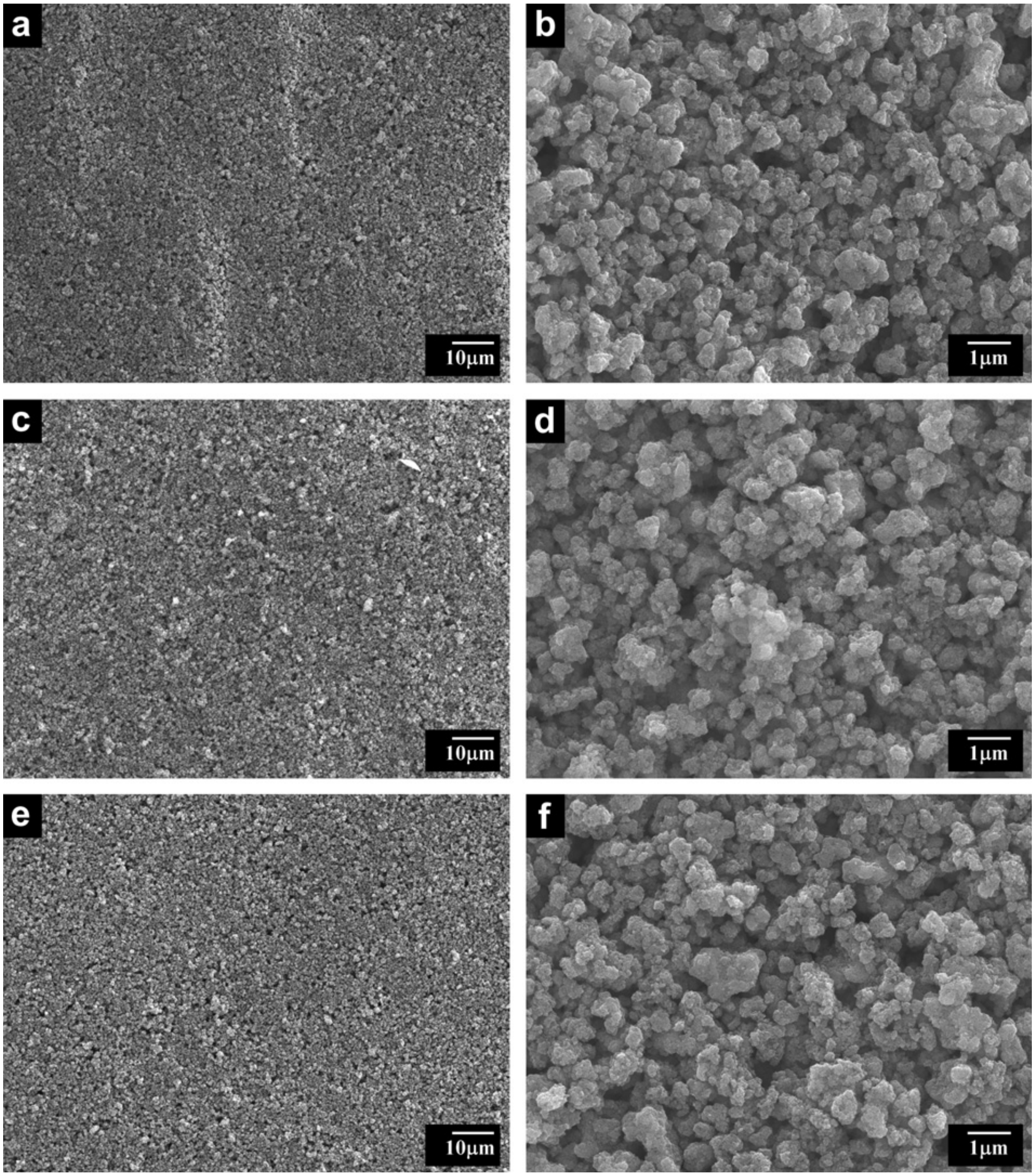

Figure 5-16 SEM images at different magnifications for deposits prepared from TiO_2 suspensions in ethanol containing 1 gL^{-1} (a and b) AR, (c and d) AY and (e and f) PV

Figure 5-16 shows SEM images of the films, which was deposited on stainless steel substrates. The films prepared using AR, AY and PV showed a similar morphology. The

SEM images at low magnification showed that the films were crack free. High magnification images indicated that deposits contained submicron particles. The films were porous with pore size in the range of 0.1–1 μm. The film porosity resulted from packing of TiO_2 particles.

5.3.2 EPD of TiO_2 nanoparticles modified with aurintricarboxylic acid ammonium salt dye

Aurintricarboxylic acid ammonium salt dye (AT–NH_4) was used for the EPD of TiO_2 films from aqueous suspensions. The structure and possible adsorption mechanism of AT–NH_4 is shown in Figure 5-17.

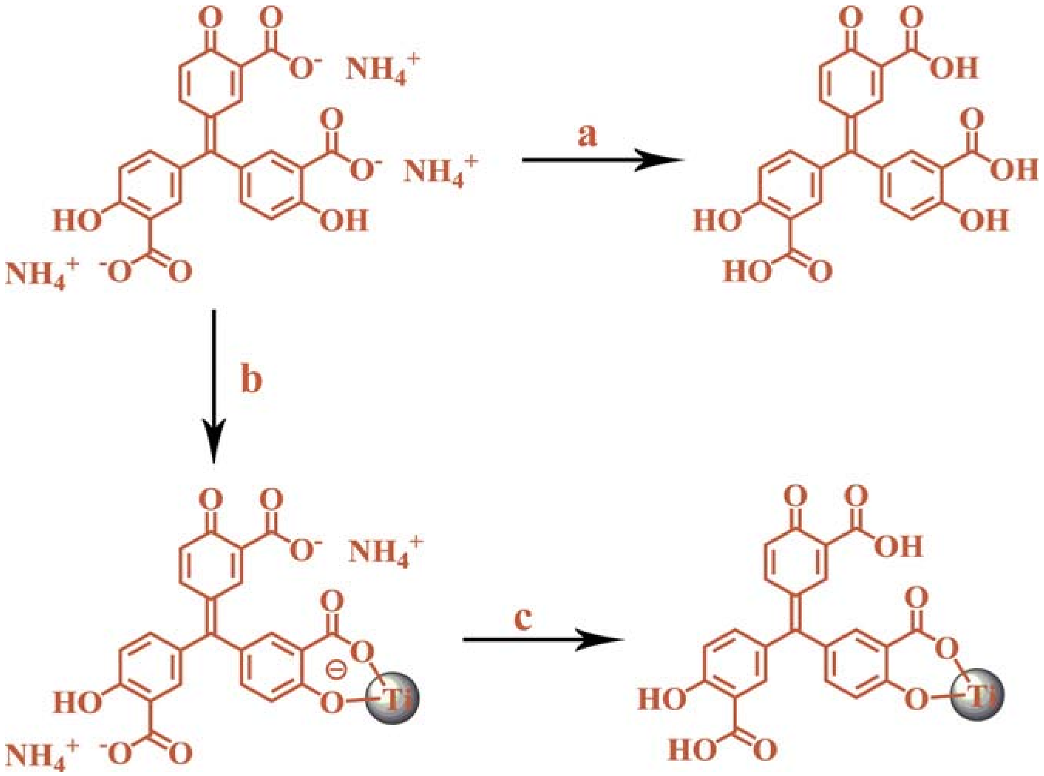

Figure 5-17 (a) Deposition of ATH from AT–NH_4 solutions, (b) adsorption of AT–NH_4 on TiO_2 and (c) deposition of TiO_2, containing adsorbed ATH.

It is found that AT–NH_4 dissociated in solution to form AT^- anions:

$$AT–NH_4 \rightarrow AT^- + NH_4^+ \tag{5-1}$$

The electric field provided electromigration of AT^- toward the anode, where pH decreased as a result of electrochemical decomposition of water:

$$2H_2O \rightarrow O_2 + 4H^+ + 4e^- \tag{5-2}$$

The formation of aurintricarboxylic acid (ATH) in the low pH region at the electrode surface was expected due to the charge compensation of the COO^- groups:

$$AT^- + H^+ \rightarrow ATH \tag{5-3}$$

It should be noted that ATH is insoluble in water. Therefore, the charge compensation of AT^- and formation of insoluble ATH promoted the film formation. Although the films were insoluble in water, they were soluble in concentrated NH_4OH solutions.

It was suggested that the adsorption mechanism of AT–NH_4 was similar to that of AY (Figure 5-12b) and salicylate [104] and involved the complexation of adjacent COO^- and OH groups (Figure 5-17b). The dye adsorption afforded a negative charge to the TiO_2 particles for EPD. The pH decrease at the anode surface (Eq. (5-2)) and protonation of AT^- (Eq. (5-3)) resulted in deposition of TiO_2, containing adsorbed ATH (Figure 5-17c). As discussed above, the charge neutralization of AT^- and formation of water insoluble ATH promoted the deposition process.

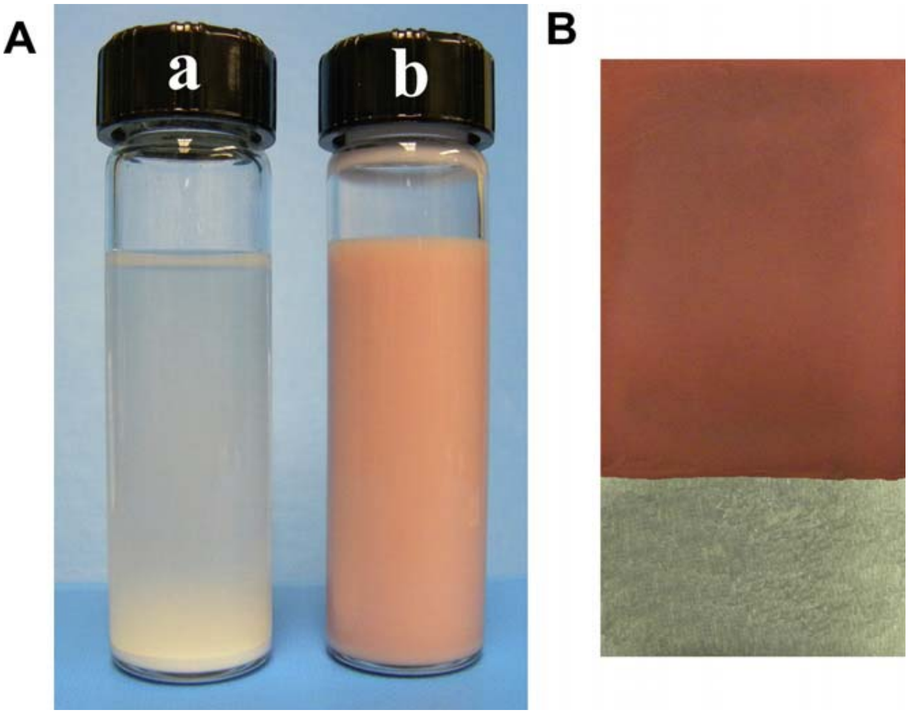

Figure 5-18 (A) TiO_2 suspension in water (a) without additive and (b) containing 1 gL^{-1} AT–NH_4; (B) TiO_2 deposit obtained from TiO_2 suspension in water, containing 1 gL^{-1} AT–NH_4

EPD was performed from 0.5–10 gL^{-1} TiO_2 suspensions in water, containing 0–1.0 gL^{-1} AT–NH_4 at deposition voltage of 3–20 V. AT–NH_4 is insoluble in ethanol. Therefore, aqueous suspensions of TiO_2 containing AT–NH_4 were utilized for EPD. The addition of AT–NH_4 to TiO_2 suspensions resulted in improved suspension stability (Figure 5-18A). Anodic deposits were gained from TiO_2 suspensions containing AT–NH_4 dye. The red color of the deposits (Figure 5-18B) showed the co-deposition of ATH with TiO_2.

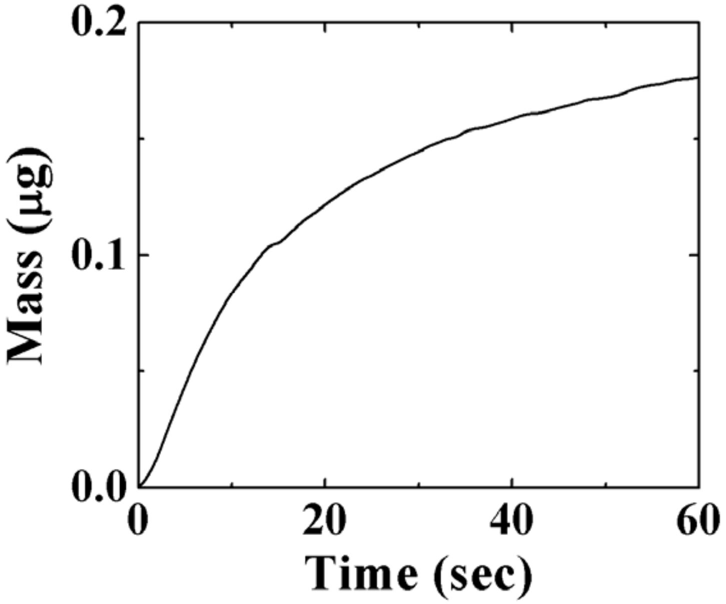

Figure 5-19 Deposit mass versus deposition time measured using QCM for 0.1 gL^{-1} AT–NH_4 solution at a deposition voltage of 4 V.

Figure 5-19 shows pure AT–NH_4 deposition yield measured using Quartz crystal microbalance (QCM) as a function of deposition time in water. The deposit mass increased with increasing time, indicating the formation of films of different mass. Therefore, the amount of the deposited material can be varied.

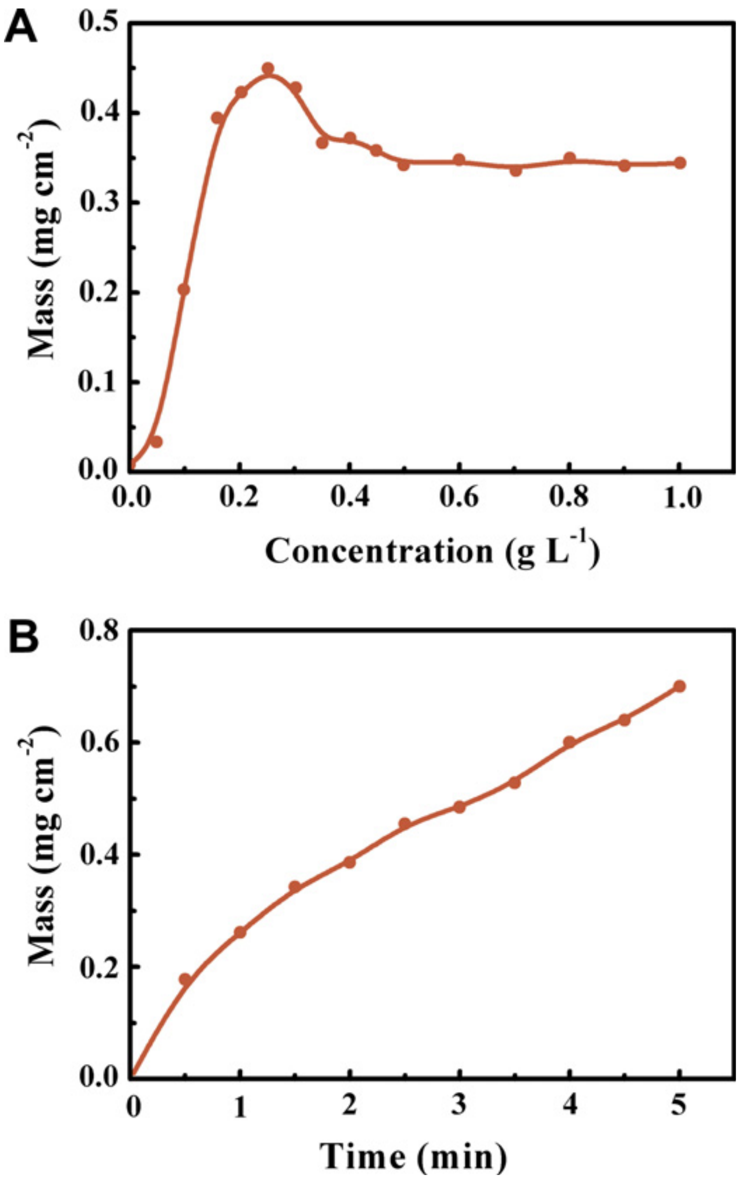

Figure 5-20 Deposition yield for deposits prepared from 10 gL^{-1} TiO_2 suspensions in water containing AT–NH_4 versus (A) AT–NH_4 concentration at a deposition time of 2 min and (B) deposition time at AT–NH_4 concentration of 1 gL^{-1}

Figure 5-20 shows deposit mass as a function of the AT–NH_4 concentration in the TiO_2 suspensions, and of the deposition time. The deposit mass increased with increased AT–NH_4 concentration (Figure 5-20A), indicated a maximum at 0.25 gL^{-1} AT–NH_4 and then decreased. The deposition yield was nearly constant in the range of 0.5–1 gL^{-1} AT–NH_4. The deposit mass increased with increasing deposition time (Figure 5-20B). Therefore, the deposition yield can be controlled by the concentration of AT–NH_4 and deposition time. The composition of the deposits can also be varied and controlled.

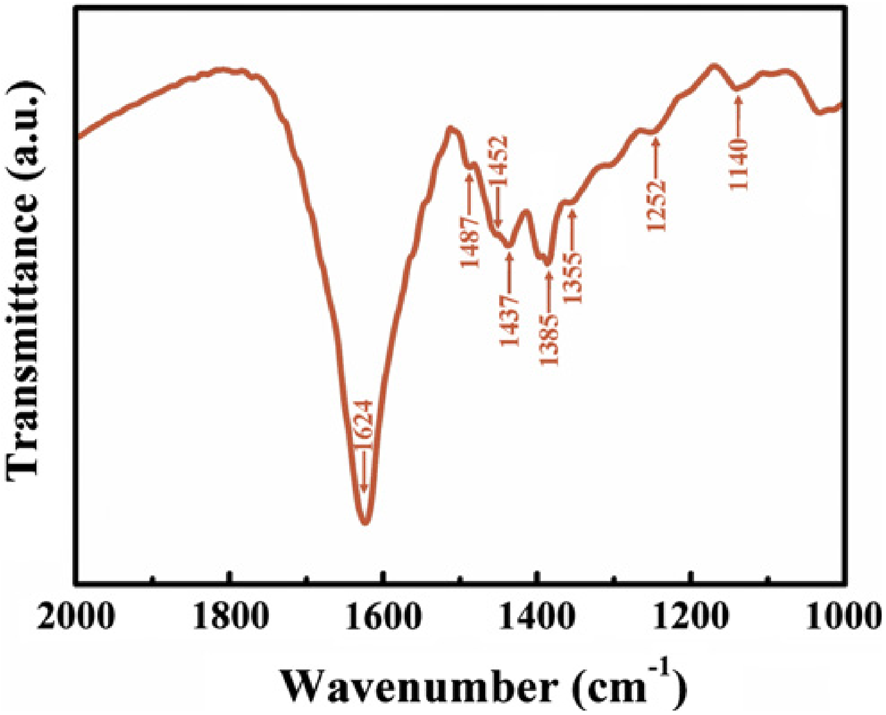

Figure 5-21 FTIR spectrum of the deposit prepared from TiO_2 suspension in water, containing 1 gL^{-1} AT–NH_4

Figure 5-21 shows the FTIR spectrum of deposits prepared using AT–NH_4 additive. The peak assignments were presented in Table 5-4. The FTIR spectrum of TiO_2 deposit shows absorptions attributed to stretching vibrations of the aromatic ring, bending vibrations of the phenolic groups and other vibrations of adsorbed AT–NH_4. The absorption, which was attributed to bending vibrations of the phenolic groups, was not observed in the spectrum of TiO_2 containing AY (Figure 5-15b). It is in this regard that one phenolic OH group of ATH was probably not involved in the complexation (Figure 5-17). Therefore, the FTIR data confirmed that the TiO_2 deposits contained adsorbed ATH.

Table 5-4 Band assignments for TiO_2 deposits obtained using AT–NH_4 [a]

AT–NH_4	Band Assignment
1624, 1487, 1452, 1437	ν(ring C−C) / ν(ring C=C) vibrations [96]
1385	Ph δ(C−OH) vibrations [96]
1355, 1252	C−O vibrations [101, 103]
1140	δ(C−H) vibrations [96, 104]

[a] The wavenumbers were given in cm^{-1}. ν = stretching mode; δ = bending mode; Ph = phenolic.

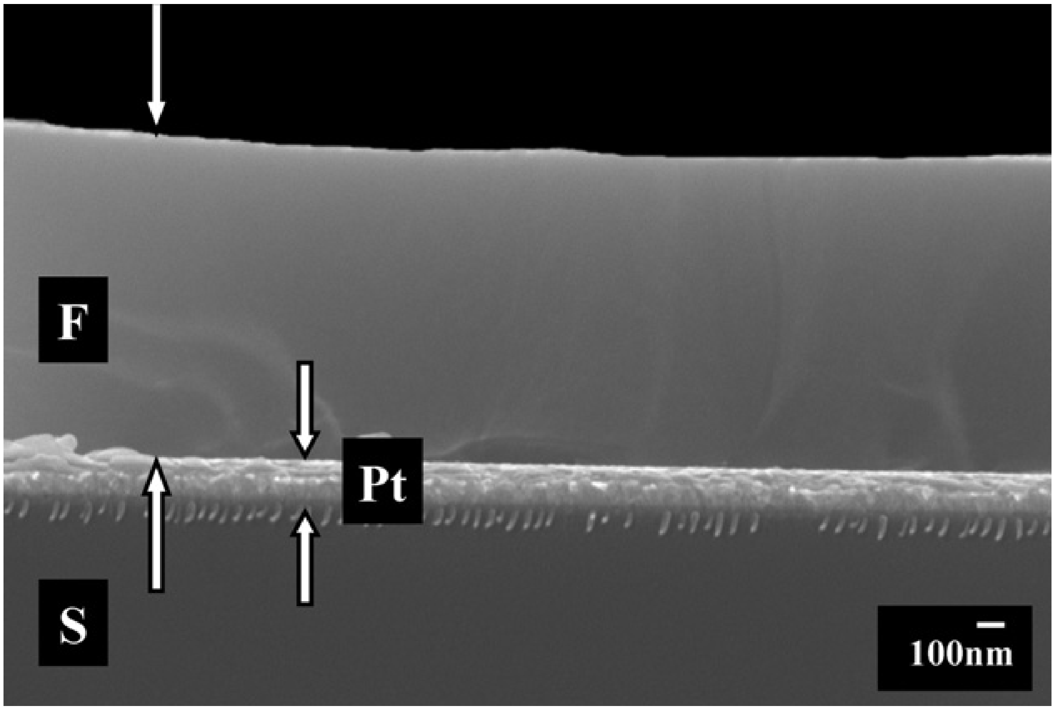

Figure 5-22 Cross section of ATH film (F) on platinized silicon wafer substrate (S), deposited from 1 gL^{-1} AT–NH_4 aqueous solutions at 5 V during 4 min, arrows show film and Pt layer

An interesting finding was the possibility of film formation from pure AT–NH_4 solutions. Figure 5-22 shows typical SEM image of film cross section. The film was relatively dense, uniform and adhered well to the substrate. The film thickness was varied in the range of 0.1–2 μm by the variation of deposition voltage in the range of 3–20 V, deposition time in the range of 1–10 min and AT–NH_4 concentration in the range of 0.1–1 gL^{-1}.

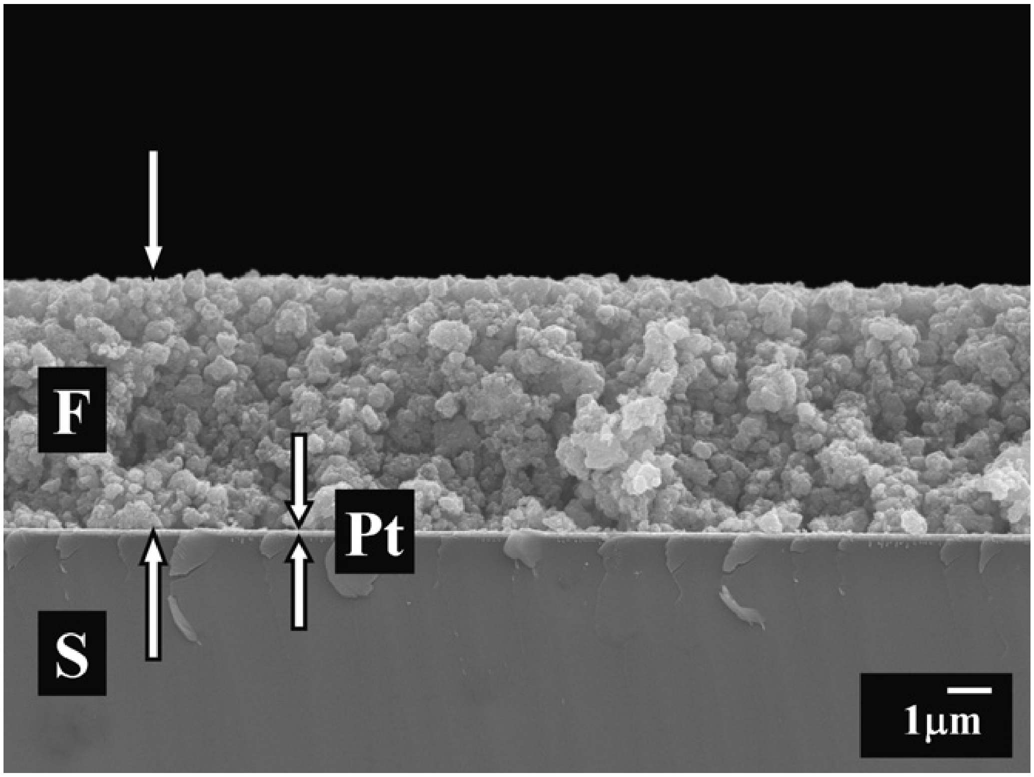

Figure 5-23 SEM image of a cross section of a deposit prepared from 1 gL^{-1} AT–NH_4 solution, containing 10 gL^{-1} TiO_2, at a deposition voltage of 10 V, F – film, S – substrate, arrows show film thickness and Pt layer thickness.

Figure 5-23 shows a typical SEM image of a film cross section, which was co-deposited TiO_2 with AT–NH_4. The image indicated film uniformity which was controlled by electric field. However, the film uniformity is limited by the size of the particles used for deposition. The thickness of the films was varied in the range of 0.5–5 μm by variation of the deposition time in the range of 1–10 min. The thickness of the composite film was thicker than the pure AT–NH_4 film. The film porosity was attributed to packing of TiO_2 particles.

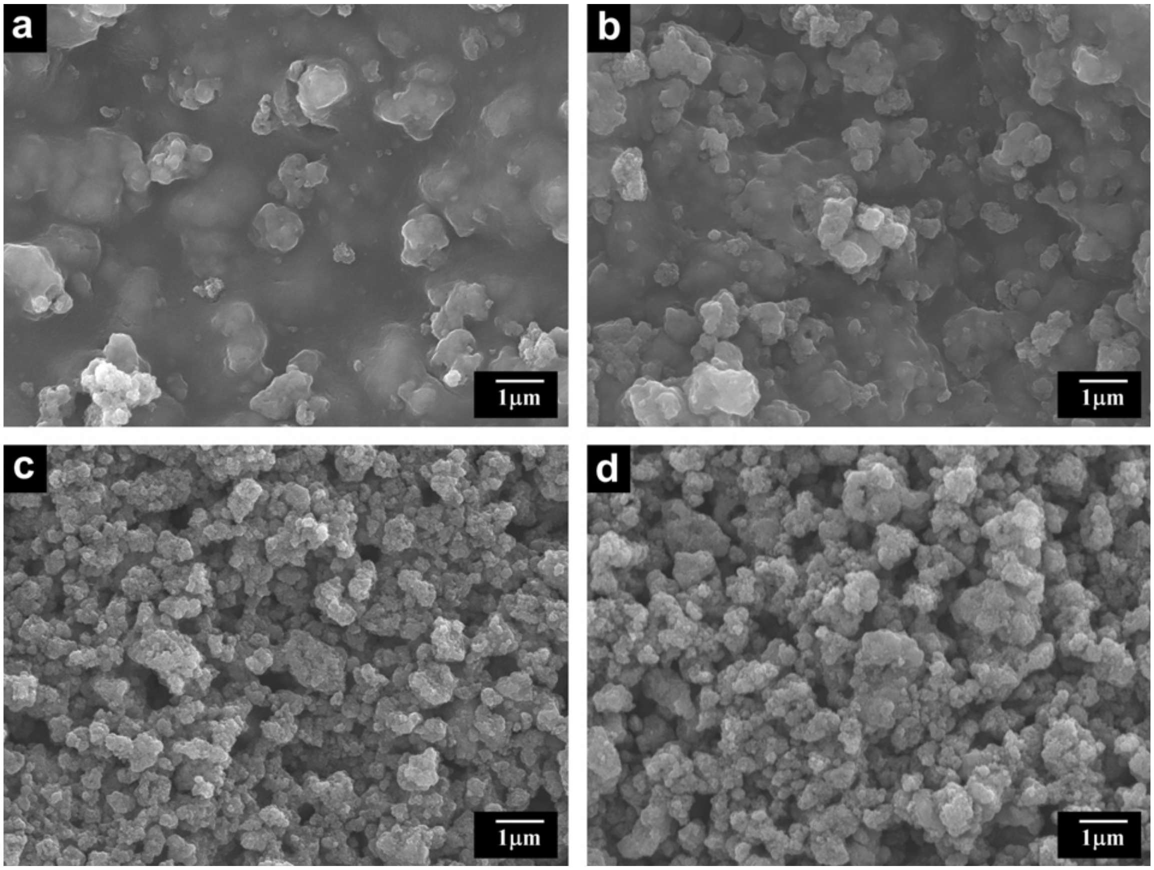

Figure 5-24 SEM images of deposits prepared from 1 gL^{-1} aqueous solution of AT–NH_4 containing (a) 0.5, (b) 1, (c) 5 and (d) 10 gL^{-1} TiO_2

Figure 5-24 shows SEM images of the deposits prepared from 1 gL^{-1} aqueous solution of AT–NH_4 containing 0.5, 1, 5 and 10 gL^{-1} TiO_2. The analysis of the SEM images showed that the increase in TiO_2 concentration in the suspensions caused increasing amount of TiO_2 in the deposits. The SEM images of deposits prepared from suspensions containing 0.5 and 1 gL^{-1} TiO_2 (Figure 5-24a and b) showed TiO_2 particles in the ATH matrix. The deposits prepared from 1 gL^{-1} AT–NH_4 aqueous solution containing 5 and 10 gL^{-1} TiO_2 contained mainly TiO_2 particles. The SEM images showed that the deposits were porous (Figure 5-24c and d). The porosity was attributed to packing of TiO_2 particles.

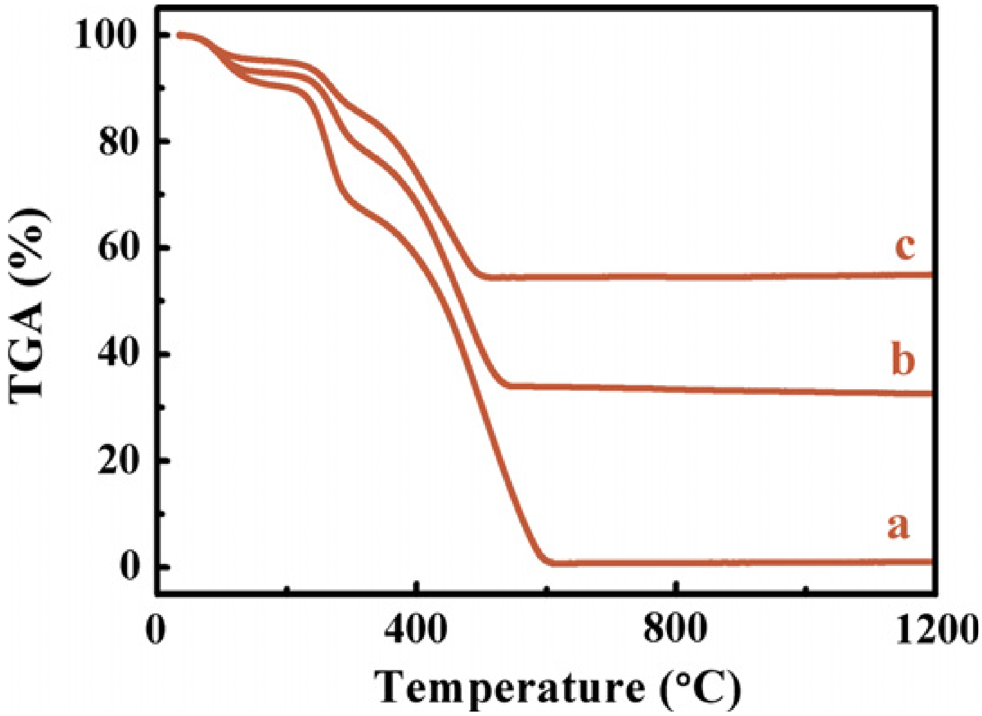

Figure 5-25 TGA data for deposits prepared from 1 gL^{-1} aqueous solution of AT–NH_4: (a) without TiO_2 and containing, (b) 0.5 and (c) 1 gL^{-1} TiO_2

Figure 5-25 shows TGA data for a deposit, prepared from 1 gL^{-1} AT–NH_4 aqueous solution. The TGA graph showed several steps in mass loss below 600 °C, attributed to burning out of ATH. The TGA data for deposits prepared from 1 gL^{-1} AT–NH_4 aqueous solution, containing 0.5 gL^{-1} and 1 gL^{-1} TiO_2, showed mass loss of 67.4 and 45.1 mass%, respectively. These results indicated the possibility of the formation of organic–inorganic composites, containing 32.6 and 54.9 mass% TiO_2. The results of TGA studies are in agreement with SEM data. The TGA results together with SEM data the indicated that organic–inorganic ATH–TiO_2 composites can be obtained.

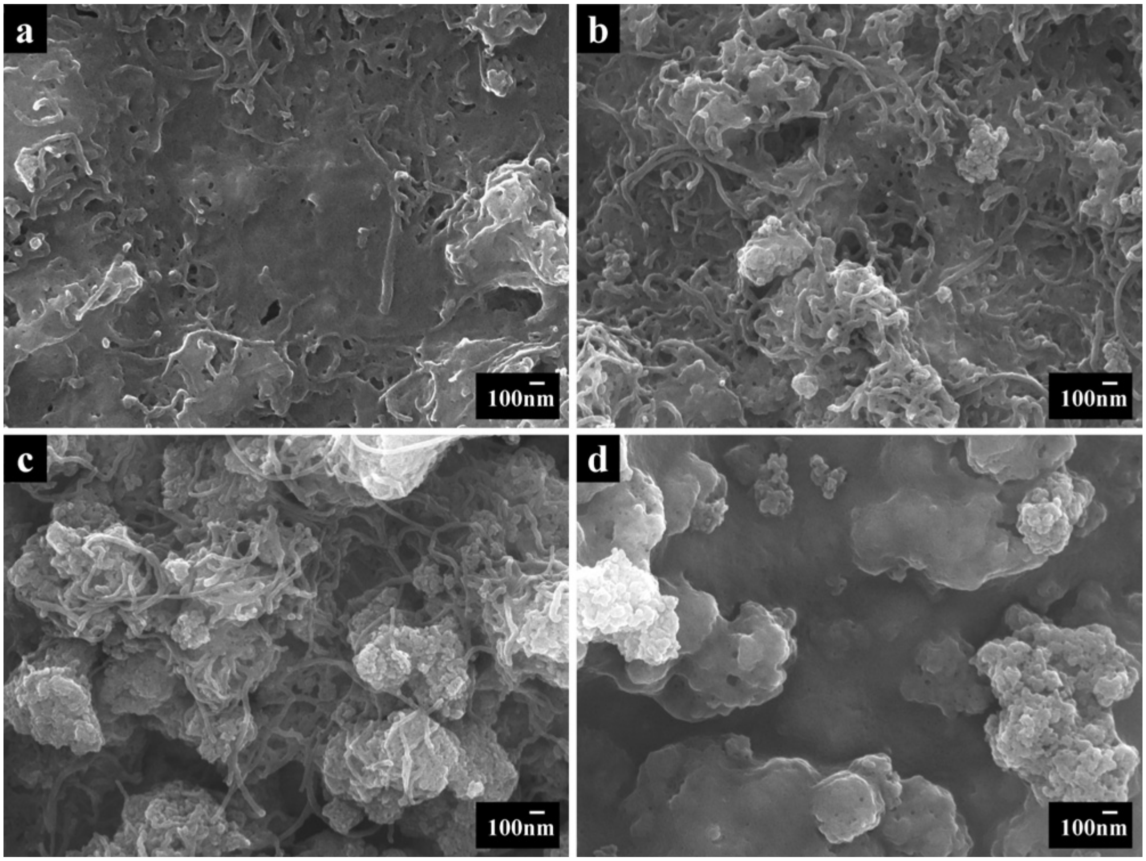

Figure 5-26 SEM images of deposits prepared from 1 gL^{-1} aqueous solution of AT–NH$_4$, containing (a) 0.5 gL^{-1} MWCNT and 0.5 gL^{-1} TiO$_2$, (b) 0.5 gL^{-1} MWCNTs and 1 gL^{-1} TiO$_2$, (c) 0.5 gL^{-1} MWCNTs and 2 gL^{-1} TiO$_2$, (d) 1 gL^{-1} TiO$_2$

Figure 5-26 shows MWCNTs and TiO$_2$ particles in the aurintricarboxylic acid matrix. The images (a, b, c) compared the deposits obtained from 0.5 gL^{-1} MWCNTs suspensions, containing different amounts of TiO$_2$. The images (b, d) compared the deposits prepared from 1 gL^{-1} TiO$_2$ suspensions with and without MWCNTs. The SEM images (a, b, c) showed that the increase in TiO$_2$ concentration in the suspensions resulted in the increased TiO$_2$ content in the deposit, as indicated by the increasing number of TiO$_2$ particles in the images from (a) to (c). The comparison of the images (b) and (d) indicated that the addition of MWCNTs to the TiO$_2$ suspensions resulted in incorporation of MWCNTs in the deposits. Therefore, the composition of the deposits can be varied. The feasibility of deposition of carbon nanotubes and TiO_2 indicated that individual materials can be co-deposited to form composite films.

In previous works on EPD of TiO_2 for photovoltaic applications, the TiO_2 particles were deposited using various charging agents and then the films were impregnated with dye solutions [105, 106]. However, the results presented above showed that dyes can also be used as charging and dispersing agents. So that, in our approach, the competitive adsorption of dyes and other charging or dispersing agents can be avoided. Moreover, the problems related to the impregnation of films with dyes and film integrity during impregnation can also be avoided, because in the proposed method, the dyes were adsorbed on TiO_2 nanoparticles in the bulk of the suspensions and incorporated in the films during EPD. It is important to note that only TiO_2 nanoparticles containing adsorbed dyes were deposited, because adsorbed dyes provided the charge, required for EPD. Therefore, the proposed approach offers advantages for the fabrication of dye-sensitized films for photovoltaic devices. The possibility of the fabrication of organic–inorganic composites using ATH demonstrated in this investigation offers new possibilities in the fabrication of composites.

The use of ATH allowed dispersion, charging and deposition of TiO_2 particles. Moreover, the film forming properties of ATH allowed the formation of composite films of controlled composition. The use of organic dyes paves the way for the fabrication of other composites. Preliminary investigations indicated that organic dyes are promising materials for the fabrication of composites, containing TiO_2 nanoparticles and carbon nanotubes with improved electrical conductivity for applications in photovoltaic devices.

5.4 Electrophoretic deposition of ceramic particles with PDAOT polymer

The protonation of the amine side chains of PDAOT with acetic acid resulted in a complete dissolution of the polymers.

$$\text{PDAOT} + \text{H}^+ \rightarrow \text{PDAOT}-\text{H}^+ \tag{5-4}$$

Electrodeposition from PDAOT$-$H$^+$ solutions resulted in the formation of cathodic deposits. The deposition mechanism involved base generation in cathodic reaction which resulted in a pH increase at the cathode surface.

$$2\text{H}_2\text{O} + 2\text{e}^- \rightarrow \text{H}_2 + 2\text{OH}^- \tag{5-5}$$

The electric field provided electrophoretic motion of the cationic PDAOT$-$H$^+$ macromolecules toward the cathode surface. The charge neutralization of the PDAOT$-$H$^+$ in the high pH region at the cathode surface resulted in the PDAOT precipitation and the formation of insoluble films:

$$\text{PDAOT}-\text{H}^+ + \text{OH}^- \rightarrow \text{PDAOT} + \text{H}_2\text{O} \tag{5-6}$$

QCM studies showed that the deposit mass increased with increasing deposition time (Figure 5-27). Therefore, the amount of the deposited material can be varied and controlled.

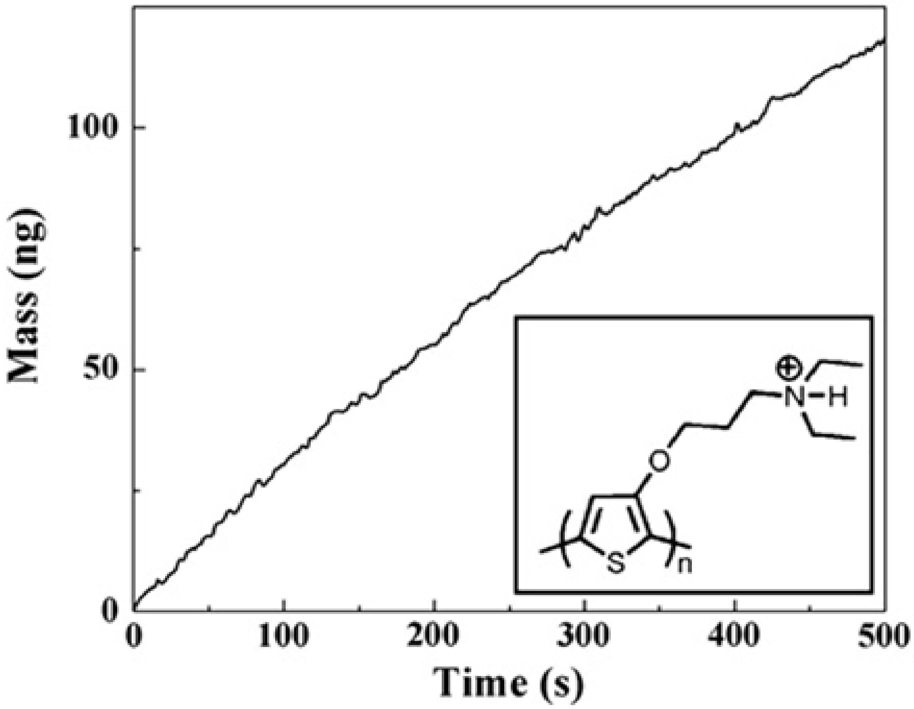

Figure 5-27 Deposit mass versus time for 0.1 gL^{-1} PDAFP at deposition voltage of 4 V (insets show structures of protonated polymers)

Figure 5-28 shows typical SEM images of the surface of the PDAOT with TiO$_2$ composite film prepared by EPD. The SEM image showed non-uniform distribution of TiO$_2$ in the PDAOT matrix. Some TiO$_2$ particles formed agglomerates, containing several particles. It is known that the incorporation of small inorganic particles into a polymer matrix presents difficulties related to the tendency of particles to agglomerate. The agglomeration can result from Van der Waals forces between particles or it can be attributed to the bridging flocculation of the particles, containing adsorbed polymer. In addition, the electric field present during EPD can promote the agglomeration of nanoparticles. However, it was found that the dispersion of TiO$_2$ in the polymer matrix can be improved using protonated dopamine (DA). Figure 5-29 shows that a more uniform distribution of TiO_2 particles with reduced particle agglomeration can be achieved using DA as a dispersant. Surface adsorption of DA leads to electrostatic repulsion of nanoparticles, producing films with significantly decreased agglomeration.

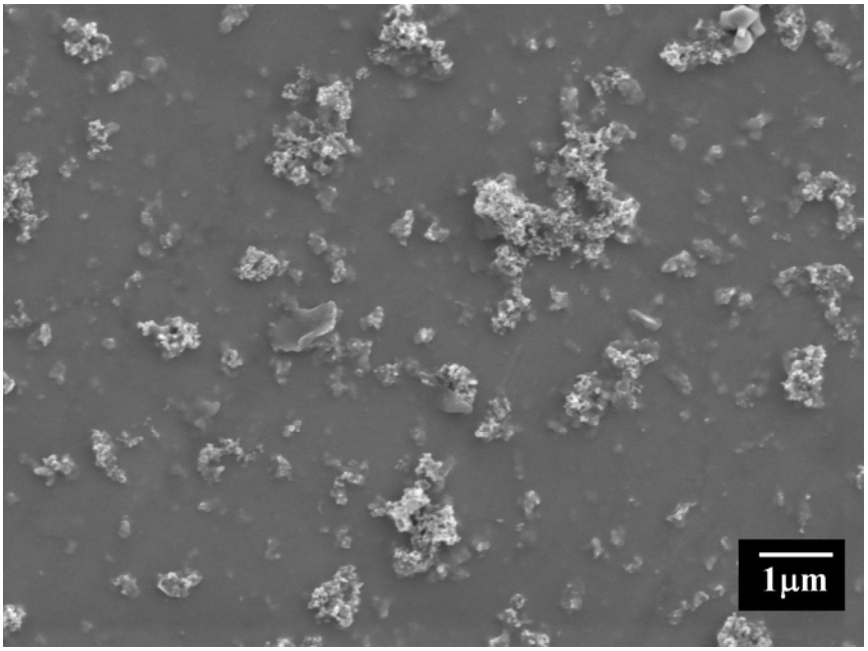

Figure 5-28 SEM images of deposits prepared from 3 gL^{-1} PDAOT water/ethanol mixed solutions containing 0.5 gL^{-1} TiO_2 at 5 V during 2 min

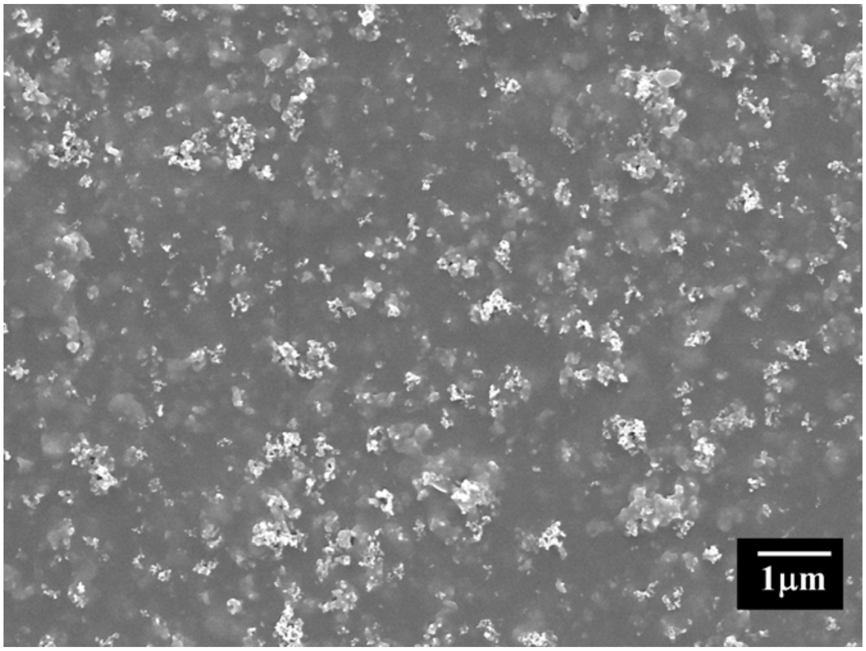

Figure 5-29 SEM images of deposits prepared from 3 gL^{-1} PDAOT water/ethanol mixed solutions containing 1.0 gL^{-1} TiO$_2$ at 15 V during 2 min

5.5 Electrophoretic deposition of ceramic particles with PEI polymer

The neutral linear polyethylenimine (PEI) is insoluble in water or ethanol. Protonation of the amino group with small amounts of acetic acid (5 vol.%) resulted in complete and rapid dissolution of the polymer in water or ethanol, forming a transparent solution. Cathodic deposits were obtained from PEI solutions in a mixed ethanol/water solvent (80/20 v/v). It is suggested that the deposition mechanism is based on the electrophoretic motion of protonated PEI—H$^+$ towards the cathode, where the pH is high due to the decomposition of water. The charge neutralization of the PEI—H$^+$ in the high pH region at the cathode surface resulted in the PEI precipitation and the formation of insoluble films:

$$\underset{\text{Soluble}}{\text{PEI}-\text{NH}_2^+} + \text{OH}^- \rightarrow \underset{\text{Insoluble}}{\text{PEI}-\text{NH}} + \text{H}_2\text{O} \tag{5-7}$$

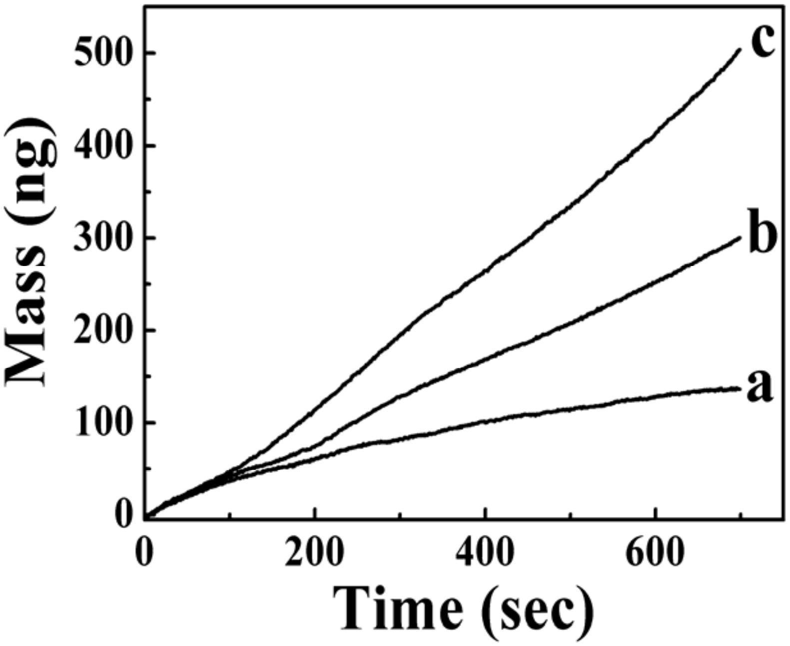

Figure 5-30 Deposit mass versus deposition time measured using QCM for 0.1 gL^{-1} PEI solution at a deposition voltage of (a) 4 V, (b) 7 V, (c) 10 V

Figure 5-30 shows pure PEI deposition yield measured using Quartz crystal microbalance (QCM) as a function of deposition time in a mixed ethanol/water solvent (80/20 v/v) at voltages in the range of 4–10 V. The deposit mass in the cathodic electrode continuously increased with increasing time and voltage, which indicates the formation of films of different mass. Therefore, the amount of the deposited material can be varied.

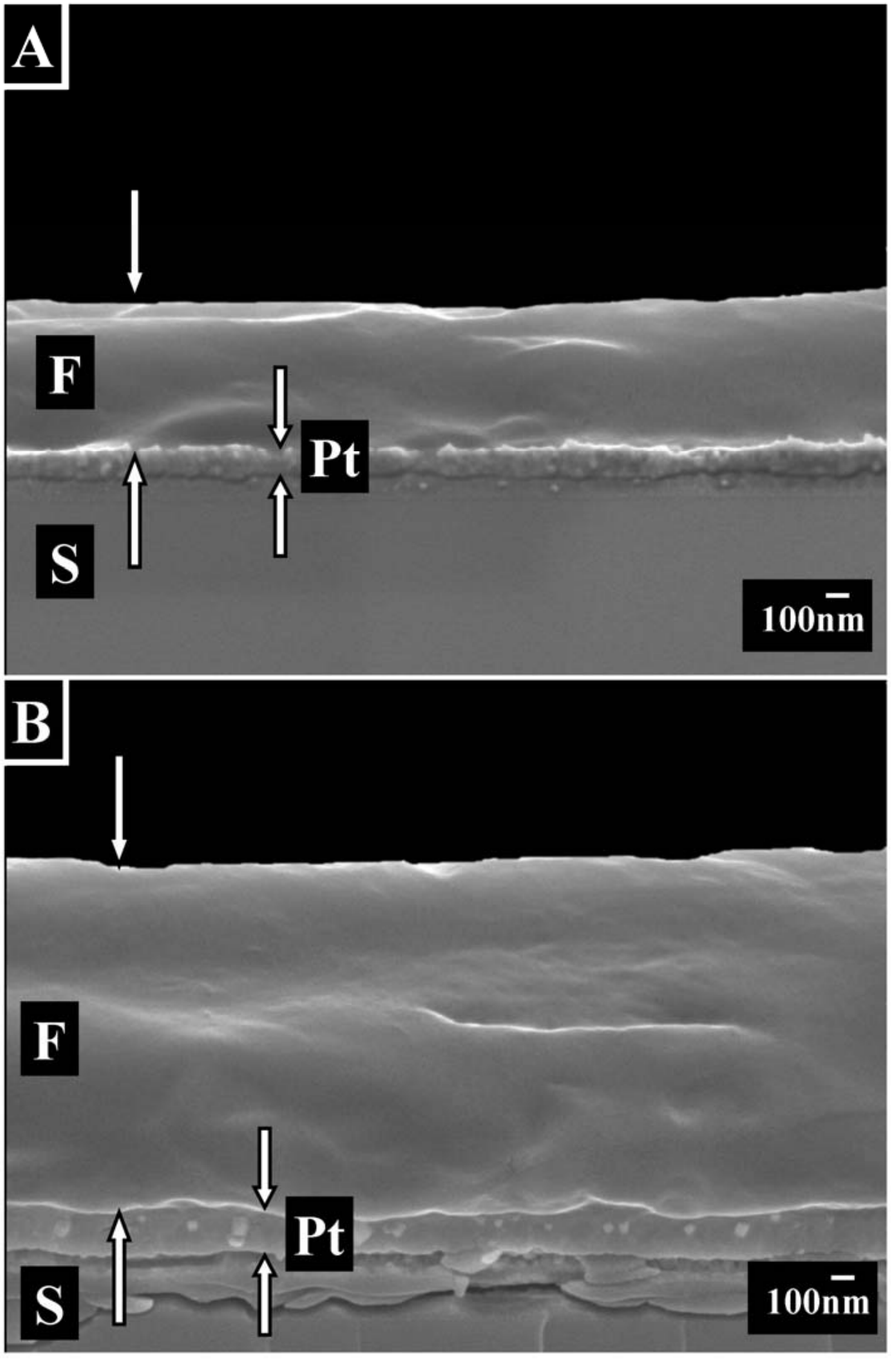

Figure 5-31 Cross section of PEI films (F) on the platinized silicon wafers (S), deposited from 10 gL^{-1} PEI water/ethanol mixed solutions at 40 V during (A) 5 min, (B) 10 min, arrows show film and Pt layer

Figure 5-31 shows typical SEM image of film cross section prepared by EPD. The film was relatively dense, uniform and adhered well to the substrate. It was found that pinhole-free films can be obtained from PEI water/ethanol mixed solutions. The film thickness was varied in the range of 0.1–1 μm by the variation of deposition voltage in the range of 10–40 V, deposition time in the range of 5–10 min. The increase in the film thickness with increasing voltage was attributed to increasing electric field in the suspension, which, in turn, increased the speed of electrophoretic motion of polymer macromolecules and resulted in higher deposition yield [5, 37, 107].

Figure 5-32 shows SEM images of the films prepared from the suspensions of TiO_2–PEI complexes in a mixed ethanol/water solvent system. The image (A) shows TiO_2 particles in the PEI matrix. The porosity can be attributed to packing of the particles and gas evolution at the electrode. The image (B) shows TiO_2–PEI composite film cross section. The films were relatively dense, adherent and uniform. The image indicated film uniformity which was controlled by electric field. However, the film uniformity is controlled by the particles size used for deposition. Film thickness could be varied in the range of 0.1–1 μm by adjusting the deposition voltage (from 30 to 40 V) and deposition time (5–10 min).

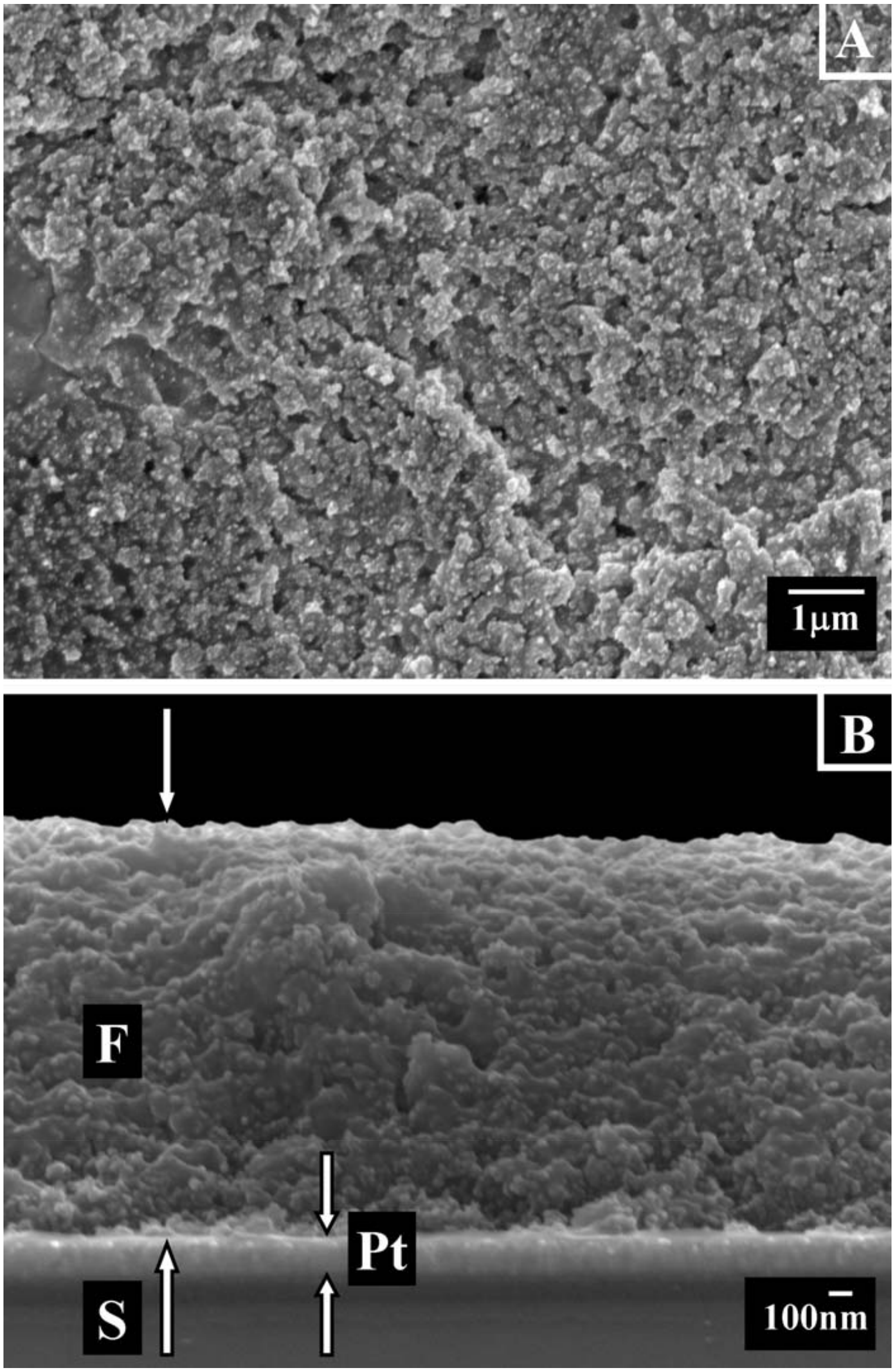

Figure 5-32 SEM images of deposits prepared from 10 gL^{-1} PEI water/ethanol mixed solutions containing 10 gL^{-1} TiO_2 at 40 V during 10 min; (A) Surface image; (B) Cross section of films (F) on the platinized silicon wafers (S), arrows show film and Pt layer

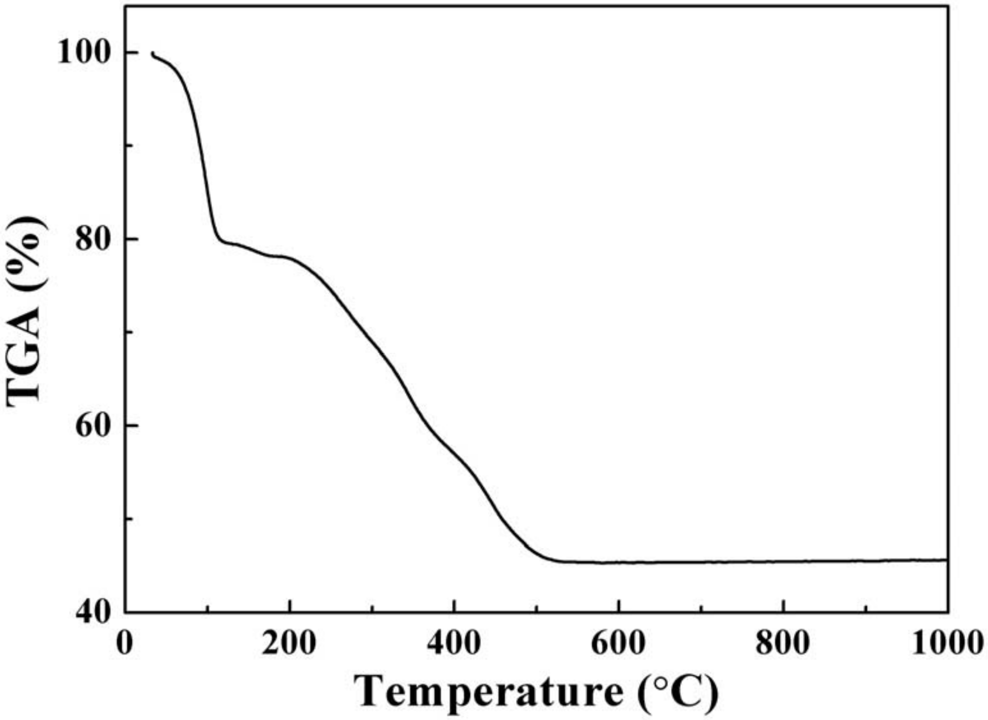

Figure 5-33 TGA data for deposits prepared from 10 gL^{-1} PEI water/ethanol mixed solutions containing 10 gL^{-1} TiO$_2$

Figure 5-33 shows TGA data for a deposit, prepared from 10 gL^{-1} PEI water/ethanol mixed solutions containing 10 gL^{-1} TiO$_2$. The TGA graph shows several steps in mass loss below 600 °C. The total mass loss at 1000 °C was found to be 54.2%. The mass loss can be attributed to film dehydration at lower temperatures and decomposition of the polymer side chains and backbone at higher temperatures. From the TGA data, the TiO$_2$ content in the sample was estimated to be 45.8 mass%. The TGA results together with SEM data indicated that organic–inorganic PEI–TiO$_2$ composites can be obtained.

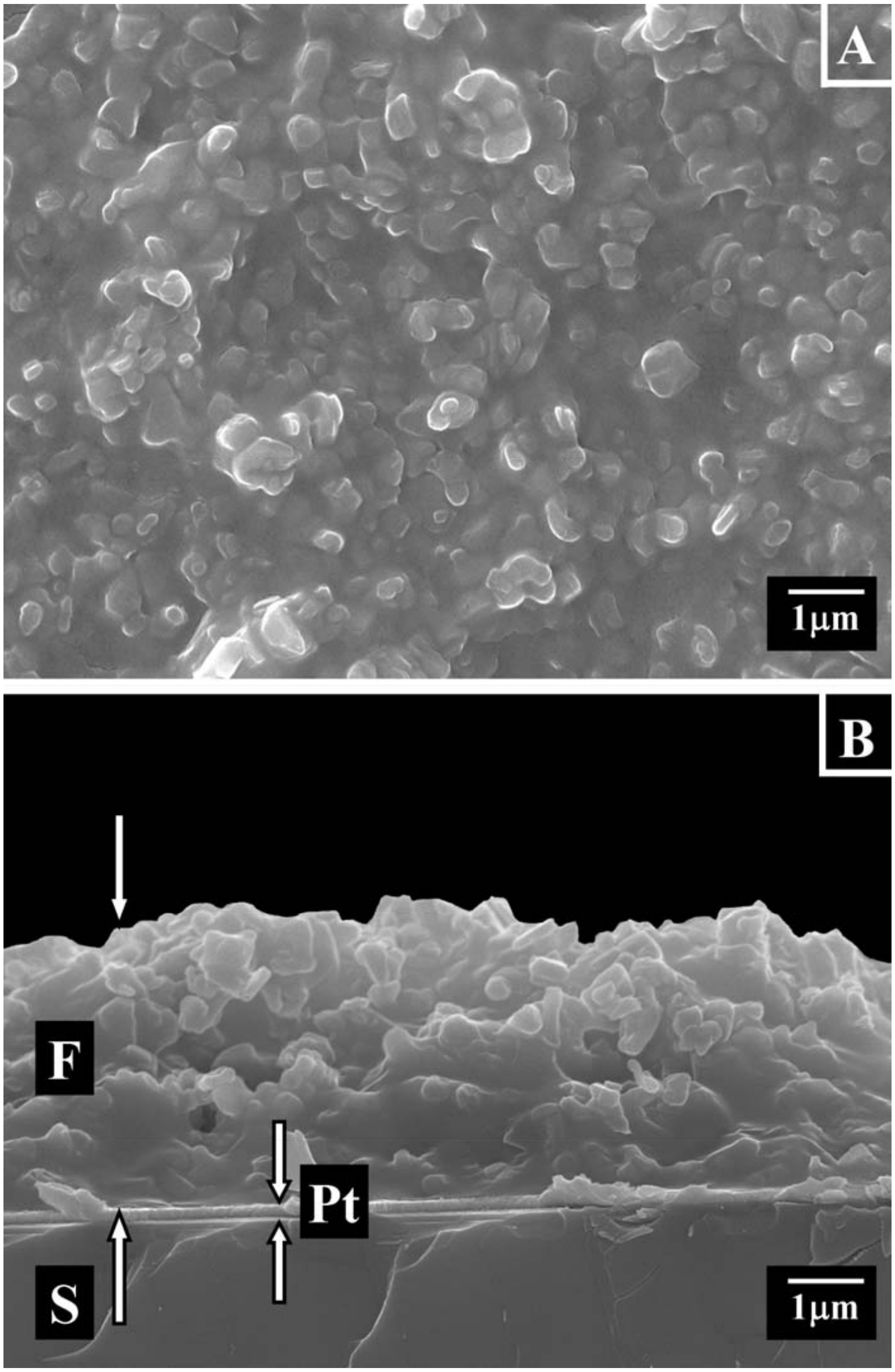

Figure 5-34 SEM images of deposits prepared from 10 gL^{-1} PEI water/ethanol mixed solutions containing 10 gL^{-1} hydrotalcite at 40 V during 3 min; (A) Surface image; (B) Cross section of films (F) on the platinized silicon wafers (S), arrows show film and Pt layer

The term hydrotalcite refers to a family of synthetic compounds with a structure based on the magnesium hydroxide ($Mg(OH)_2$)-like layers in which some of the divalent cations have been replaced by trivalent ones. Hydrotalcite ($Mg_6Al_2(OH)_{16}(CO_3)\cdot 4H_2O$), which is also known as aluminum–magnesium layered double hydroxide (LDH), is a synthetic compound that was widely investigated in the past few years because of its many potential applications, such as clinic anti-acid, catalyst support, adsorptive flotation, acid scavengers in polymer composites and as a raw material for high temperature insulating porous ceramics [108].

Figure 5-34 shows SEM images of the films prepared from the suspensions of hydrotalcite–PEI complexes in a mixed ethanol/water solvent system. The image (A) shows a surface of hydrotalcite particles in the PEI matrix. The image (B) shows hydrotalcite–PEI composite film cross section, which presented hydrotalcite incorporated into the polymer matrix. The films were relatively dense, adherent and thick. Film thickness could be varied in the range of 2–4 μm by adjusting the deposition voltage (from 30 to 40 V) and deposition time (5–10 min).

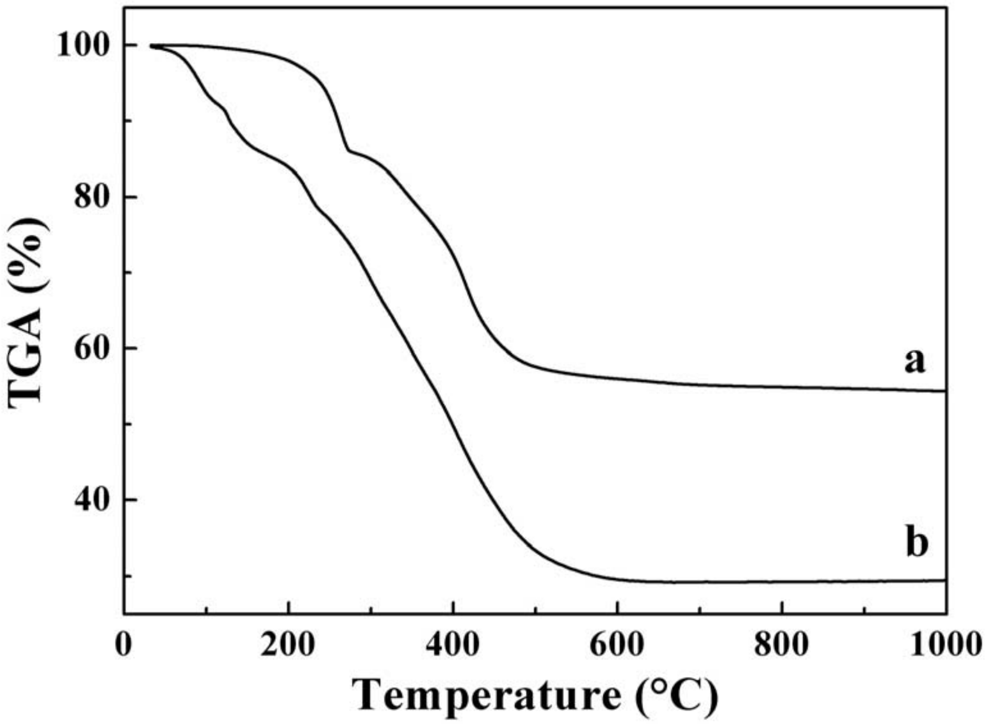

Figure 5-35 TGA data for (a) as-received hydrotalcite; (b) deposits prepared from 10 gL^{-1} PEI water/ethanol mixed solutions containing 10 gL^{-1} hydrotalcite

The films were studied by TGA. Figure 5-35 compares the TGA data for as-received hydrotalcite (curve a) and hydrotalcite deposits, prepared from suspensions, containing PEI polymer (curve b). The curve (a) indicated two major weight losses at around 250 °C and 400 °C. It is well understood that the two major weight losses at temperature below 500 °C are attributed to dehydration of the material (physically adsorbed, crystalline, and H-bound water in the interlayer) and dehydroxylation of OH groups [109]. The curve (b) shows several steps in mass loss below 600 °C, mainly attributed to dehydration and burning out of PEI. The total mass loss at 1000 °C was found to be 70.7%. From the TGA data, the hydrotalcite content in the sample was estimated to be 29.3 mass%. The results of TGA studies are in agreement with SEM data.

The TGA results together with SEM data the indicated that organic–inorganic PEI–hydrotalcite composites can be obtained.

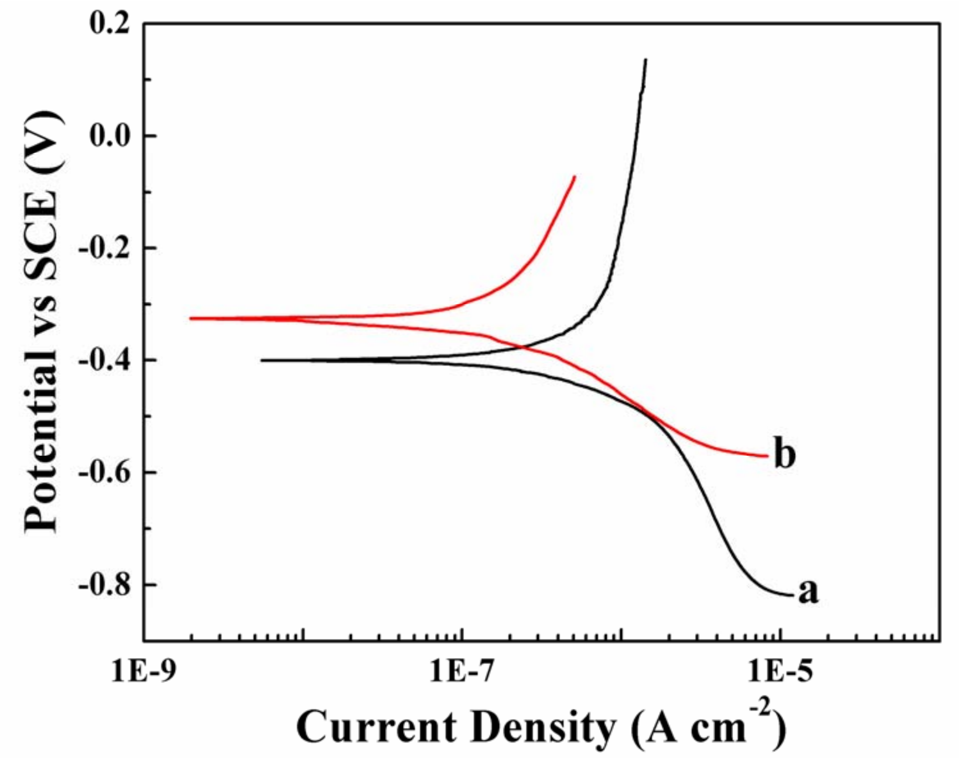

Figure 5-36 Tafel plot for (a) uncoated stainless steel substrate; (b) films coated stainless steel substrate. The films were prepared from 10 gL^{-1} PEI water/ethanol mixed solutions at a deposition voltage of 40 V during 2 min

The PEI polymer films prepared by electrodeposition were used for the corrosion protection of stainless steel substrates. Figure 5-36 compared Tafel plots for the uncoated (curve a) and PEI coated stainless steel (curve b). It can be noted that the corrosion current and therefore the rate of corrosion of the coated sample was reduced by the coating. In addition, the coated substrate shows a higher corrosion potential. These results indicated that the PEI film worked as a protective layer and provided corrosion protection of the stainless steel substrates. Moreover, the possibility of film formation on conductive substrates paves the way for other applications, such as fuel cells, sensors and catalysis.

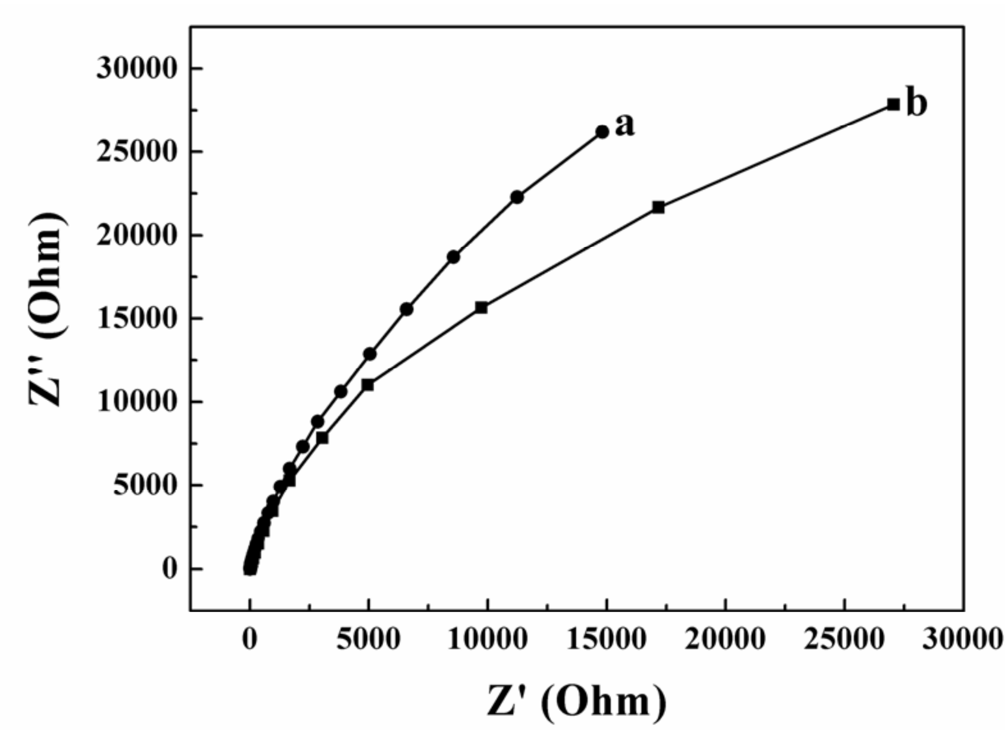

Figure 5-37 Nyquist plots of complex impedance $Z^* = Z' - iZ''$ for (a) uncoated stainless steel substrate; (b) films coated stainless steel substrate. The films were prepared from 10 gL^{-1} PEI water/ethanol mixed solutions at a deposition voltage of 40 V during 2 min

The PEI film working as a protective layer was confirmed by the impedance spectroscopy data in Figure 5-37, which compared Nyquist plots for the uncoated (curve a) and PEI coated stainless steel (curve b). The PEI film coated substrates (curve b) shows higher Z' impedance. Therefore, the coated substrate provided a barrier for electrolyte diffusion and corrosion protection of the substrates.

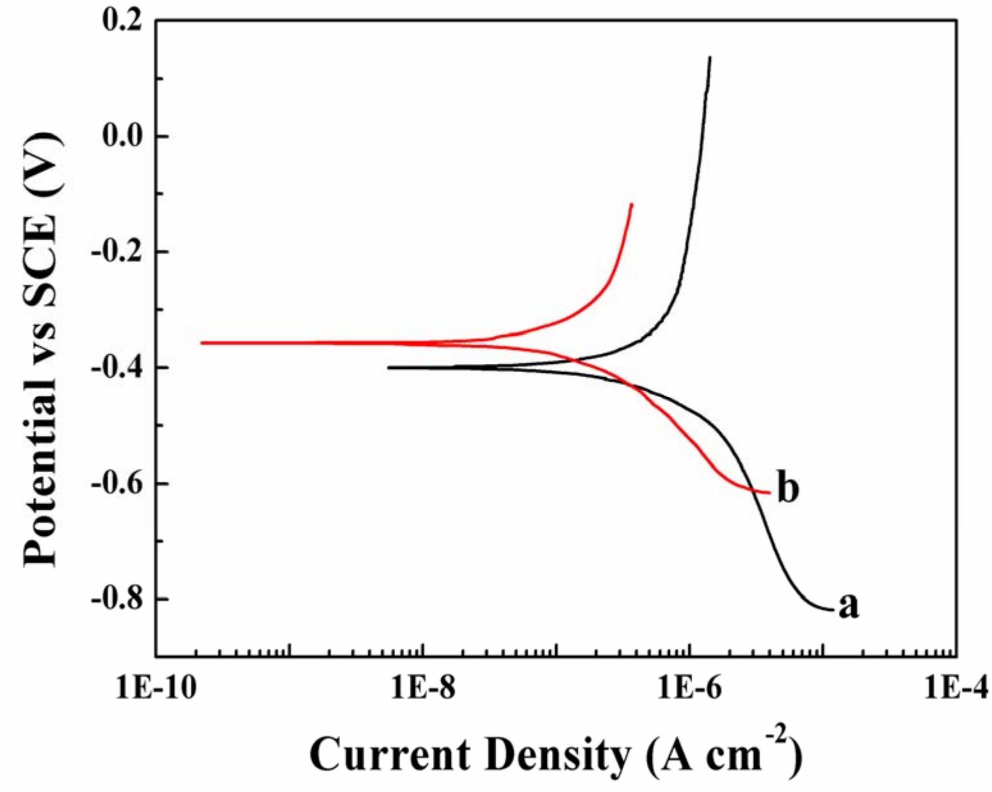

Figure 5-38 Tafel plot for (a) uncoated stainless steel substrate; (b) coated stainless steel substrate. The films were prepared from 10 gL^{-1} PEI water/ethanol mixed solutions containing 10 gL^{-1} TiO_2 at a voltage of 40 V during 5 min

Figure 5-38 compared Tafel plots for the uncoated stainless steel (curve a) and coated stainless steel with PEI−TiO_2 (curve b). It can be seen that the corrosion current and the rate of corrosion of the coated sample was reduced by the PEI−TiO_2 coating. Moreover, the coated stainless steel shows a higher corrosion potential. The composite films showed improved corrosion resistance, compared to the uncoated stainless steel. Therefore, these results indicated that the composite film acted as a barrier protective layer, which provided corrosion protection of the stainless steel substrate.

6 Conclusions

The main conclusions are summarized as follows:

- CA, DCA, PCA and TCA are efficient additives for dispersion, charging and EPD of TiO_2 particles. Anodic deposition was achieved using CA. In contrast, cathodic deposition was achieved using DCA, PCA and TCA. The difference in particle charge can be attributed to competitive adsorption of the anionic molecules and H^+. The deposition yield measurements showed that the amount of the deposited material can be varied and controlled. FTIR studies showed that strong adsorption of CA is attributed to catecholate type of bonding. CA is a promising dispersant for EPD of TiO_2 films with advanced functionality.
- Fundamental adsorption mechanism of organic molecules with COOH groups and OH groups has been investigated.
  - The adsorption of 2,6-DHBA, 2,3-DHBC, CA, which are belong to catecholate and salicylate family, are strong, whereas the adsorption of 5-SSA, TCA, PCA, DCA, which are belong to phenol and carboxyl group, are weak.
  - These organic molecules can be used to disperse, charge and functionalize metal oxide nanoparticles.
- Electrophoretic deposition method has been developed for the deposition of TiO_2 nanoparticles modified with organic dyes. The electrophoretic deposition method offers advantages for the fabrication of dye-sensitized TiO_2 films.
  - AR, AY and PV violet dyes were used for the dispersion and charging of TiO_2 in ethanol and anodic EPD of TiO_2 films. The deposition yield was varied by the

  changing the dye concentration in the suspensions and deposition time. The method resulted in the formation of porous crack free films.
  - AT–NH_4 dye was used for the deposition of TiO_2 from aqueous suspensions. It was found that thin films of pure ATH and composite ATH–TiO_2 films can be obtained. ATH film thickness was varied in the range of 0.1 – 2 μm by variation of the deposition time at a constant voltage. The composition and microstructure of the composite films and the amount of the deposited material can be varied by the variation of TiO_2 and AT–NH_4 concentration in suspensions and deposition time.
- EPD has been developed for the fabrication of cathodic PDATO–TiO_2 composites. It was shown that cationic DA can be used as charging additives and dispersants. The adsorption mechanism was based on the complexation of the metal ions at the nanoparticle surfaces. The agglomeration of TiO_2 nanoparticles significantly reduced after adding DA.
- EPD has been developed for the fabrication of cathodic pure PEI films and PEI–TiO_2, PEI–hydrotalcite composites.
  - Electrochemical tests showed that the PEI and PEI–TiO_2 coated stainless steel substrate exhibited a higher corrosion potential and a lower corrosion rate which indicated that PEI film worked as a protective layer and provided corrosion protection of the stainless steel substrates.

7 References

1. Antony Falk., Dürschner Christian., Remmers, and Karl-Heinz, *Photovoltaics for professionals: solar electric systems marketing, design and installation*. Berlin: London: Solarpraxis AG, 2007.
2. Juan Bisquert, David Cahen, Gary Hodes, Sven Ru1hle, and Arie Zaban, *Physical Chemical Principles of Photovoltaic Conversion with Nanoparticulate, Mesoporous Dye-Sensitized Solar Cells*. J. Phys. Chem. B, 2004. **108**: p. 8106-8118
3. F. Sun, X. Pang, I. Zhitomirsky, *Electrophoretic deposition of composite hydroxyapatite–chitosan–heparin coatings*. Journal of materials processing technology, 2009. **209**: p. 1597–1606.
4. I. Zhitomirsky, *Electrophoretic deposition of organic-inorganic nanocomposites*. J Mater Sci, 2006. **41**: p. 8186–8195.
5. I. Zhitomirsky, *Cathodic electrodeposition of ceramic and organoceramic materials. Fundamental aspects*. Advances in Colloid and Interface Science, 2002. **97**: p. 277-315.
6. Partho Sarkar, and Patrick S. Nicholson, *Electrophoretic deposition (EPD) mechanisms kinetics and application to ceramics*. Journal of the American Ceramic Society, 1996. **79(8)**: p. 1987-2002.
7. Walther Schwarzacher, *Electrodeposition: A technology for the future*. The Electrochemical Society Interface, 2006. p. 32-35.
8. A. R. Boccaccini1, S. Keim, R.Ma, Y. Li, and I. Zhitomirsky, *Electrophoretic*

deposition of biomaterials. J. R. Soc. Interface, 2010. **7**: p. S581–S613.

9. B.derjaguin, and L. Landau, *Theory of the stability of strongly charged lyophobic sols and of the adhesion of strongly charged particles*. Acta Physicochimica, 1941. **14**: p. 633-662.
10. E. J. W Verwey, and J. Th. G Overbeek, *Theory of the stability of lyophobic colloids*. Journal of Colloid Science, 1955. **10**: p. 224-225.
11. Guozhong Cao, *Nanostructures and nanomaterials synthesis, properties and applications*. London: Imperial college press, 2004.
12. X. L. Chu, A. D. Nikolov, and D. T. Wasan, Journal of Chemical Physics, 1995. **103**: p. 6653.
13. C. Xu, H. Gu, R. Zheng, H. Liu, X. Zhang, Z. Guo, and B. Xu, Journal of the American Chemical Society, 2004. **126**: p. 9938.
14. J. E. Sader, and D. Y. C. Chan, J. Colloid Interface Sci., 1999. **218**: p. 423.
15. M. Trau, D. A. Saville, and I. A. Aksay, Langmuir, 1997. **13**: p. 6375.
16. I. S. Lavrov, and O. V. Smirnov, Journal of applied chemistry of the USSR, 1969. **42**: p. 1459.
17. P. A. Kralchevsky, K. Nagayama, Langmuir, 1994. **10**: p. 23.
18. Ilaria Corni, Mary P. Ryan, and Aldo R. Boccaccini, *Electrophoretic deposition: From traditional ceramics to nanotechnology*. Journal of the European Ceramic Society, 2008. **28**: p. 1353–1367.
19. Hamaker, H. C., *Formation of deposition by electrophoresis*. Trans. Farad. Soc., 1940. **36**: p. 279–283.

20. Hamaker, H. C. and Verwey, E. J. W., *The role of the forces between the particles in electrodeposition and other phenomena*. Trans. Farad. Soc., 1940. **3**: p. 180–185.
21. Koelmans, H., Philips Res. Rep., 1955. **10**: p. 161–193.
22. Begona Ferrari, and Rodrigo Moreno, Journal of the European Ceramic Society, 2010. **30**(5): p. 1069–1078.
23. Omer O. Van der Biest, Luc J. Vandeperre, *Electrophoretic deposition of materials*. Annual Review of Materials Science, 1999. **29**: p. 327-352.
24. M. E. Labib, R. Williams, Journal of Colloid and Interface Science, 1984. **97**: p. 356.
25. K. Yamashita, M. Nagai, T. Umegaki, J. Mater. Sci., 1997. **32:** p. 6661.
26. R. Damodaran, and B.M. Moudgil, Colloids Surf. A: Physicochem. Eng. Aspects, 1993. **80**: p. 191.
27. J. VanTassel, and C.A. Randall, J. Eur. Ceram. Soc., 1999. **19**: p. 955.
28. F. Harbach, and H. Nienburg, J. Eur. Ceram. Soc., 1998. **18**: p. 675.
29. S. Okamura, T. Tsukamoto, N. Koura, Jpn. J. Appl. Phys., 1993. **32**: p. 4182.
30. Y. Takayama, H. Negishi, S. Nakamura, N. Koura, Y. Idemoto, and F. Yamaguchi, J. Ceram. Soc. Jpn., 1999. **107**: p. 119.
31. P.F. Grosso, R.E. Rutherford Jr, and D.E. Sargent, J. Electrochem. Soc., 1970. **117**: p. 1456.
32. I. Zhitomirsky, Adv Colloid Interface Sci., 2002. **97**: p. 279-317.
33. Rivas BL, Geckeler KE, Adv Polym. Sci., 1992. **102**: p. 171.

34. Griffiths PC, Paul A, Stilbs P, and Petterson E, Macromolecules, 2005. **38**: p. 3539.

35. U. Paik, V.A. Hackley, S. C. Choi, and Y. G. Jung, Colloid Surf. A: Physicochem. Eng. Aspects, 1998. **135**: p. 77.

36. T. Chartier, E. Streicher, and P. Boch, Bull. Am. Ceram. Soc., 1987. **66**: p. 1653.

37. I. Zhitomirsky, and A. Petric, J. Eur. Ceram. Soc., 2000. **20**: p. 2055.

38. I. Zhitomirsky, L. Gal-Or, in Intermetallic and Ceramic Coatings, N. B. Dahotre, T. S. Sudarshan, Eds. (Marcel Dekker Inc., New York, 1999), p. Chapter 3.

39. I. Zhitomirsky, NanoStructured Materials, 1997. **8**: p. 521.

40. P. Sarkar, X. Huang, and P. S. Nicholson, *Zirconia/Alumina Functionally Gradient Composites by Electrophoretic Deposition*. J. Am. Ceram. Soc., 1993. **76**: p. 1055-1056.

41. H. C. Hamaker, *Formation of Deposition by Electrophoresis*. Trans. Faraday Soc., 1940. **36**: p. 279-287.

42. Z. Zhang, Y. Huang, and Z. Jiang, *Electrophoretic Deposition Forming of SiC-TZP Composites in a Nonaqueous Sol Media*. J. Am. Ceram. Soc., 1994. **77**: p. 1946-1949.

43. J.J. Hermans, J. Polym. Sci., 1955. **18**: p. 527.

44. H. Ohshima, J. Colloid Interface Sci., 2000. **228**: p. 190.

45. P.M. Biesheuvel, and H. Verweij, J. Am. Ceram. Soc., 1999. **82**: p. 1451.

46. H. Ohshima, Colloids Surf. A: Physicochem. Eng. Aspects, **1995**. 103: p. 249.

47. J. Mizuguchi, K. Sumi, and T. Muchi, Journal of the Electrochemical Society,

1983. **130**: p. 1819.

48. J. M. Andrews, A. H. Collins, D. C. Cornish, and J. Dracass, Proceedings of the British Ceramic Society, 1969. **12**: p. 211.

49. I. Zhitomirsky, Journal of Materials Science Letters, 1998. **17**: p. 2101.

50. I. Zhitomirsky, JOM-e 52, (1) http://www.tms.org/pubs/journals/JOM/0001/Zhitomirsky/Zhitomirsky-0001.html as on 20 February 2000

51. Sasaki T, Ebina Y, Tanaka T, Harada M, and Watanabe M, Chemisty of Materials, 2001. **13**: p. 4661-4667.

52. Cassagneau T, Guerin F, and Fendler JH, Langmuir, 2000. **16**: p. 7318.

53. Bon P, I. Zhitomirsky, and Embury JD, Mater. Chem. Phys., 2004. **86**: p. 44.

54. I. Zhitomirsky, and Petric A, Ceram. Int., 2001. **27**: p. 149.

55. I. Zhitomirsky, and Petric A, Mater. Lett., 2000. **46**: p. 1.

56. Mcnally EA, Zhitomirsky I, and Wilkinson DS, Mater. Chem. Phys., 2005. **91**: p. 391.

57. I. Zhitomirsky, J. Appl. Electrochem., 2004. **34**: p. 235.

58. Nagarajan N, Humadi H, and I. Zhitomirsky, Electrochim. Acta., 2006. **51**: p. 3039.

59. Pang X, and Zhitomirsky I, Langmuir, 2004. **20**: p. 2921.

60. Cao J, Zhitomirsky I, and Niewczas M, Mater. Chem. Phys., 2006. **96**: p. 289.

61. Shchukin DG, Radtchenko IL, and Sukhorukov GB, J. Phys. Chem. B, 2003. **107**: p. 86.

62. Bardetsky D, and Zhitomirsky I, Surf. Eng., 2005. **21**: p. 125.

63. Wu LQ, Yi H, Li S, Rubloff GW, Bentley WE, Ghodssi R, and Payne GF, Langmuir, 2003. **19**: p. 519.

64. Wu LQ, Gadre AP, Yi H, Kastantin MJ, Rubloff GW, Bentley WE, Payne GF, and Ghodssi R, Langmuir, 2002. **18**: p. 8620.

65. Wu LQ, Lee K, Wang X, English DS, Losert W, and Payne GF, Langmuir, 2005. **21**: p. 3641.

66. Gorelikov I, and Kumacheva E, Chem. Mater., 2004. **16**: p. 4122.

67. Hasegawa K, Tatsumisago M, and Minami T, J. Ceram. Soc. Jpn., 1997. **105**: p. 569.

68. Pang X, and Zhitomirsky I, Int. J. Nanosci., 2005. **4**: p. 409.

69. Robert Langer, *Drugs on Target*. Science, 2001. **292**: p. 58-59.

70. P. Alivisatos, Nat. Biotechnol., 2004. **22**: p. 47.

71. Lee, H., Dellatore, S. M., Miller, W. M. and Messersmith, P. B., Science, 2007. **318**: p. 426–430.

72. G. A. Young, D. J. Crisp, in Adhesion, K. W. Allen, Ed. Applied Science, 1982. vol 6,

73. J. Herbert Waite, *Mussel Power*. Nature Materials, 2008. **7**: p. 8-9.

74. M. Yu, J. Hwang, and T. J. Deming, J. Am. Chem. Soc., 1999. **121**: p. 5825.

75. H. Lee, N. F. Scherer, and P. B. Messersmith, Proc. Natl. Acad. Sci., 2006. **103**: p. 12999.

76. Y. Li, M. Liu, C. Xiang, Q. Xie, and S. Yao, Thin Solid Films, 2006. **497**: p. 270.

77. C. G. Pierpont, and C. W. Lange, Prog. Inorg. Chem, 1994. **41**: p. 331.

78. M. Gratzel, *Heterogeneous Photochemical Electron Transfer*. Boca Raton, Fla: CRC press, 1989.

79. X. Fan, L. Lin, J. L. Dalsin, and P. B. Messersmith, J. Am. Chem. Soc., 2005. **127**: p. 15843.

80. C. Xu, K. Xu, H. Gu, R. Zheng, H. Liu, X. Zhang, Z. Guo, and B. Xu, J. Am. Chem. Soc., 2004. **126**: p. 9938.

81. J. Xie, K. Chen, H.-Y. Lee, C. Xu, A. R. Hsu, S. Peng, X. Chen, andS. Sun, J. Am. Chem. Soc., 2008. **130**: p. 7542.

82. Y. Kikuchi, K. Sanada, T. Iyoda, K. Hashimoto, and A. Fujishima, J. Photochem. Photobiol. Chem., 1997. **106**: p. 51.

83. B. O'Regan, and M. Gratzel, Nature, 1991. **353**: p. 737.

84. J. Moser, S. Punchihewa, P.P. Infelta, and M. Gratzel, Langmuir, 1991. **7**: p. 3012.

85. Ivana A. Jankovic, Zoran V. Saponjic et al., *New Hybrid Properties of TiO_2 Nanoparticles Surface Modified with Catecholate Type Ligands*. Nanoscale Research Letters, 2010 **5**: p. 81-88.

86. Yang Z, Choi D, Kerisit S, Rosso KM, Wang D, Zhang J, et al., J. Power Sources, 2009. **192**: p. 588–98.

87. Cao B, Yao W, Wang C, Ma X, Feng X, and Lu X., *Simple fabrication of rutile titanium dioxide whiskers*. Mater. Lett., 2010. **64**: p. 1819–1821.

88. Li Y, Hagen J, Schaffrath W, Otschik P, and Haarer D., Sol Energy Mater Sol Cells, 1999. **56**: p. 167–174.

89. Boccaccini AR, Roether JA, Thomas BJC, Shaffer MSP, Chavez E, Stoll E, et al. ,

J. Ceram. Soc. Jpn., 2006. **114**: p. 1–14.

90. Ye Q, Zhou F, and Liu W., Chem. Soc. Rev., 2011. **40**: p. 4244–4258.

91. Gulley-Stahl H, Hogan PA, Schmidt WL, Wall SJ, Buhrlage A, and Bullen HA. Environ. Sci. Technol., 2010. **44**: p. 4116–4121.

92. K. V. S. Devi, B. R. Raju, and G. N. Rao, Acta Chim. Slovenica., 2010. **57**: p. 398.

93. J. P. Cornard, and C. Lapouge, J. Phys. Chem. A, 2004. **108**: p. 4470.

94. T. Rajh, L. X. Chen, K. Lukas, T. Liu, M. C. Thurnauer, and D. M. Tiede, J. Phys. Chem. B, 2002. **106**: p. 10543.

95. Zhitomirsky I, and Petric A. J. Mater. Sci., 2004. **39**: p. 825–831.

96. I.A. Jankovic, Z.V. Saponjic, M.I. Comor, and J.M. Nedeljkovic, J. Phys. Chem. C, 2009. **113**: p. 12645.

97. Wu K, and Zhitomirsky I, Int. J. Appl. Ceram. Technol., 2011. **8**: p. 920–927.

98. K. Wu, Y. Wang, and I. Zhitomirsky, J. Colloid Interface Sci., 2010. **352**: p. 371.

99. Xiao-Hong Guan, Chii Shang et al., Chemosphere, 2006. **65**: p. 2074–2081.

100. Shun-Xing Li, Shu-Jie Caia, and Feng-Ying Zheng, Dyes and Pigments, 2012. **95**: p. 188-193.

101. P. M. Jayaweera, and T. A. U. Jayarathne, Surface Science Leters, 2006. **600**: p. L297-L300.

102. M. Guedes, J. M. F. Ferreira, and A. C. Ferro, J. Colloid Interface Sci., 2009. **330**: p. 119.

103. S. Pirillo, M. L. Ferreira, and E. H. Rueda, *The effect of pH in the adsorption of Alizarin and Eriochrome Blue Black R onto iron oxides*. J. Hazard. Mater., 2009.

168: p. 168-178.

104. K. D. Dobson, and A. J. McQuillan, Spectrochimica Acta. Part A: Molecular and Biomolecular Spectroscopy, 2000. **56**: p. 557.

105. W. Jarernboon, S. Pimanpang, S. Maensiri, E. Swatsitang, and V. Amornkitbamrung, Thin Solid Films, 2009. **517**: p. 4663.

106. H. Chang, H. T. Su, W. A. Chen, K. David Huang, S. H. Chien, S. L. Chen, C. C. Chen, Sol. Energy, 2010. **84**: p. 130.

107. I. Zhitomirsky, and L. Gal-Or, J. Mater. Sci.: Mater. Med., 1997. **8**: p. 213.

108. Rafael Salomao, L.M. Milena, M.H. Wakamatsu, and Victor C. Pandolfelli, *Hydrotalcite synthesis via co-precipitation reactions using MgO and* $Al(OH)_3$ *precursors.* Ceramics International, 2011. **37**: p. 3063–3070.

109. Jia Zhang, Yun Feng Xu Guangren Qian, Zhi Ping Xu, Chun Chen, and Qiang Liu, J. Phys. Chem. C, 2010. **114**: p. 10768–10774.